

# For Reference

NOT TO BE TAKEN FROM THIS ROOM

Ex LIBRIS  
UNIVERSITATIS  
ALBERTAEÆNSIS







THE UNIVERSITY OF ALBERTA

RELEASE FORM

NAME OF AUTHOR        Theodore W. J. Frauenfeld  
TITLE OF THESIS        Non-Isothermal Miscible Displacement  
DEGREE FOR WHICH THESIS WAS PRESENTED    Master of Science  
YEAR THIS DEGREE WAS GRANTED    Fall, 1981

Permission is hereby granted to THE UNIVERSITY OF ALBERTA LIBRARY to reproduce single copies of this thesis and to lend or sell such copies for private, scholarly or scientific research purposes only.

The author reserves other publication rights, and neither the thesis nor extensive extracts from it may be printed or otherwise reproduced without the author's written permission.

---

## THE STATE

THE STATE OF NEW YORK

IN SENATE

JANUARY 1, 1901.

REPORT

OF THE

COMMISSIONERS OF THE LAND OFFICE

FOR THE YEAR 1900.

ALBANY:

JOHN W. BAKER, PRINTERS.

THE UNIVERSITY OF ALBERTA

RELEASE FORM

NAME OF AUTHOR	Theodore W. J. Frauenfeld
TITLE OF THESIS	Non-Isothermal Miscible Displacement
DEGREE FOR WHICH THESIS WAS PRESENTED	Master of Science
YEAR THIS DEGREE WAS GRANTED	Fall, 1981

Permission is hereby granted to THEODORE W. J. FRAUENFELD to present to the School of Graduate Studies, University of Alberta, for acceptance, a thesis entitled "Non-Isothermal Miscible Displacement". Further, permission is hereby granted to THE UNIVERSITY OF ALBERTA LIBRARY to reproduce single copies of this thesis and to lend or sell such copies for private, scholarly or scientific research purposes only.

---



THE UNIVERSITY OF ALBERTA

Non-Isothermal Miscible Displacement

by



Theodore W. J. Frauenfeld

A THESIS

SUBMITTED TO THE FACULTY OF GRADUATE STUDIES AND RESEARCH

IN PARTIAL FULFILMENT OF THE REQUIREMENTS FOR THE DEGREE

OF Master of Science

IN

Petroleum Engineering

Department of Mineral Engineering

EDMONTON, ALBERTA

Fall, 1981



Digitized by the Internet Archive  
in 2019 with funding from  
University of Alberta Libraries

<https://archive.org/details/Frauenfeld1981>

THE UNIVERSITY OF ALBERTA  
FACULTY OF GRADUATE STUDIES AND RESEARCH

The undersigned certify that they have read, and recommend to the Faculty of Graduate Studies and Research, for acceptance, a thesis entitled Non-Isothermal Miscible Displacement submitted by Theodore W. J. Frauenfeld in partial fulfilment of the requirements for the degree of Master of Science in Petroleum Engineering.



## ABSTRACT

This study investigates isothermal and non-isothermal miscible displacement in a porous medium. The effects of several parameters on dispersion are studied, including the effect of a temperature front on the process. The work done includes a series of experimental measurements of thermal and concentration profiles for two component displacement and numerical simulations of several experiments. The development of the numerical simulation program is described. This simulation is unique in that the equations are linked by temperature. A dimensional scaling study of the one dimensional equations and of the displacement parameters is also included.



## ACKNOWLEDGEMENTS

The author wishes to thank Dr. S. M. Farouq Ali for suggesting this study and for guidance throughout this investigation, the Alberta Oil Sands Technology and Research Authority for financial assistance, and the Research Council of Alberta for educational leave provisions and for permission to use the data contained in this work.



## Table of Contents

Chapter	Page
I. SURVEY OF THE LITERATURE . . . . .	3
II. EXPERIMENTAL APPARATUS AND PROCEDURE . . . . .	9
III. DISCUSSION OF RESULTS . . . . .	15
A. Experimental Data . . . . .	15
Velocity Effects . . . . .	20
Mixing at an Unfavourable Viscosity Ratio . . . . .	23
Dispersion at $M=1.0$ . . . . .	23
Effect of Inlet Temperature . . . . .	26
Movement of Thermal Front . . . . .	28
Pressure Profiles . . . . .	32
Dispersion in a Water-Wet Sandpack . . . . .	32
IV. NUMERICAL ANALYSIS . . . . .	34
A. Numerical Procedures . . . . .	34
B. Numerical Results . . . . .	36
Tests of the Numerical Program . . . . .	36
Results of Numerical Simulations . . . . .	41
C. Results of Scaling Study . . . . .	55
V. CONCLUSIONS . . . . .	60
A. Experimental and Numerical Results . . . . .	60
B. Scaling Study . . . . .	61
C. Practical Application . . . . .	62
D. Recommendations for Future Work . . . . .	62
VI. BIBLIOGRAPHY . . . . .	64
VII. APPENDIX A . . . . .	67



A.	Inspectional Analysis of Miscible Displacement Equations . . . . .	67
B.	Dimensional Analysis of Non-Isothermal Miscible Displacement Equations . . . . .	73
VIII.	APPENDIX B . . . . .	79
A.	Convection-Diffusion Equation . . . . .	79
B.	Heat Transfer Equation . . . . .	83
C.	Fluid Flow Equation in One Dimension . . . . .	84
D.	Pressure Equation . . . . .	85
IX.	APPENDIX C . . . . .	91
A.	Stability Analysis . . . . .	91
X.	APPENDIX D . . . . .	93
A.	Heat Transfer Calculations for Miscible Displacement Test Core . . . . .	93
XI.	APPENDIX E . . . . .	95
A.	Miller Stability Criterion for Stable Thermal Displacement Front . . . . .	95
XII.	APPENDIX F . . . . .	98
A.	Experimental Data and Work-Up . . . . .	98



## List of Tables

Table	Description	Page
1	Properties of Oils Used	12
2	Experimental Data	21
3	Numerical Data	44
4	Numerical Stability Data	47
5	Summary of Experimental Data	111



## List of Figures

Figure	Title	Page
1	Schematic of Experimental Apparatus	10
2	Experimental Concentration Profiles, R5	16
3	Experimental Concentration Profiles, R9	17
4	Experimental Concentration Profiles, R11	18
5	Unfavourable Mobility Ratio Displacement	19
6	Effect of Velocity on Dispersion	22
7	Mixing Coefficient at Unfavourable Mobility Ratio	24
8	Isothermal Displacement Data	25
9	Effect of Inlet Temperature on Mixing Coefficient	27
10	Temperature Profile of Heated Displacement, R9	29
11	Temperature Profile of Heated Displacement, R13	30
12	Temperature Profile of Chilled Displacement, R12	31
13	Numerical Solution at $C(0,t) = 1.0$	37
14	Numerical Solution at Larger $\Delta x$	38
15	Numerical Solution at $C(0,0) = 0.0$	39
16	Numerical Solution at $C(0,0) = 0.5$	40
17	Numerical Solution at $\Delta t = 120$ sec.	42
18	Numerical Solution at One and Three Iterations	43
19	Comparison of Experimental and Numerical Solution, R3	45
20	Numerical Simulation Data for 20-30 Mesh Pack	48
21	Simulation of Highly Favourable Mobility Displacement, R8	50
22	Numerical Simulation of Unfavourable Mobility Ratio Displacement	52
23	Numerical Simulation of Thermal Profile	53



Figure	Title	Page
24	Viscosity Ratio Profile at $t=3600$ s, R3	54
25	Pressure Solution for R3	56
26	Experimental Pressure Profile	57
27	Numerical Solution for R3 Using Pressure Equation	58
28	Comparison of Sleeve and Pack Heat Transfer	94
29	Flow Chart of Numerical Simulation	99
30	Experimental Strategy	100
31	Example Experimental Probability Plot	101
32	Example Numerical Probability Plot	102
33	Harmony 44-111 Mixtures, Refractive Index	103
34	Varsol-Harmony 111 Mixtures, Refractive Index	104
35	Harmony 44-87 Mixtures, Refractive Index	105
36	Harmony 87-111 Mixtures, Refractive Index	106
37	Harmony 53-87 Mixtures, Refractive Index	107
38	Harmony 44-53 Mixtures, Refractive Index	108
39	Varsol-Harmony 44 Mixtures, Refractive Index	109
40	Viscosity Correlations for Mixtures	110



## Nomenclature

$C_i^n$	concentration at time step $n$ , node $i$	volume fraction
$c_p$	fluid specific heat	J/gm.C
$c_{pr}$	specific heat of sand grains	J/gm.C
$d_p$	mean sand grain size	cm
$D_0$	diffusion coefficient	cm <sup>2</sup> /s
$k$	permeability (darcys)	$\mu\text{m}^2$
$k_d$	dispersion coefficient	cm <sup>2</sup> /s
$k_h$	thermal conductivity	J/s.cm.C
$L$	length of sandpack	cm
$M$	local viscosity ratio	$\frac{\mu_{\text{displaced}}}{\mu_{\text{displacing}}}$
$p_i^n$	pressure at time step $n$ , node $i$	bar
$T_i^n$	temperature at time step $n$ , node $i$	C
$v$	bulk fluid velocity	cm/s
$\Delta p$	pressure drop	bar
$\Delta T$	temperature drop	C
$\Delta t$	time step	s
$\Delta x$	distance step	cm
$\varepsilon$	dimensionless length	$x/L$
$\varepsilon$	truncation error term	$\frac{\text{gm}}{\text{cm}^3 \cdot \text{s}}$ or $\frac{\text{J}}{\text{cm}^3 \cdot \text{s}}$
$\rho$	oil density	gm/cm <sup>3</sup>
$\rho_r$	density of sand grains	gm/cm <sup>3</sup>
$\sigma$	mixing coefficient	$K_d/vd_p$
$\tau$	dimensionless time	sec/(sec at 1.P.V.)
$\mu$	oil viscosity	mPa.s
$\phi$	porosity	dimensionless
$\omega$	truncation cancellation term	dimensionless



## INTRODUCTION

Miscible floods have been used quite successfully in some types of conventional oil reservoirs to improve the recovery of oil. In these floods, solvent (high pressure gas, propane or liquid carbon dioxide) is used to displace oil.

For heavy oil recovery the use of a solvent driven by steam or by a hot water bank has been proposed. This method has been studied by a number of investigators, including Farouq Ali(1). It has the characteristics of both miscible displacement and steam flooding. Attempts to study this process by scale models must scale both heat transfer and the displacement process. This leads to difficulties in satisfying the relevant criteria.

The problem was therefore defined as follows:

"A porous medium is saturated with a hydrocarbon fluid which is displaced by a second hydrocarbon fluid. The displacement front moves at a constant velocity. The displacement front is accompanied by a thermal front moving at a different velocity. The pressure drop within the porous medium is a function of the viscosity of the moving fluid. This viscosity is a function of fluid temperature and composition".

The problem was approached by two methods:

1. An experimental approach, in which thirty-six experiments in three sand packs were used to explore the effects of fluid velocity, inlet mobility ratio, inlet temperature gradient and sand particle size on dispersion. Of particular interest was the interaction between the displacement front and the thermal front.
2. A numerical simulation, in which the equations for diffusion, heat transfer, and pressure drop were solved by a finite difference



method.

The goal of the numerical model was to simulate the interactions of the thermal front and the dispersion front, as determined experimentally. The study included a scaling analysis of the problem which demonstrated the incompatibility of the scaling groups.



## I. SURVEY OF THE LITERATURE

The use of laboratory models to study displacement processes in oil reservoirs requires that the models be properly scaled. The scaling process determines the dimensionless groups relevant to the process under study and adjusts the variables of the model so that the values of the dimensionless groups for the field and the model are equal.

There are two methods for deriving the relevant dimensionless groups. The first method is dimensional analysis. In this method, variables are repeatedly combined until a useful set of dimensionless groups is obtained. This technique only requires that the complete set of relevant variables are known. The procedure has been described by Greenkorn (2) and by Geertsma, Croes and Schwartz (3). The second method is inspectional analysis. In this procedure, the equations governing the system under study are written in dimensionless form and the resulting dimensionless parameters are combined to yield a set of dimensionless groups. Geertsma, Croes and Schwartz (3) have described this procedure and have derived scaling groups for waterflooding, hot waterflooding, and miscible displacement. The results of dimensional and inspectional analyses on the non-isothermal miscible displacement problem can be found in Appendix A.

The results of these analyses show that the problem cannot be scaled satisfactorily due to conflicting scaling criteria. The fluid flow and heat transfer groups demand that the model flow velocity and permeability be higher than the prototype values, but the dispersion scaling group demands that the term  $vd_p$  (flow rate  $\times$  particle diameter) be equal to the prototype value. Since the miscible displacement-heat transfer problem cannot be adequately modelled in the



laboratory, it is necessary to predict field performance by a numerical model.

The effect of different variables (velocity, permeability, temperature, viscosity) on the dispersion coefficient  $k_d$  is of interest to anyone who would like to predict the performance of a laboratory or field experiment. Miscible displacement experiments have been described by a number of investigators. Brigham, Reed and Dew(4) reported experiments in which the parameters velocity, length, particle size, viscosity ratio and core diameter were studied. They determined that:

1. At favourable viscosity ratios ( $M < 1$ ) the displacement was adequately described by a theoretical solution.
2. The dispersion coefficient  $k_d$  changed by a factor of 5.7 when the mobility ratio was changed by the same factor (from 0.175 to 0.998). This implied a linear relationship between mobility ratio and dispersion.
3. When the viscosity ratio became unfavourable, the theoretical error function curve could no longer describe the recovery profile.
4. Viscous fingering or bypassing of the displaced oil by solvent was evident at unfavourable mobility ratios.
5. At low rates of flow, the dispersion coefficient  $k_d$  was found to be independent of velocity.
6. At higher flow rates the dispersion coefficient was a function of velocity and of particle diameter.

These results form the basis of the equation  $k_d = D_0 + \sigma v d_p$ .

Pozzi and Blackwell(6) derived a set of scaling criteria for isothermal miscible displacement. Their experiments were performed primarily in the unfavourable mobility ratio region and were used to



validate the scaling criteria developed by inspectional analysis. The regions in which these scaling criteria are valid were also defined.

Blackwell(5) reported an experimental study in which a dimensionless dispersion number  $k_d/D_0$  was plotted against a dimensionless velocity group  $vd_p/D_0$ . From this plot the regions in which diffusion dominates ( $vd_p/D_0 < 0.4$ ), and in which convective mixing dominates ( $vd_p/D_0 > 4$ ) were determined.

Van der Pol(7) reported results which indicate that diffusion is the dominant mechanism under field conditions. He also reported that small core experiments in both the mixing-dominated range and the diffusion-dominated range produced results which agreed well with Blackwell's work. It was concluded that the dispersion coefficients determined in laboratory core models would make scaling of dispersion difficult or impossible in the laboratory.

Experiments on dispersion of thermal energy were reported by Green, Perry and Babcock(8). They presented a numerical solution to the heat transfer problem. This solution was a convection-diffusion equation and provided valid solutions as long as stable flow prevailed. Stable flow was maintained by injecting a chilled liquid in order to produce a favourable mobility ratio.

The calculations of thermal dispersion by Green et al(8) show that thermal diffusion may occur through two mechanisms. At low rates, conduction predominates and the static conductivity of the system is the effective diffusion rate. A plot of  $vd_p$  vs  $k_h$  indicated that at higher rates dispersion begins to dominate the heat transfer process. This transition occurs at  $vd_p/k_h = 0.005 \frac{\text{cm}^3 \text{ C}}{\text{J}}$ . At



rates below the value of  $vd_p/k_h = 0.0025$ , the heat transfer coefficient  $k_h$  may be represented by a constant. At higher rates, the conduction coefficient will include a velocity dependent term.

Perkins and Johnston(9) reviewed a number of papers on dispersion and miscible displacement, and covered the topics discussed above. They also discussed the effect of an immobile gas saturation on dispersion coefficients.

In order to test the validity of the equations and coefficients used to describe the miscible displacement process, it is necessary to solve these equations using finite difference techniques. A number of authors (10, 11, 12, 13) have presented techniques for dealing with the equations describing the heat and mass transfer. Peaceman and Rachford(10) used a combined backward and central difference approximation and solved the resulting equations by an iterative technique using an implicit difference formulation. Their solution also included a pressure solution for two-dimensional isothermal incompressible flow.

Chaudhari(11) discussed some of the limitations of Peaceman and Rachford's method and suggested a scheme which would eliminate most of the errors inherent in this technique. Chaudhari used an explicit finite difference technique in which the numerical error was cancelled.

Laumbach(12) presented a high-accuracy, semi-implicit technique known as the Truncation Cancellation Procedure. This method uses a system of equations at three spatial levels and two time levels which gives rise to a tridiagonal matrix. The results presented for this solution system indicate that good results may be obtained even when a small number of points are used. A further advantage of this method is that it is stable for large  $\Delta t$  values. This procedure was used by



Awang(13) to simulate one-dimensional heat and mass transfer in a porous medium.

Awang performed several heated injection miscible displacements in order to examine non-isothermal dispersion. A numerical simulation of the convection-diffusion equation for both heat and mass transfer was performed. The results of these experiments showed that a dispersion coefficient as a function of  $vd_p$  only could not be used to model a heated miscible displacement. The results also indicated that the local viscosity ratio was not constant throughout the experiment and was a function of fluid composition and temperature. The dispersion obtained in these experiments was found to be temperature sensitive, as it varied with the thermal gradient in the pack. The results of this work combined with the results of Brigham, Reed and Dew(4) suggest that the thermal gradient in the pack may produce a viscosity ratio variation which influences the local dispersion coefficient  $k_d$ .

Leventhal(14) described a fourth degree accurate procedure known as the Operator Compact Implicit (OCI) method. This method achieves high accuracy without resorting to the large number of points required to solve each equation by standard fourth degree implicit systems. In the OCI system the operators defining the function at the  $i-1$  node, the  $i$  node, and the  $i+1$  node are generated using only these three points rather than the five points normally required for a fourth degree one-dimensional system. Solutions to the Buckley-Leverett displacement problem were presented, which demonstrated a solution which is more accurate than the solutions obtained by a conventional finite difference method or by the Galerkin method.

Miller(24) has discussed extensively the effect of condensation



fronts and thermal fronts on the stability of a moving fluid interface in a porous medium. His work on the stability of a steam front involved the derivation of a stability criterion in which he assumed a displacement front which contained a small wave-like perturbation. The regions in which the perturbation would grow, decay or remain constant were then delineated by a summation of the forces tending to cause instability or to damp the perturbation. Miller concluded that a decrease in volume of fluids at a condensation front or a thermal front would tend to favour the stability of the front. He presented the example of a steam front, which would remain stable in spite of the unfavourable viscosity ratio between water and steam. His analysis also considered the effect of the heat released by condensation on the stability of a thermal front.

Miller(23) also examined the stability of moving interfaces due to phase transformation or mass transfer. The effect of interfacial tension on interface stability was examined and it was found that interfacial tension had a stabilizing effect in most systems.

Miller and Jain(22) described the stability criterion for another type of system consisting of the vaporization or condensation of a dilute fog. They determined that the gain or loss of volume due to the thermal energy absorbed or released by the process was the factor which stabilized or destabilized the process.



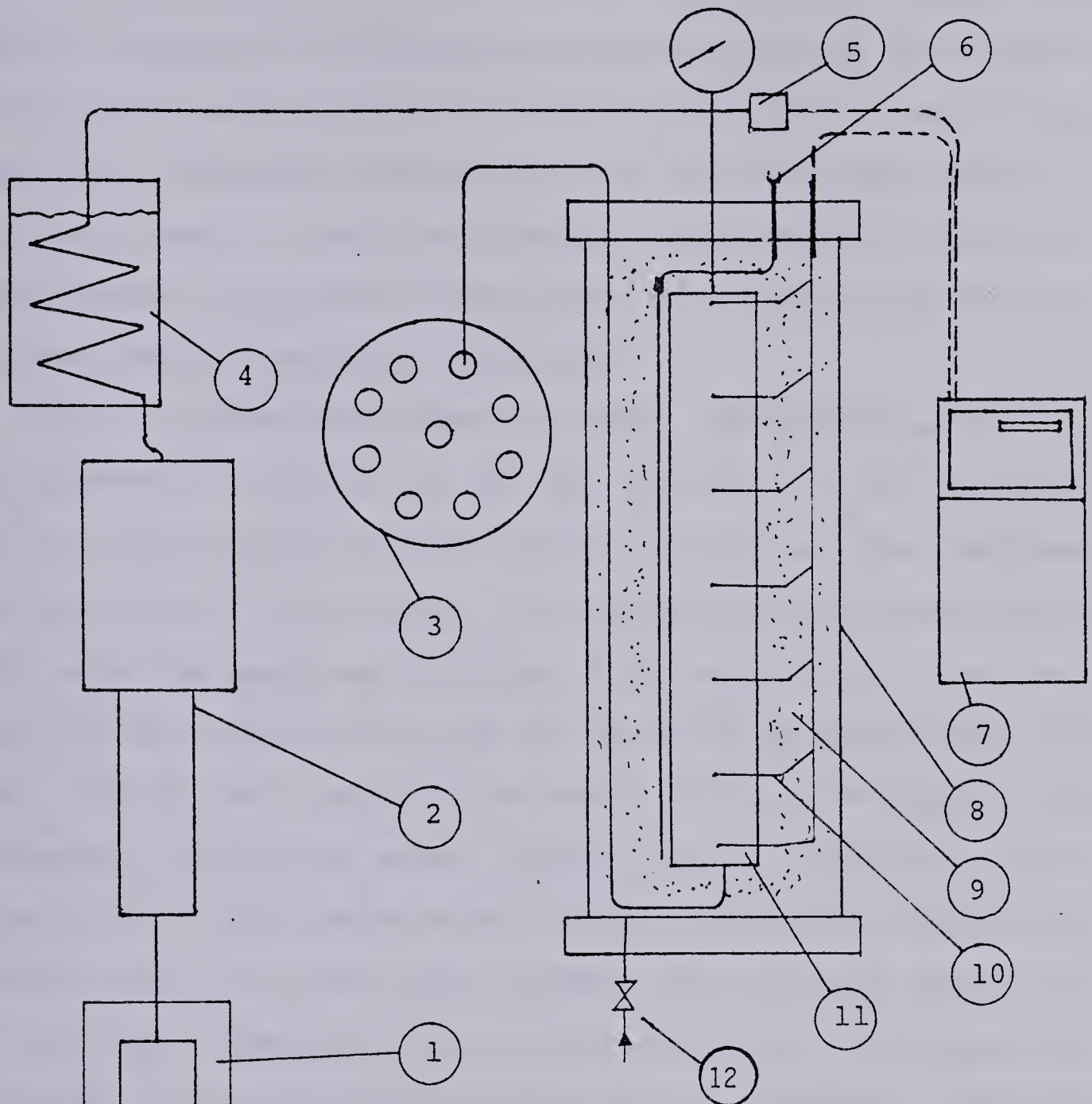
## II. EXPERIMENTAL APPARATUS AND PROCEDURE

The apparatus, as illustrated in Figure 1, was similar to that employed by Awang(13) and by Brigham et al.(4) Modifications specific to this project are:

1. A 4:1 flow multiplying cylinder is used in the system in order to provide flow rates beyond those available from a Ruska pump.
2. The insulated core assembly is enclosed in a pressure vessel in order to allow for the use of a confining overburden pressure during tests at high injection pressures. This modification allows for the operation of the system at high temperatures (above the oil bubble point) or at low temperatures (where high fluid viscosities produce high pressure drops). The arrangement had the advantage of allowing for the use of a positive net overburden on the core at all times. The overburden could be increased as required to prevent internal pressure from expanding the sleeve and thereby changing the packing within the core. This possibility was considered to be more serious than the changes in permeability caused by overburden pressure variations.
3. The core sleeve is fabricated from 0.010" (0.25 mm) stainless steel in order to provide a sleeve wall with a low thermal conductivity and to produce a durable core assembly. Appendix D contains heat transfer calculations considered in the design of this sleeve system.
4. The sleeve is provided with fittings through which six thermocouples are inserted.
5. The core assembly was mounted vertically and fluids were displaced downwards so that gravity would favour the stability of the fluid fronts.



Figure 1 Schematic of Experimental Apparatus



Clockwise from lower right:

1. Ruska pump
2. 4:1 displacing cylinder
3. Sample collector
4. Constant temperature bath
5. Pressure transducer
6. Electric heater plug
7. Data logger
8. Pressure vessel
9. Insulation
10. Thermocouple
11. Core assembly
12.  $N_2$  overburden supply



The core assembly is 7.93 cm in diameter and 78.7 cm long. The sleeve is packed with 80-120  $\mu\text{m}$  (20-30 mesh) or 20-30  $\mu\text{m}$  (80-120 mesh) Ottawa silica sand by means of a particle distributor as described by Wygal(20). This packing technique consists in slowly adding sand to a dry core by means of a particle distributor consisting of five layers of coarse screens. The filled core was sealed with an end cap and the core was ready for leak testing and insulation.

Prior to running displacement experiments, the porosity of the core was determined by weighing the core dry, evacuating it, and saturating the core with deaerated distilled water. The core was then reweighed and the volumes of sand and water were calculated assuming densities of  $2.645 \text{ gm/cm}^3$  for quartz and  $0.9983 \text{ gm/cm}^3$  for water at  $25^\circ\text{C}$ . The final porosities were found to be 0.328 for the 80-120  $\mu\text{m}$  (20-30 mesh) sand pack, 0.368 for pack 2 and 0.356 for pack 3 (20-30  $\mu\text{m}$  sand packs). The differences in porosities suggest that the particle distributor is more effective with large size particles. This was confirmed by packing some practice cores. The cores were reweighed after drying to ensure that all water was removed prior to saturating with oil. The cores were insulated, placed in the pressure vessel and evacuated before saturating with oil.

The hydrocarbons used in these experiments were a group of commercially available oils, the Gulf Harmony series of hydraulic oils. These oils ranged in viscosity from 25. mPa·s to 256. mPa·s at  $40^\circ\text{C}$ . Varsol was used where a viscosity of 1. mPa·s was desired. A complete summary of oil properties appears in Table 1.

The experiments were carried out as follows: The core was saturated with the oil to be used as the displaced fluid by injecting



Table 1  
Properties of Oils Used

Oil	Kinematic Viscosity at 40°C mm <sup>2</sup> /s(cs)	Density at 40°C gm/cm <sup>3</sup>	Kinematic Viscosity at 100°C mm <sup>2</sup> /s(cs)	Density at 100°C gm/cm <sup>3</sup>	Refractive Index at 25°C
Harmony 44	30.48	0.847	5.28	0.803	1.4696
Harmony 53	65.3	0.857	8.71	0.818	1.4759
Harmony 87	210.3	0.868	19.12	0.832	1.4816
Harmony 111	302.5	0.875	24.95	0.841	1.4891
Varsol	1.	0.767	-	-	1.4400

Note: Viscosity values are manufacturer's data. Density values are measurements made on a Haake densitometer.



this oil at  $v = .02$  cm/s until the refractive index of the effluent matched that of the injected oil. Velocity is defined as flow rate/core cross section. This displacement required a minimum of three pore volumes when the fluid initially in place was more viscous than the injected fluid. The displacing cylinder was then loaded with the second oil used. The constant temperature bath was adjusted to the desired injection temperature and injection was started.

Effluent samples were taken at one minute intervals for favourable mobility experiments and at three minute intervals for unfavourable mobility runs. Sampling was done at proportionately longer or shorter intervals for higher or lower rate displacements to maintain a sampling interval of one percent pore volume for favourable mobility tests. Sampling was continued until 1.25 pore volumes were displaced in the favourable mobility ratio experiments and until 1.5 pore volumes for the unfavourable mobility ratio experiments. Heated injection fluid or chilled injection fluid experiments were run to three pore volumes in order to log temperature profiles for the pack.

The composition of the effluent was determined by refractive index measurements. Concentration values as a percentage of displacing fluid were obtained from a calibration curve of refractive index vs concentration (Appendix F).

A total of 36 tests were performed. Of these, 17 runs were carried out on a 80-120  $\mu\text{m}$  sand pack and 19 runs on 20-30  $\mu\text{m}$  sand packs. Four of the tests in the 80-120  $\mu\text{m}$  pack were repeat experiments. The tests in the coarse pack included experiments at four favourable and two unfavourable mobility ratios. Also included were three tests with a heated displacing fluid and one test with chilled displacing fluid. One



test at a low flow rate was also performed.

The 20-30  $\mu\text{m}$  packs were used for experiments at six favourable and one unfavourable viscosity ratio. These experiments include seven heated injection displacements and one chilled injection displacement. One low rate and one very low rate experiment were included. A set of three displacements in a water-wet pack was also performed.



### III. DISCUSSION OF RESULTS

#### A. Experimental Data

The concentration of displacing fluid in the effluent from all experiments was plotted vs time on linear axes to yield smooth curves which characterize the miscible displacement process at a favourable mobility ratio. These plots closely resemble the error function solution described by Brigham(21) for the miscible displacement problem. Several such plots are shown. Figures 2, 3 and 4 illustrate the displacement curves obtained from an isothermal experiment, a heated injection displacement and an isothermal displacement at a lower velocity, respectively. The corresponding numerical solutions are also shown. Note that the curves are plotted using a cubic spline to fit the data points.

In order to determine the dispersion coefficients for each experiment, the concentration data was plotted as concentration vs a pore volume number  $\frac{V-V_p}{\sqrt{V}}$  on probability paper (Appendix F). Volume displaced at a given time is  $V$  and  $V_p$  is the fluid contained in one pore volume. The slope of the resulting straight line was used to calculate the dispersion coefficient  $k_d$  and a mixing coefficient for each experiment.  $(k_d = \frac{(V_{90}-V_{10})^2}{3.625} \frac{V}{\phi})$ . The pore volume number at 90% concentration is  $V_{90}$  and  $V_{10}$  is the pore volume number at 10% concentration.

The displacements carried out at unfavourable mobility ratios were also plotted on linear axes. These plots did not produce a smooth curve, and exhibited early breakthrough and an irregular profile characteristic of viscous fingering, (Figure 5). When the data from these experiments were plotted on probability paper, the resulting



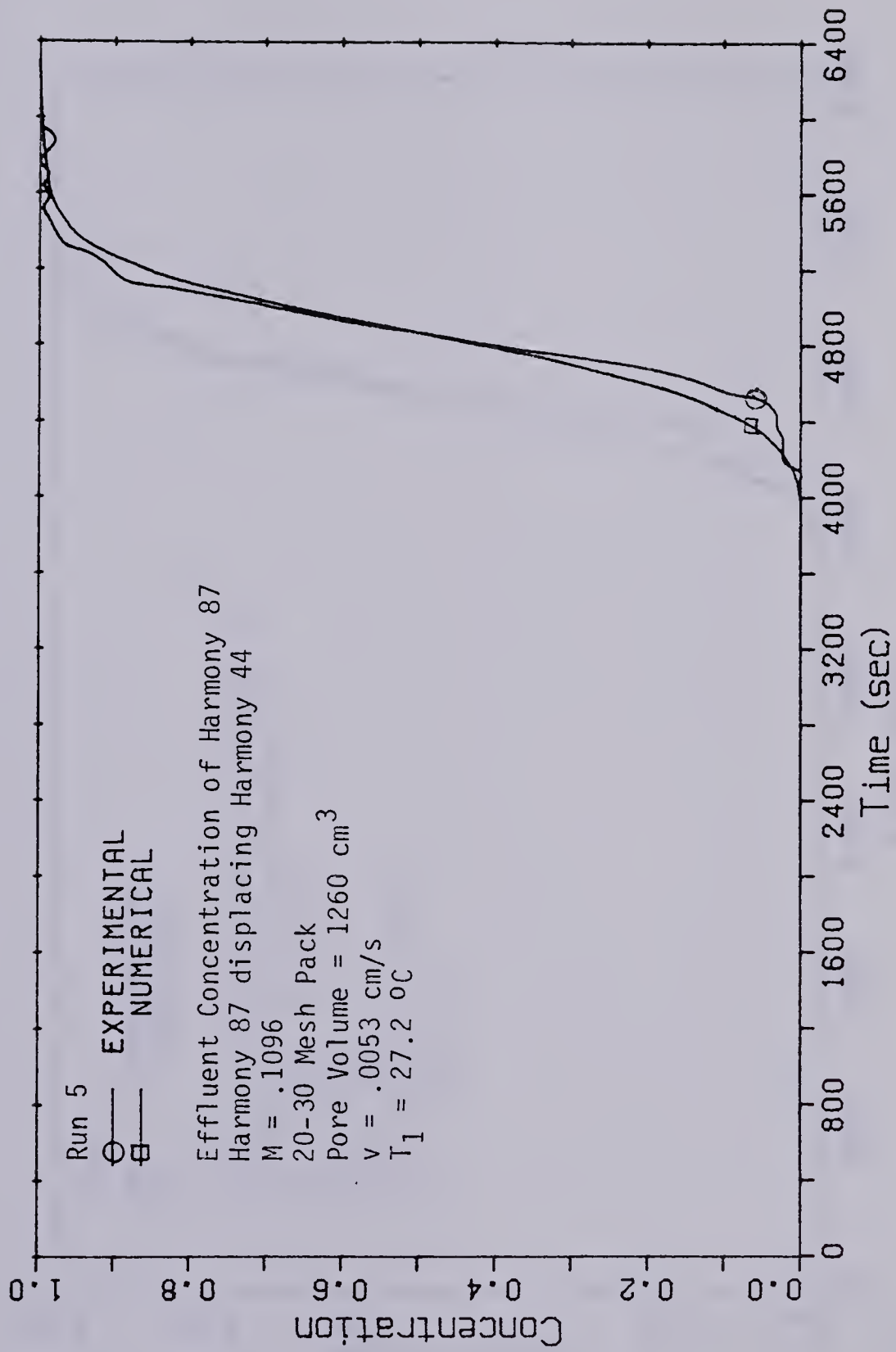


Figure 2 NUMERICAL SOLUTION FOR R5



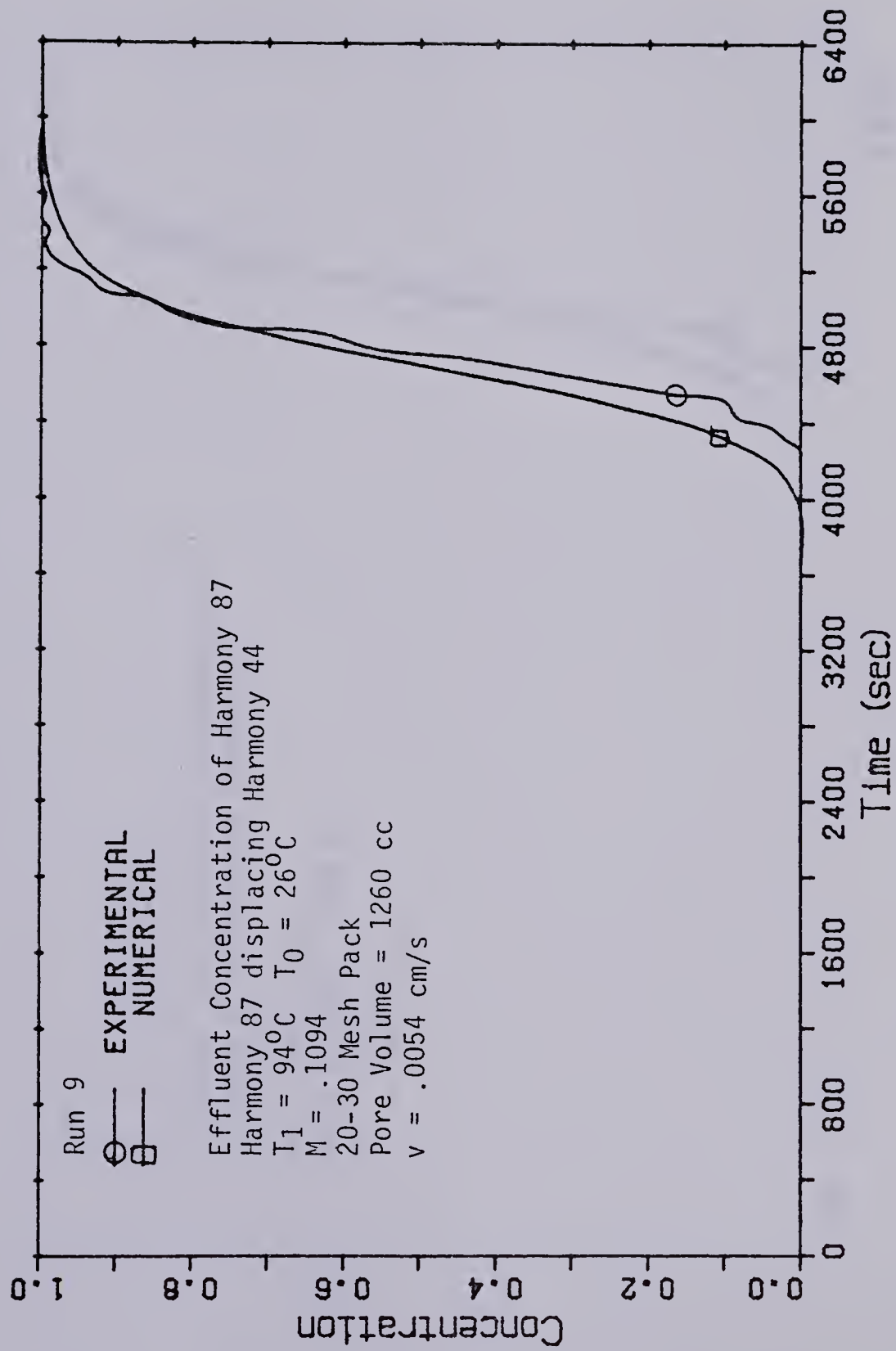


Figure 3 NUMERICAL SOLUTION FOR R9



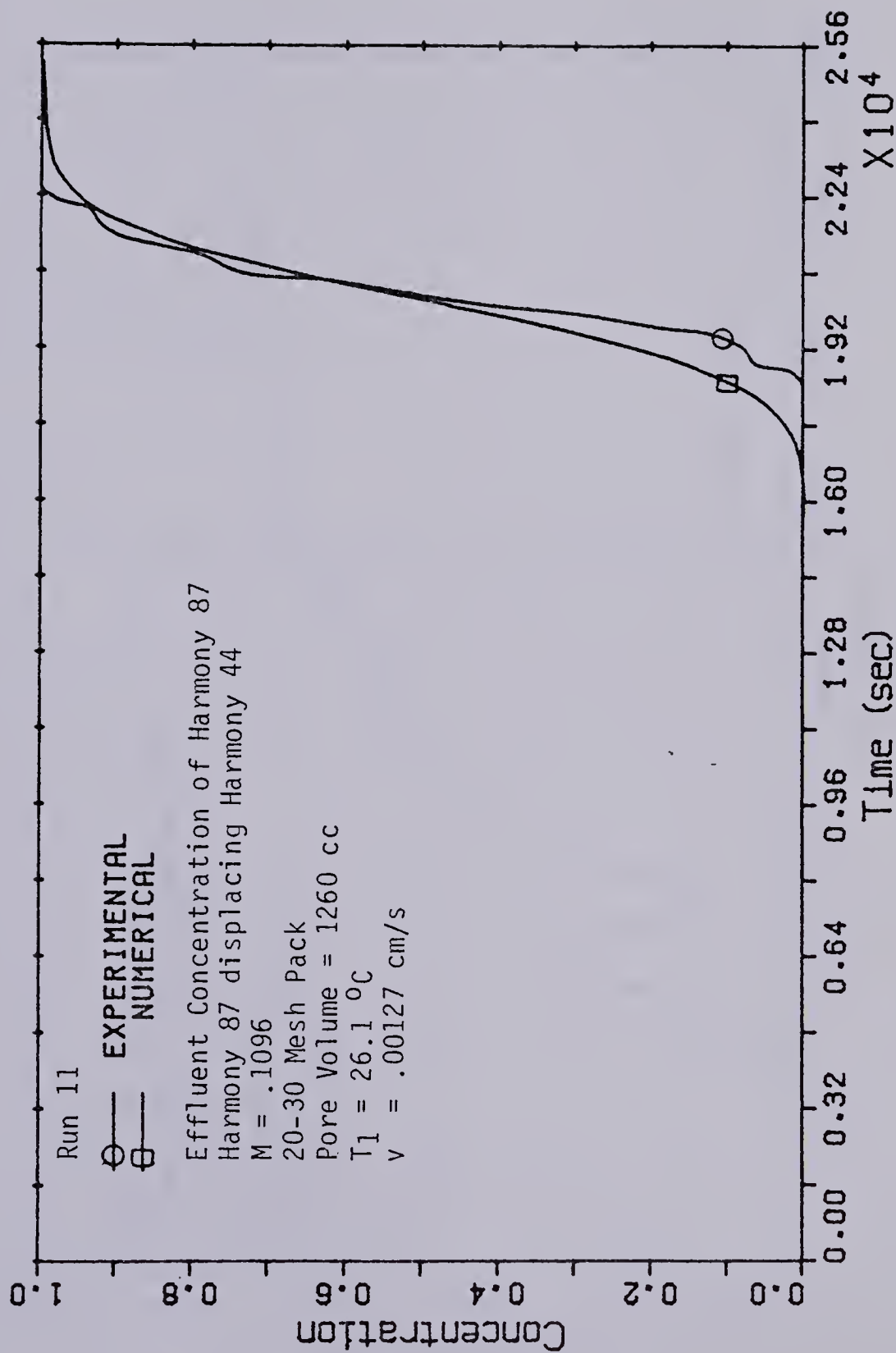


Figure 4 NUMERICAL SOLUTION FOR R11



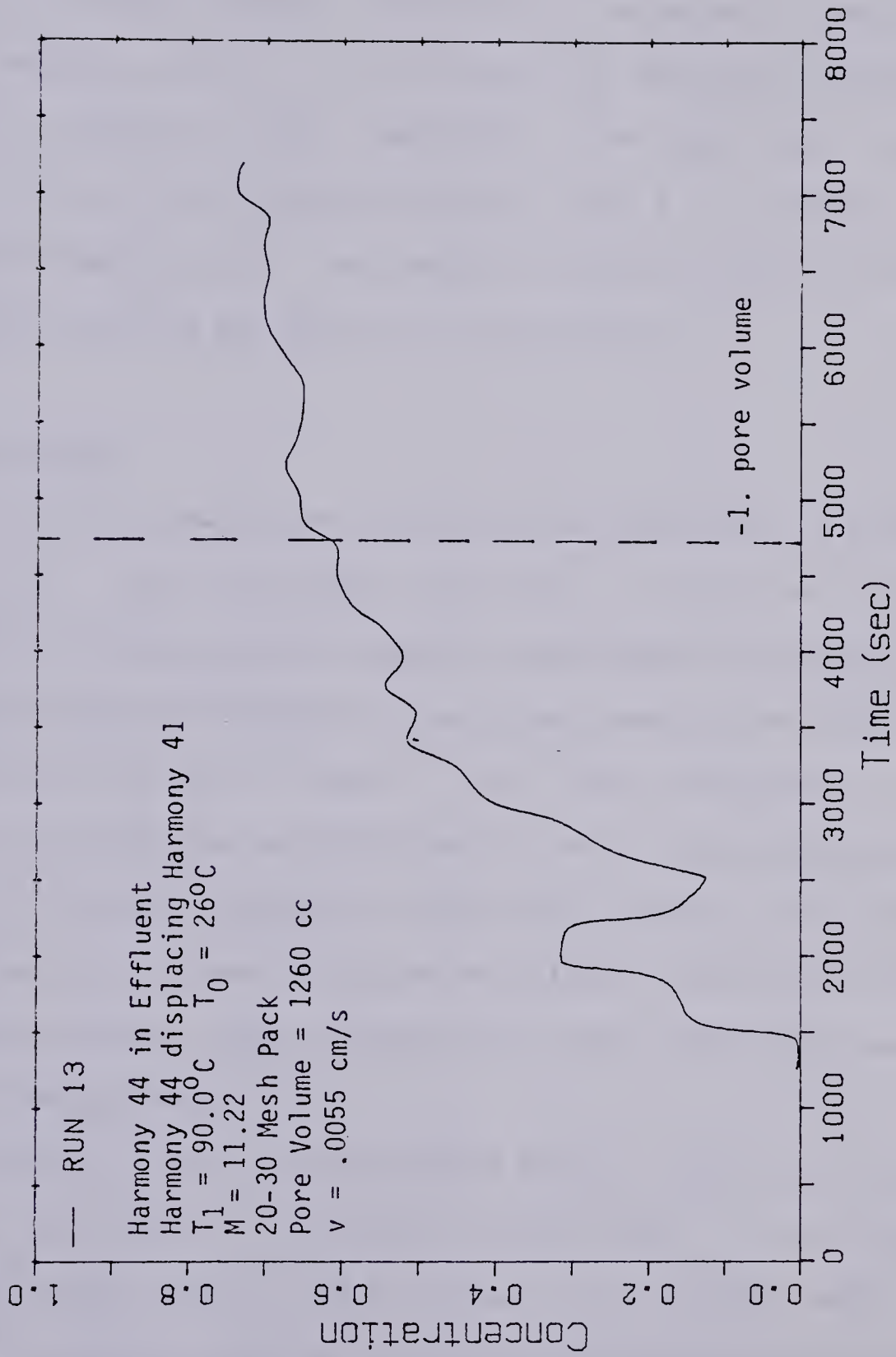


Figure 5 UNFAVOURABLE MOBILITY DISPLACEMENT, R13



values of  $k_d$  and  $\sigma$  were found to be very large and should be considered to be the averaged results for viscous fingering and not as the result of dispersion at a stable front.

The  $k_d$  values or their dimensionless counterpart  $\sigma$  were plotted (i) vs velocity and (ii) vs inlet mobility ratio to illustrate the effects of velocity, inlet temperature, sand pack size and inlet mobility ratio on the dispersion process. Table 2 is a complete summary of the experimental data. Breakthrough is defined as the earliest time that displacing fluid was detected in the effluent.

### Velocity Effects

The effect of velocity on the dispersion coefficient is illustrated in Figure 6. The displacement experiments at three velocities are represented in this plot of dispersion coefficient vs velocity. The dispersion coefficient appears to be proportional to the velocity for the 20-30 and 80-120  $\mu\text{m}$  packs. This linear relationship between velocity and dispersion was discussed by Perkins and Johnston(9). The plot also illustrated an effect of grain size on mixing. This effect is probably due to a decrease in packing efficiency in the 20-30  $\mu\text{m}$  pack as discussed by Brigham, Reed and Dew(4) who noted that finer sand packs were less homogeneous.

The dispersion plot was extrapolated to zero velocity to obtain the diffusion coefficient for the 20-30  $\mu\text{m}$  sand pack. For Harmony 87 displacing Harmony 44 in a 20-30  $\mu\text{m}$  pack,  $D_0 = 0.00005 \text{ cm}^2/\text{s}$ . This value is in agreement with the diffusion coefficient obtained by using the diffusion formula found in (15), p.574,  $D_0 = A\mu^{-.5}$ , where A is the reference diffusivity for a viscosity of one cp. This diffusion is



Table 2  
Experimental Data

Run	T <sub>i</sub> (°C)	Inlet M	k <sub>d</sub> (cm <sup>2</sup> /s)	pore vol at brkthru	σ	v (cm/s)	Comments
			Pack 1				80-120 μm
1	27.4	0.089	0.0013	0.89	0.84	.0052	(F) favourable
2	23.5	11.2	1.09		167.	.0215	(U) unfavourable
3	92.0	0.089	0.00136	0.87	0.86	.0052	F heated run
4	25.6	11.22	0.267	0.29	167.	.0052	U
5	27.2	0.110	0.00165	0.86	1.02	.0053	F 87 disp. 44
6	26.7	0.708	0.00188	0.85	1.30	.0048	F 111 disp. 87
7	27.5	708.0	2.28	0.15	1380	.0054	U
8	28.2	0.0014	0.0072	0.95	0.46	.0054	F
9	94.0	0.110	0.0014	0.91	0.87	.0054	F heated
10	96.0	0.708	0.00226	0.94	1.38	.0054	F heated
11	26.1	0.110	0.00032	0.92	0.81	.00127	F low rate
12	19.5	0.708	0.0015	0.91	0.93	.00538	F chilled run
13	90.0	11.2	0.84	0.34	507.	.00547	U heated
14	26.7	0.110	0.00134	0.91	0.800	.00550	F repeat of 5
15	28.0	0.708	0.00284	0.84	1.71	.0054	F repeat of 6
16	27.8	0.089	0.00132	0.90	0.81	.0054	F repeat of 1
17	27.2	0.708	0.00214	0.91	1.34	.0052	F repeat of 6
			Pack 2				20-30 μm
18	26.8	0.110	0.000454	0.94	1.27	.0052	F
19	25.3	0.708	0.00079	0.90	2.32	.0049	F
20	24.4	11.22	0.180	0.41	518.	.0050	U
21	91.5	0.110	0.000539	0.95	1.41	.0055	F heated
22	92.4	0.708	0.00139	0.90	3.66	.0055	F heated
23	89.0	11.2	0.249	0.35	652.	.0055	U heated
24	26.9	0.110	0.000408	0.92	1.19	.0050	F chilled
25	30.0	0.110	0.000183	0.92	2.35	.0011	F low rate
26	29.3	0.110	0.000053	0.94	2.16	.00035	F very low rate
			Pack 3				20-30 μm
27	29.2	0.110	0.00092	0.93	2.14	.0062	F water wet
28	27.5	0.708	0.00163	0.92	3.96	.0061	F water wet
29	27.8	11.22	0.21	0.38	498.	.0061	U water wet
30	92.0	0.028	0.00072	0.92	1.76	.0057	F heated
31	25.8	0.116	0.00055	0.93	1.42	.0054	F repeat of 18
32	27.5	0.708	0.00118	0.92	3.18	.0053	F repeat of 19
33	86.4	0.089	0.00054	0.94	1.40	.0054	F
34	92.5	0.375	0.00072	0.93	1.78	.0056	F 53 disp. 44
35	89.2	0.290	0.00050	0.94	1.28	.0053	F 87 disp. 53
36	91.5	0.028	0.00046	0.91	1.14	.0057	F heated



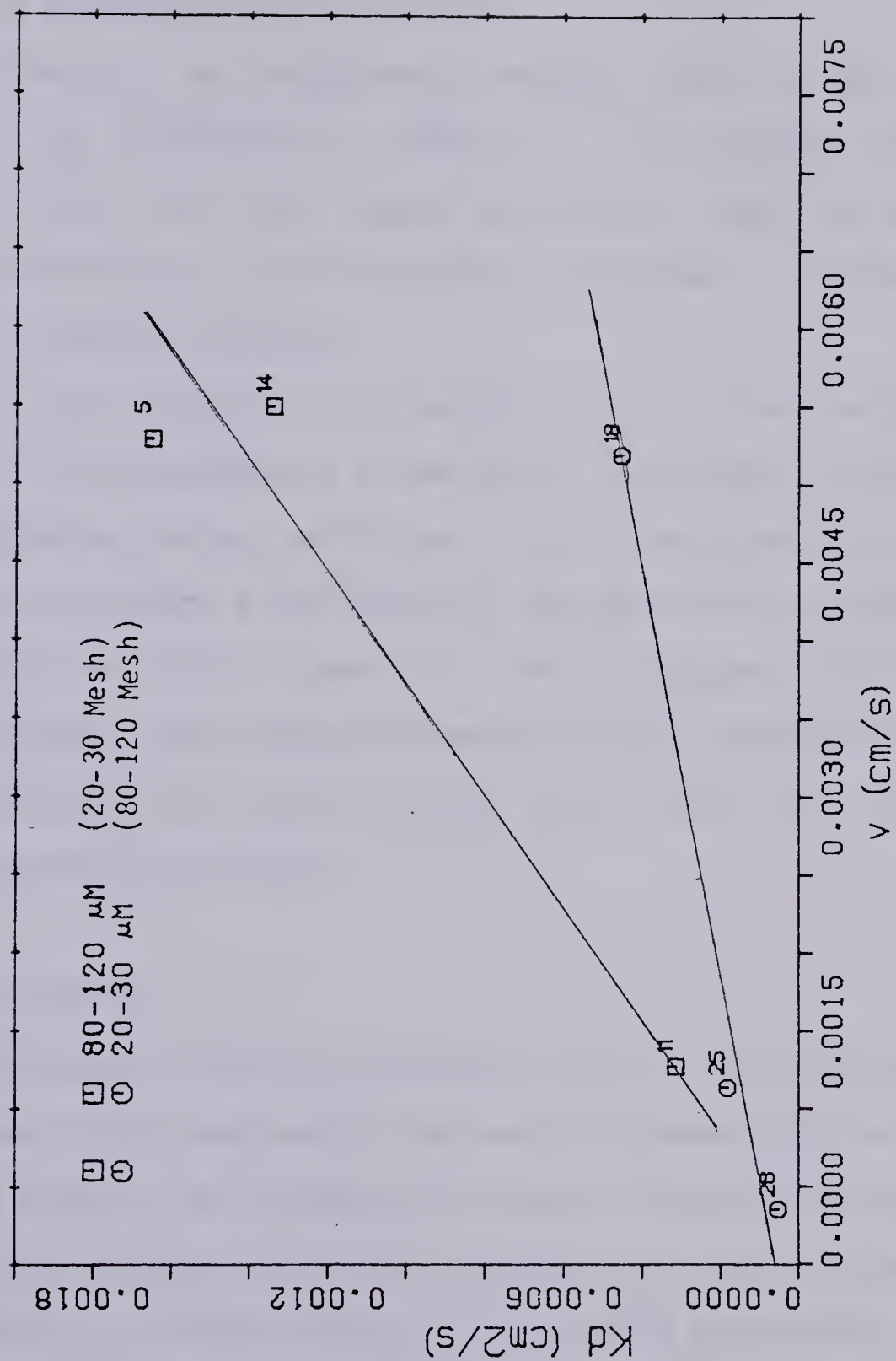


Figure 6 Effect of Velocity on Dispersion



too small to have an effect on mixing at experimental flow rates.

### Mixing at an Unfavourable Viscosity Ratio

The effect of an unfavourable mobility ratio on the mixing coefficient is illustrated in Figure 7. The heated injection experiments tests (13, 23) display more mixing than the matching isothermal tests (4, 20). Here the mixing coefficient  $\sigma$  is defined as a dimensionless number ( $\sigma = k_d / v d_p$ ).

Perkins and Johnston(9) have defined  $\sigma$  as  $k_d = \sigma v d_p$  where  $\sigma$  is a measure of the inhomogeneity of the pack. In this work  $\sigma$  is defined as a dimensionless mixing coefficient. All of the unfavourable ratio displacements exhibited a high degree of mixing and early breakthrough of the displacing fluid (Figure 5). These characteristics suggest viscous fingering. The unfavourable mobility ratio experiments using a heated displacing fluid exhibited higher mixing coefficients than the matching isothermal experiments.

### Dispersion at $M=1.0$

In the region of favourable mobility ratios, a set of experiments was performed in both sand packs. The results of these tests are plotted in Figure 8 to illustrate the trend of increasing mixing as mobility ratio increased. The lines through the two sets of points may be extrapolated to provide estimates of the mixing coefficients as the mobility ratio approaches unity. This extrapolation yields a value of  $\sigma=2.5$  for the mixing coefficient in the 20-30  $\mu\text{m}$  pack and  $\sigma=1.5$  for the 80-120  $\mu\text{m}$  pack. These values are of the same magnitude as the value of 1.75 for sand packs suggested by Blackwell(5). The increase of  $\sigma$  with



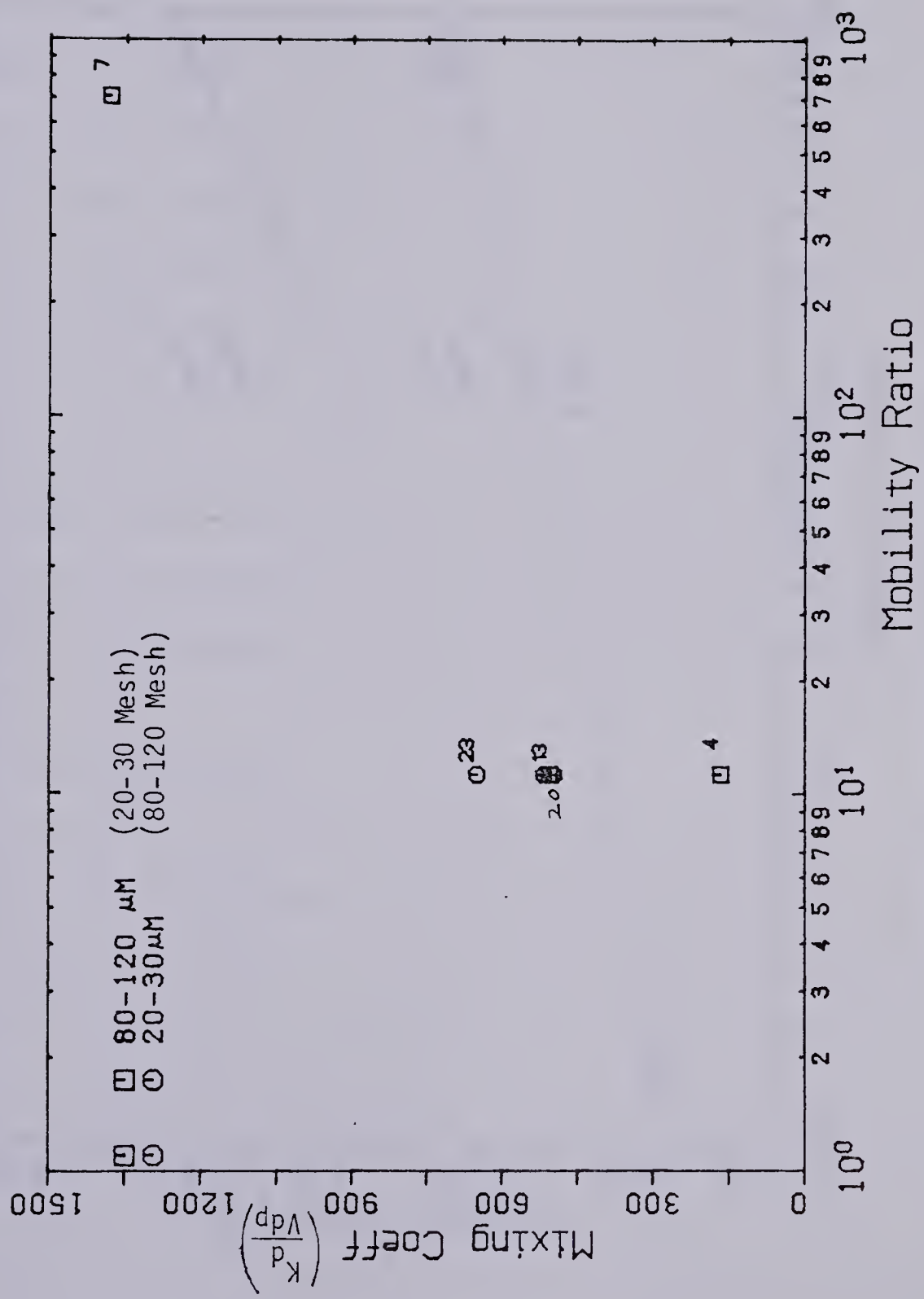


Figure 7 Mixing Coefficients at Unfavourable Mobility Ratio



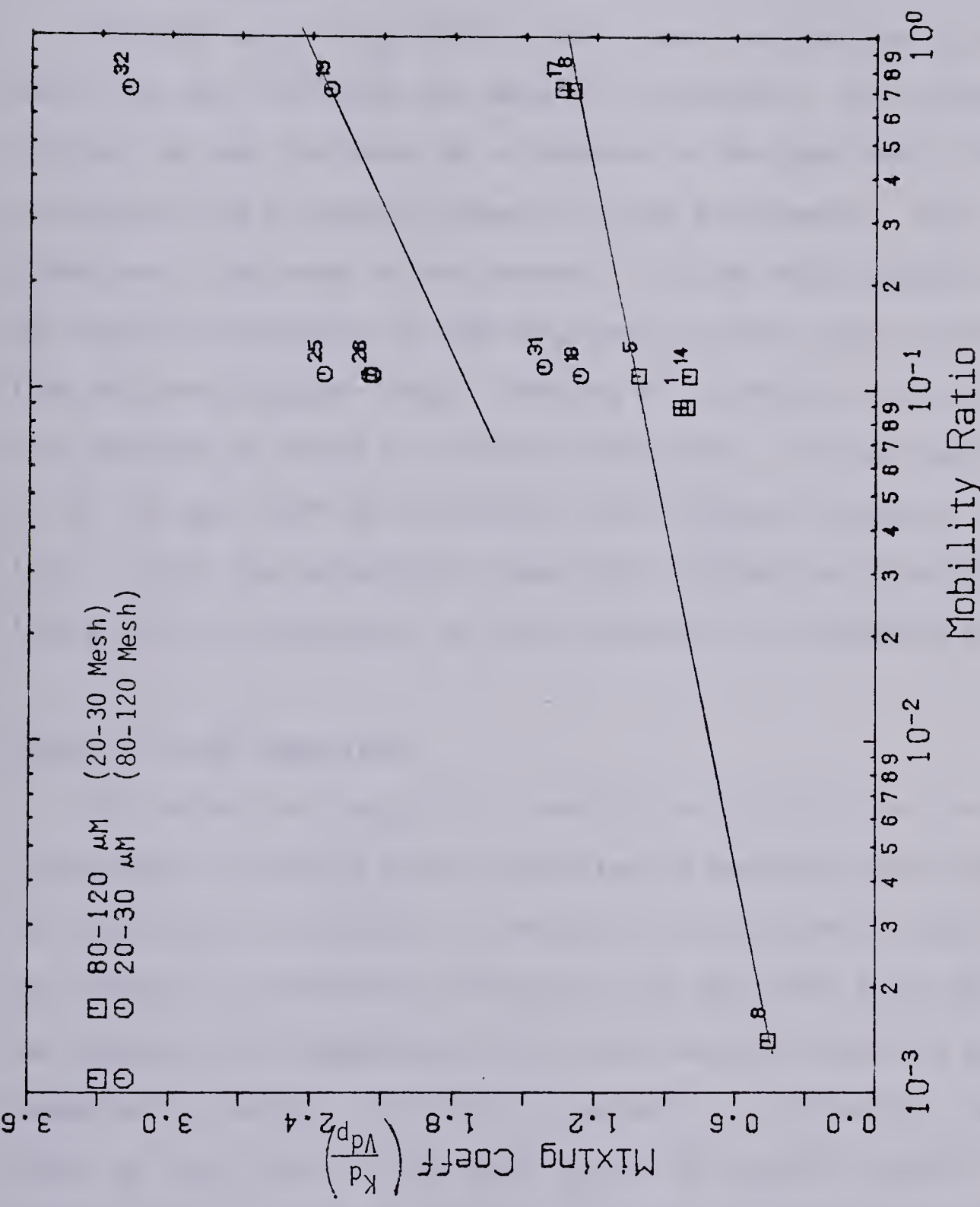


Figure 8 Isothermal Displacement Data



decreasing particle size agrees with the results discussed by Perkins and Johnston(9) who noted that pack inhomogeneity tends to increase as particle size is reduced.

The 20-30  $\mu\text{m}$  pack was found to have a small residual gas saturation which may have increased the amount of dispersion. The presence of residual gas was indicated by a decrease in the pack pore volume as calculated from a material balance on some experiments. This volume change was of the order of four percent. This gas would dissolve in the oil during displacements at high pressure, and would cause the effluent from the core to appear cloudy. Reducing the overburden pressure on the core appeared to reduce or eliminate the problem. The gas was assumed to be nitrogen from the overburden which entered through a fitting leak. Perkins and Johnston(9) noted that a residual gas saturation had little effect on dispersion, so this problem was not considered serious.

### Effect of Inlet Temperature

The effect of heating or cooling the inlet fluid was also investigated. A plot of mixing coefficient vs mobility ratio (Figure 9) for sand pack 2 illustrates an increase in mixing when a heated fluid was injected. A decrease in mixing was also noted when a chilled fluid was injected. The magnitude of this effect was quite small in spite of temperature gradients sufficient to produce an unfavourable mobility ratio at the inlet to the core during the heated injection fluid displacements. Similar behaviour was noted in sandpack 1. The heated injection tests in sand pack 3 did not appear to have an increased dispersion, possibly because the removal of residual water was not completely successful.



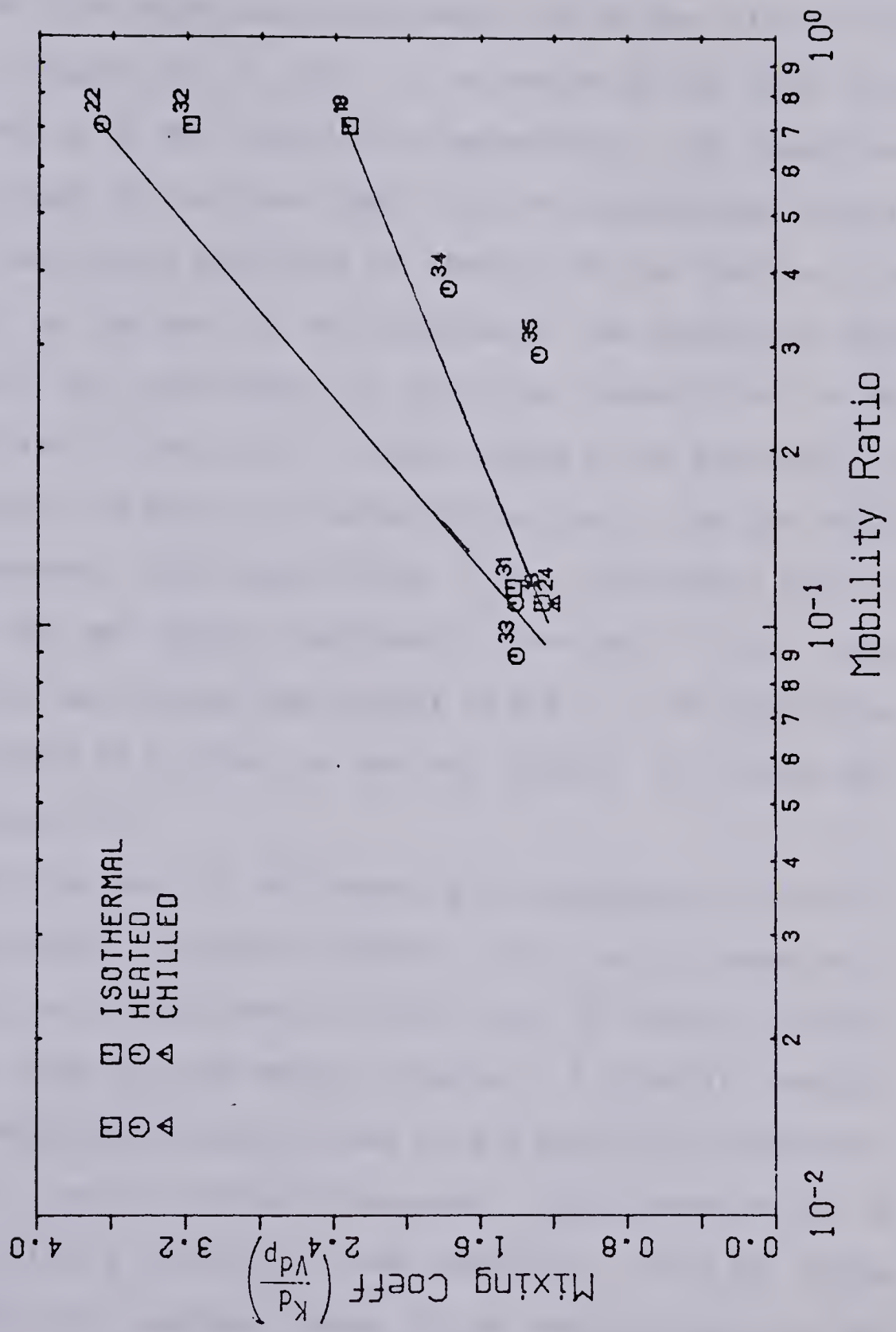


Figure 9 Effect of Inlet Temperature on Dispersion



## Movement of Thermal Front

The temperature profiles at several points in the core were plotted for some of the high temperature displacements and for one chilled fluid displacement, (Figures 10, 11, 12).  $T_i$  is defined as the inlet fluid temperature and  $T_0$  as the initial core temperature. The temperature front moves through the core more slowly than the concentration front as may be seen from Figure 3 and Figure 10. Because the two fronts will be coincident only at the start of the displacement, the temperature front can only affect the displacement by initiating instabilities in the concentration front at this time. At later stages of the experiment the thermal front will lag behind the concentration front so the two fronts will be independent. The thermal front in the unfavourable mobility displacements did not differ significantly from that in the stable displacements as may be seen from Figures 10 and 11. The jogs in the curves were thought to be errors in the data logging. All curves were plotted by a spine fit.

A stability analysis of the thermal and concentration fronts was carried out by Miller's stability criterion. The results appearing in Appendix E confirm the experimental evidence that the thermal front was stable in the range of experiments conducted. A stability analysis of the concentration front was performed using a stability criterion for a miscible front moving vertically downwards. This criterion may be obtained from Miller's criterion or from Chuoke(26). Since the fluids used were completely miscible, there is no capillary term in the stability number. The resulting equation implies that sand pack diameter is not a factor in the stability criterion. This is not true for the case where capillary forces are present. The only



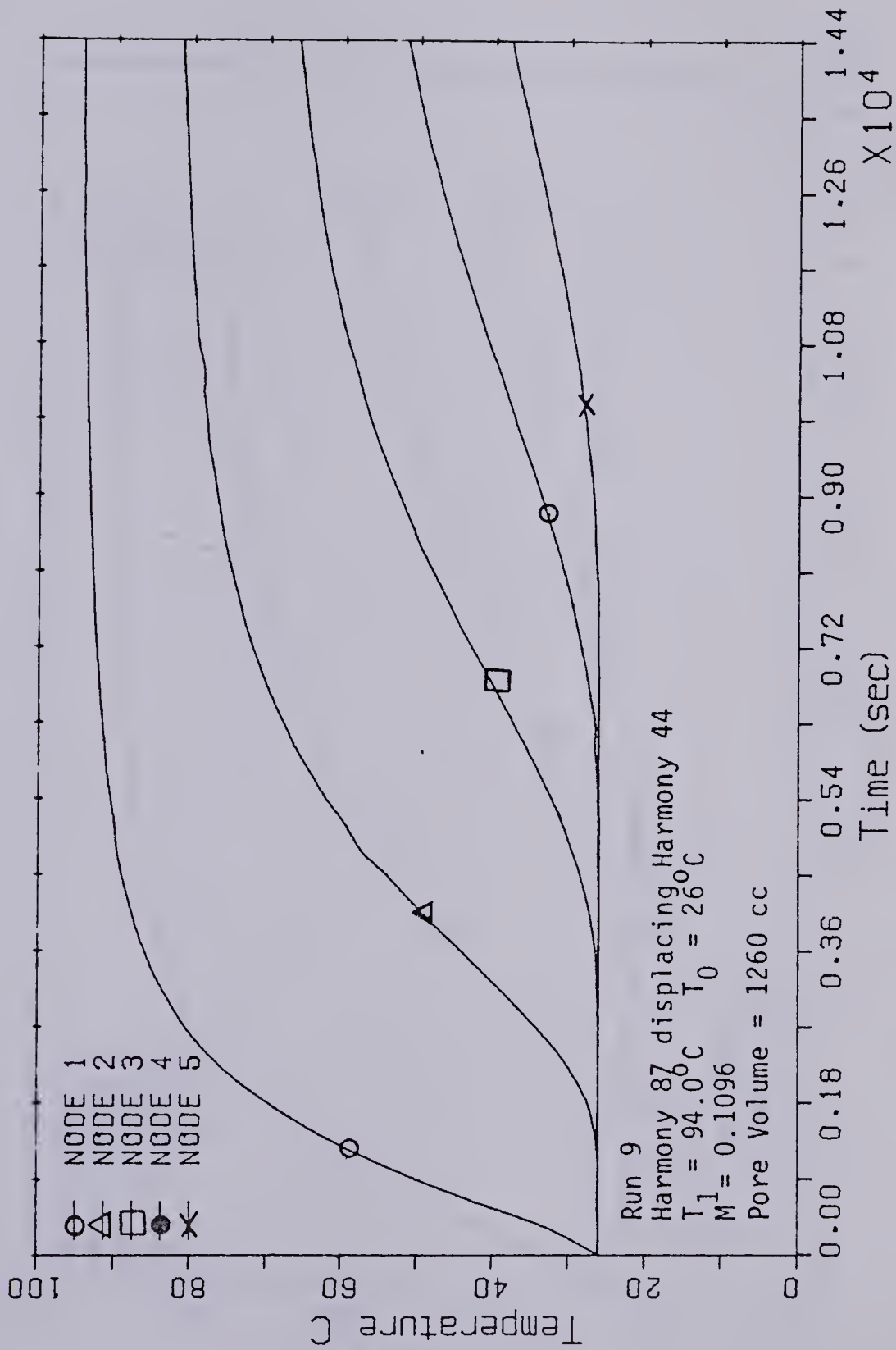


Figure 10 EXPERIMENTAL TEMPERATURE PROFILES, R9



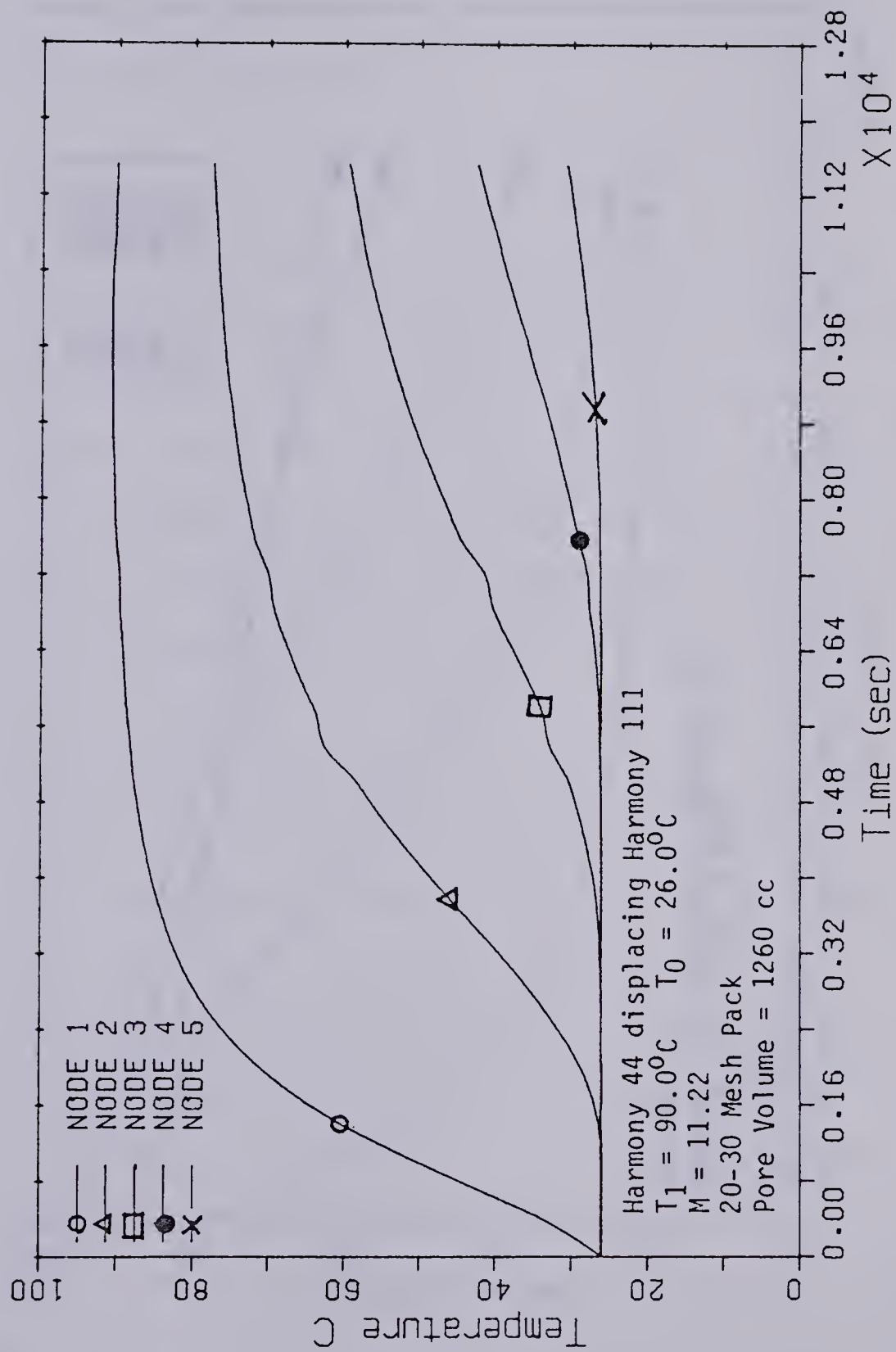


Figure 11 EXPERIMENTAL TEMPERATURE PROFILES, R13



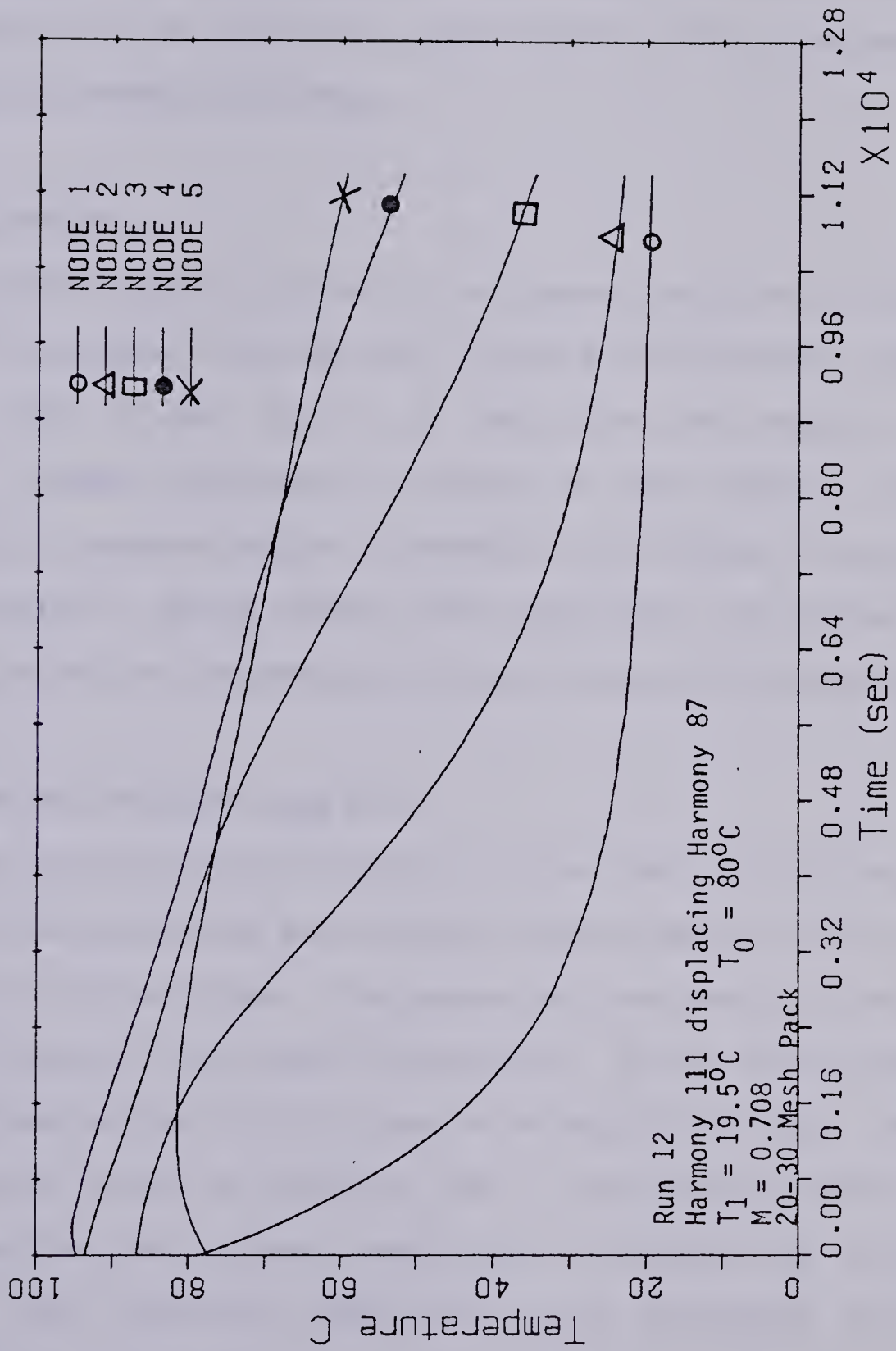


Figure 12 EXPERIMENTAL TEMPERATURE PROFILES, R12



stabilizing force in the experimental system was gravity, and the gravitational force was calculated to be much smaller than the viscous forces present at the experimental flow rates. This was confirmed experimentally by the finding of instabilities in all the unfavourable mobility displacements performed.

### Pressure Profiles

Favourable mobility isothermal displacements exhibited a continuous increase of pressure with time until the core was completely saturated with the more viscous fluid. At this point the pressure became constant. Heated displacements displayed the same pressure increase, followed by a pressure decline as movement of the thermal front reduced fluid viscosity. During chilled fluid injections, the pressure drop increased as the low temperature front moved through the sand pack.

### Dispersion in a Water-Wet Sand Pack

Three experiments were performed in a sand pack initially saturated with distilled water which was displaced from the pack by the oil to be used as the displaced phase. Displacement was continued until the water phase was reduced to an immobile saturation. The oil in the core was then displaced by the oil to be used as the displacing fluid. Effluent samples were taken at intervals and a displacement profile was calculated from the effluent compositions as measured by refractive index. The dispersion coefficients were calculated from the concentration vs time curves.

The experiments in water-wet sand packs produced results similar to those for single phase experiments. The dispersion was found to



increase as the mobility ratio became less favourable. At an unfavourable mobility ratio, early breakthrough and viscous fingering were observed. The displacement tests at favourable mobility ratios were found to have a higher dispersion than similar single phase oil displacements. The unfavourable mobility displacement was found to have a lower mixing coefficient than the matching displacement with no residual water saturation. It is possible that water mobilized by the high injection rates had an effect on this test. The results of tests in water packs 27-29 agree with the results of Kasraie(25) who noted that dispersion in sand packs decreased, then increased as the water saturation in the core was increased to the residual saturation point. The effect of residual saturations was not explored further in this work, but it was noted that pack 3 heated injection experiments did not behave as did the experiments in packs 1 and 2. The dispersion in tests 33-35 appeared to be less than the corresponding dispersion for isothermal tests. This suggested that the removal of residual water from the pack with isopropyl alcohol was not completely successful.



#### IV. NUMERICAL ANALYSIS

##### A. Numerical Procedure

A major portion of this study involved a numerical simulation of the convection-diffusion equations for simultaneous heat and mass transfer, when a liquid at a constant temperature displaces a second miscible liquid, initially at a different temperature.

The equations describing the process are:

Heat Transfer

$$\frac{\partial}{\partial x} \left( k_h \frac{\partial T}{\partial x} \right) - \frac{\partial (\rho v c_p T)}{\partial x} = \frac{\partial ([ (1-\phi) \rho_r c_{p_r} + \phi \rho c_p ] T)}{\partial t}$$

Mass Transfer

$$\frac{\partial}{\partial x} \left( k_d \frac{\partial (\rho C)}{\partial x} \right) - \frac{\partial (\rho v C)}{\partial x} = \phi \frac{\partial \rho C}{\partial t}$$

Pressure

$$-\frac{\partial}{\partial x} \left( \frac{-\rho k}{\mu} \frac{\partial p}{\partial x} \right) = \phi \frac{\partial \rho}{\partial t}$$

Gravity has been neglected as it is small relative to the pressure forces at experimental flow rates .

or, Velocity

$$\frac{\partial (\rho v)}{\partial x} = - \phi \frac{\partial \rho}{\partial t}$$

The numerical solution technique selected was the truncation cancellation procedure described by Laumbach(12). This technique produces a finite difference approximation to the convection-diffusion equation which solves for the n+1st time step using a semi-implicit formulation. The equations are solved for a one-dimensional system, so the solutions are valid for the stable flow regime only. The system of equations and the finite difference formulations are found in Appendix B. Awang(13) performed a truncation error analysis on this system of



equations and demonstrated that they are second order accurate for all values of  $\omega$  and that they are fourth order accurate for  $\omega = (\frac{\tau+1}{6} + \frac{1}{3})$ .  $\omega$  is a weighting term for the truncation error cancellation. The truncation error terms and their application to the convection diffusion equation appear in Appendix B.

The computer program utilized solved for temperature and displacing fluid concentration by a semi-implicit procedure. The velocity values at each node may be solved directly, or the pressures in the system may be used to calculate velocity. The temperature and concentration at three points at the  $n$ th time level are used to solve for the temperature and concentration at the  $n+1$ st level. A tridiagonal matrix was generated using rock and fluid properties at the  $n$ th time level and the matrix is solved by the Thomas algorithm. The values of temperature, pressure and concentration obtained were used to update the fluid and rock properties and the results were used to update the solution matrix. The solution was repeated until a convergence criterion of  $\Delta C = .0001$ ,  $\Delta T = .01$  °C,  $\Delta P = .001$  bar, was achieved, (Appendix F).

A one-dimensional set of equations was established using the system properties calculated at each time step. Solution of the resulting matrix yielded temperature and concentration values for the next time step. The fluid flow equation was solved by two methods.

1. The velocity at each node was calculated by a direct solution approach.
2. The pressure equation was solved by an implicit procedure and velocity was calculated from the pressure values. A description of the solution method appears in Appendix B. The three equations were coupled by temperature.



The parameters distance step  $\Delta x$  and time step  $\Delta t$  for each set of computer runs were determined by comparing the numerical solution obtained at a given value of  $k_d$  with the analytical solution at the same value of  $k_d$ . The validation of the numerical solution is described more fully in the Discussion of Numerical Results.

## B. Numerical Results

### Tests of the Numerical Program

A comparison of the numerical solution with the analytical solution is presented in Figures (13 - 16). These plots show that:

1. The boundary condition  $C(0,0)=0$  causes the numerically calculated concentration profile to lag behind the profile produced by the analytical solution (Figure 15). An overshoot may also be produced in the numerical solution.
2. The boundary condition  $C(0,t)=1$  causes the numerically calculated profile to lead the analytical solution (Figure 13).
3. The use of a smaller distance increment causes the numerically produced profile to follow the analytical solution more closely. Conversely, an increase in the distance step (Figure 14) increases the error and can cause an overshoot in the numerical solution.
4. Changing the boundary condition to  $C(0,0)=0.5$ ,  $C(0,t)=1.0$  resulted in a numerically generated profile which matched the analytical solution (Figure 16). This boundary condition eliminates the lag or lead of the numerical solution due to the finite width of the distance step  $\Delta x$  in the numerical solution.

One simulation was attempted using the Crank-Nicholson method, but this system proved unsatisfactory as the large numerical dispersion



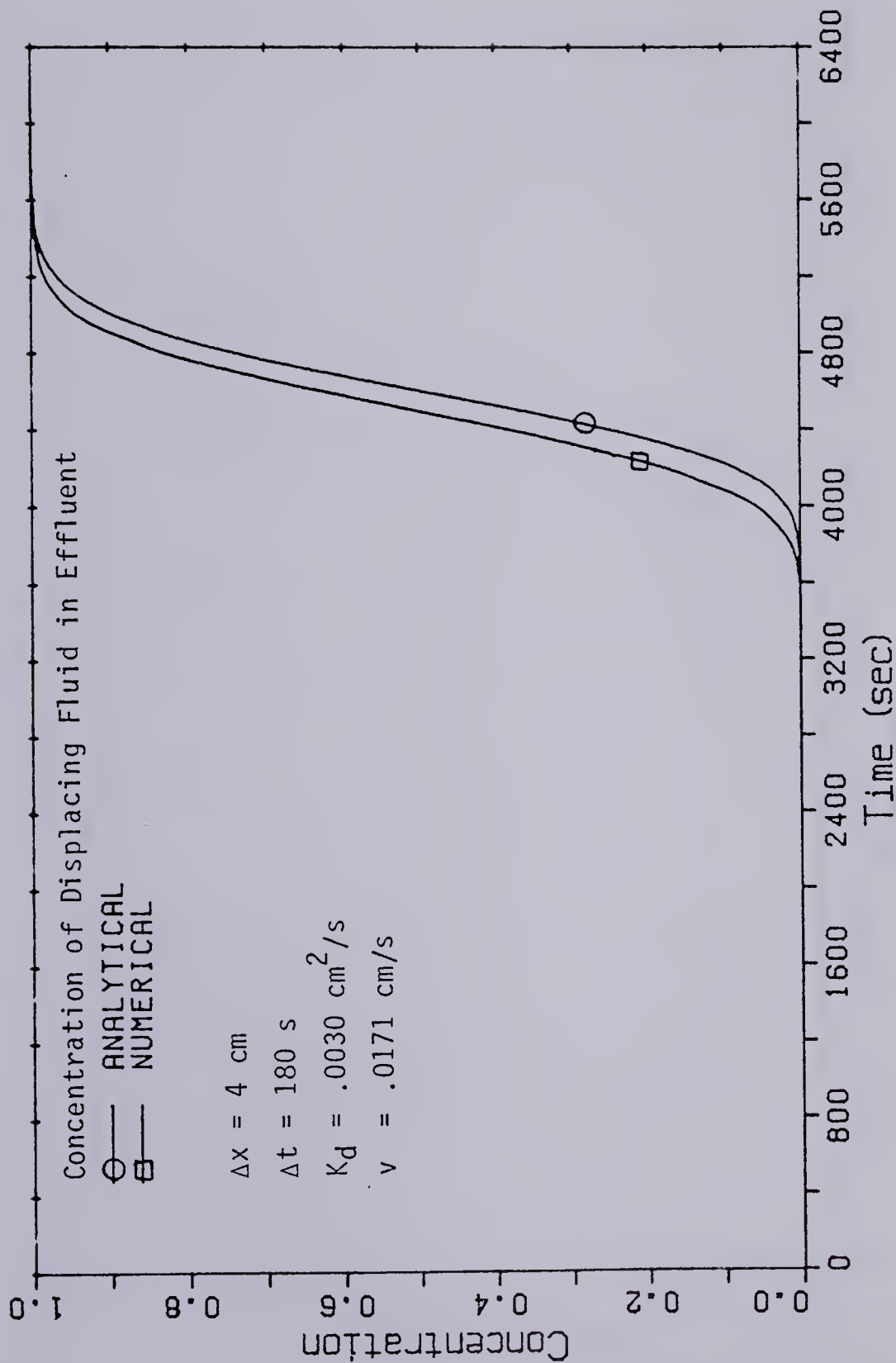


Figure 13 NUMERICAL SOLUTION AT  $C(0,0)=1.0$



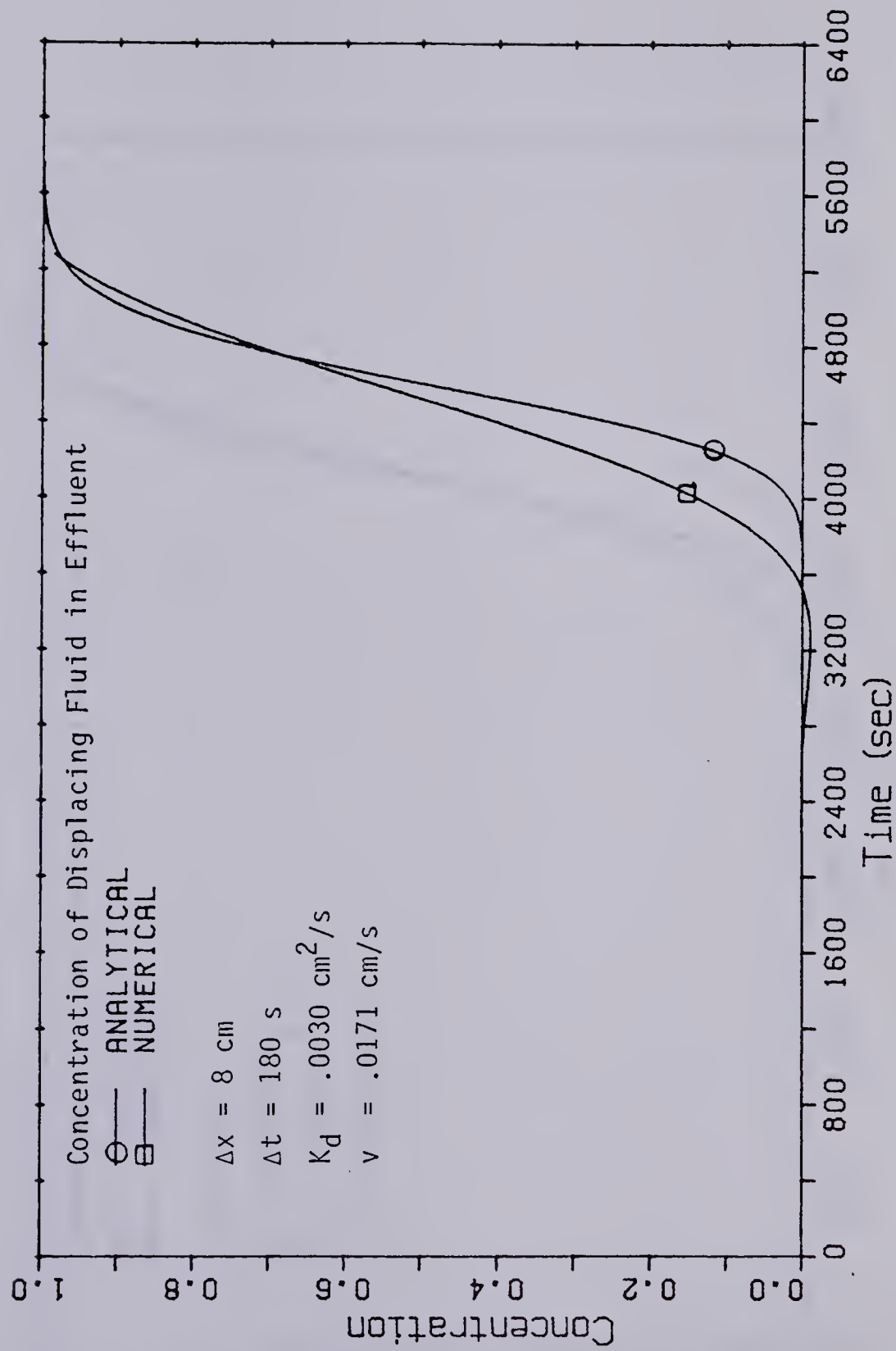


Figure 14 NUMERICAL SOLUTION AT  $\Delta x=8 \text{ cm}$



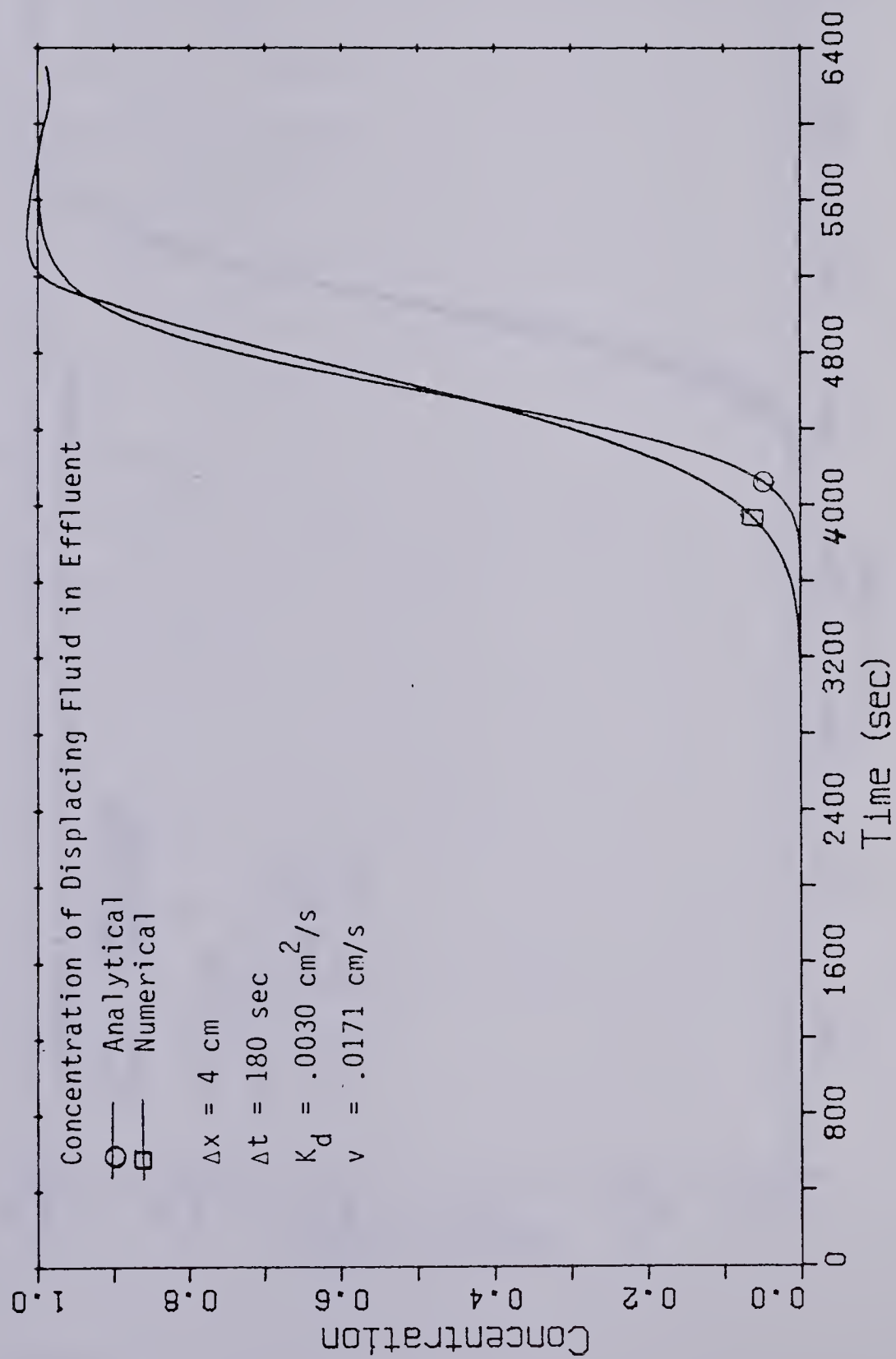


Figure 15 Numerical Solution at  $C(0,0)=0$



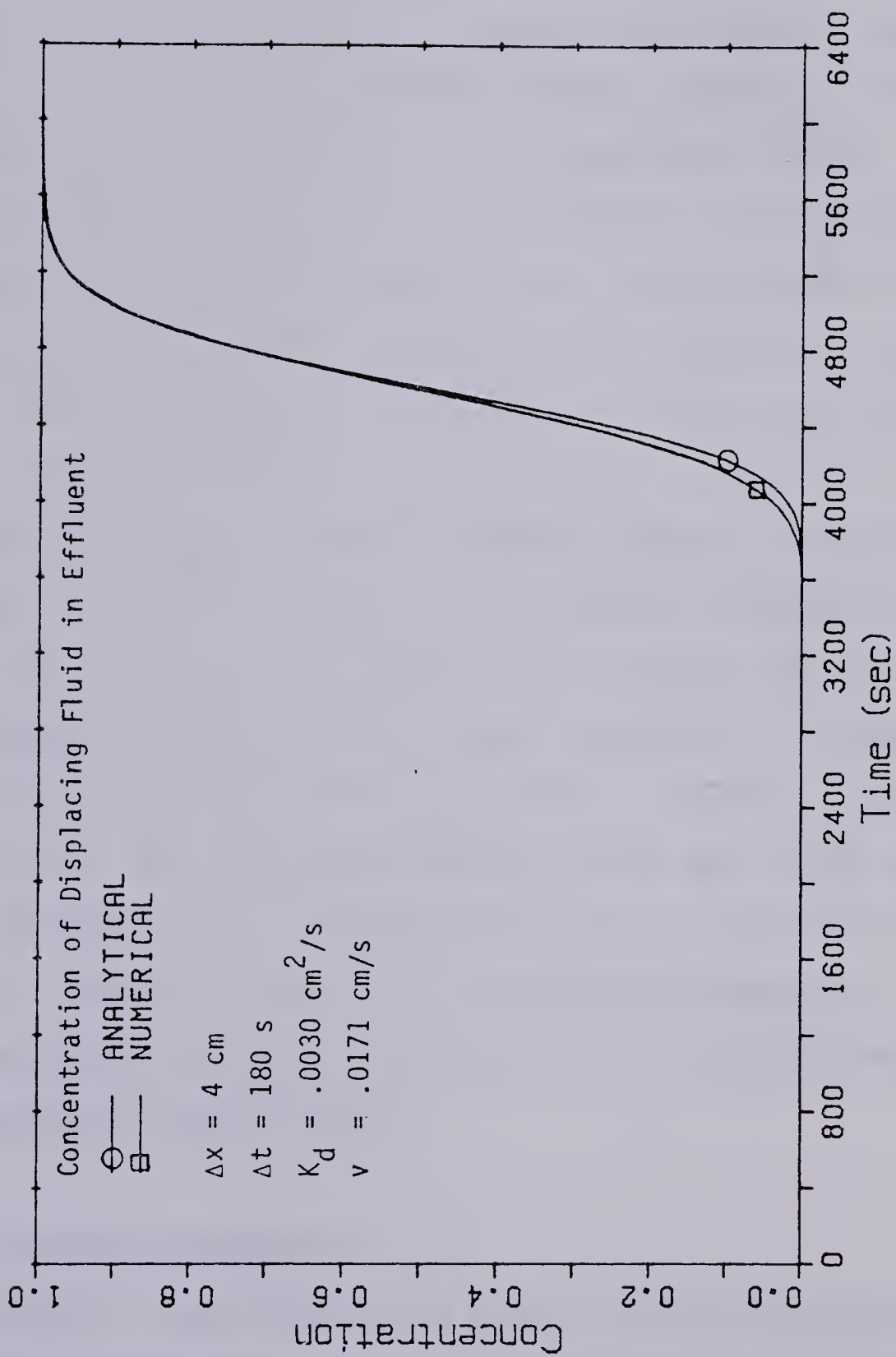


Figure 16 NUMERICAL SOLUTION AT  $C(0,0)=0.5$



overshadowed the actual dispersion. The effect of numerical dispersion on solutions to the convection-diffusion equation and on similar equations is discussed by Peaceman(27). Peaceman noted that the convection term in a convection-diffusion equation will produce a numerical dispersion in several types of finite difference solutions. This dispersion may appear as a smearing of the concentration profile, as an overshoot or undershoot behaviour, or as instability in the solution.

Comparisons of simulations carried out at varying values of  $\Delta t$  and  $\Delta x$  indicate that some runs were unstable and that there was an overshoot in other runs. A good fit for the numerical solution occurs between  $\Delta t=180$  s and  $\Delta x=4$  cm (Figures 16) and  $\Delta t=120$  s (Figure 17). The improvement in accuracy obtained by iterative updating is also evident (Figure 18). A stability analysis of the truncation cancellation procedure by the Karplus Criterion (Appendix C) indicates that the system will be stable if  $\Delta t < 300$  s, if  $\Delta x=4$  cm and  $v=.0056$  cm/s. The numerical runs performed indicate that the actual region of stability is  $\Delta t < 240$  s (see Table 3). This stability criterion may be most easily met by adjusting the time step to an appropriate value for a given set of run parameters. The Karplus criterion is not completely rigorous as it does not include boundary conditions. This omission is a possible reason for the discrepancy in stability times.

## Results of Numerical Simulations

The numerical program was used to simulate some of the experimental displacements (Figures 2-4, Figure 19) to assess the ability of the numerical system described to predict the effects of mobility ratio and inlet temperature on the displacement process. The results of these



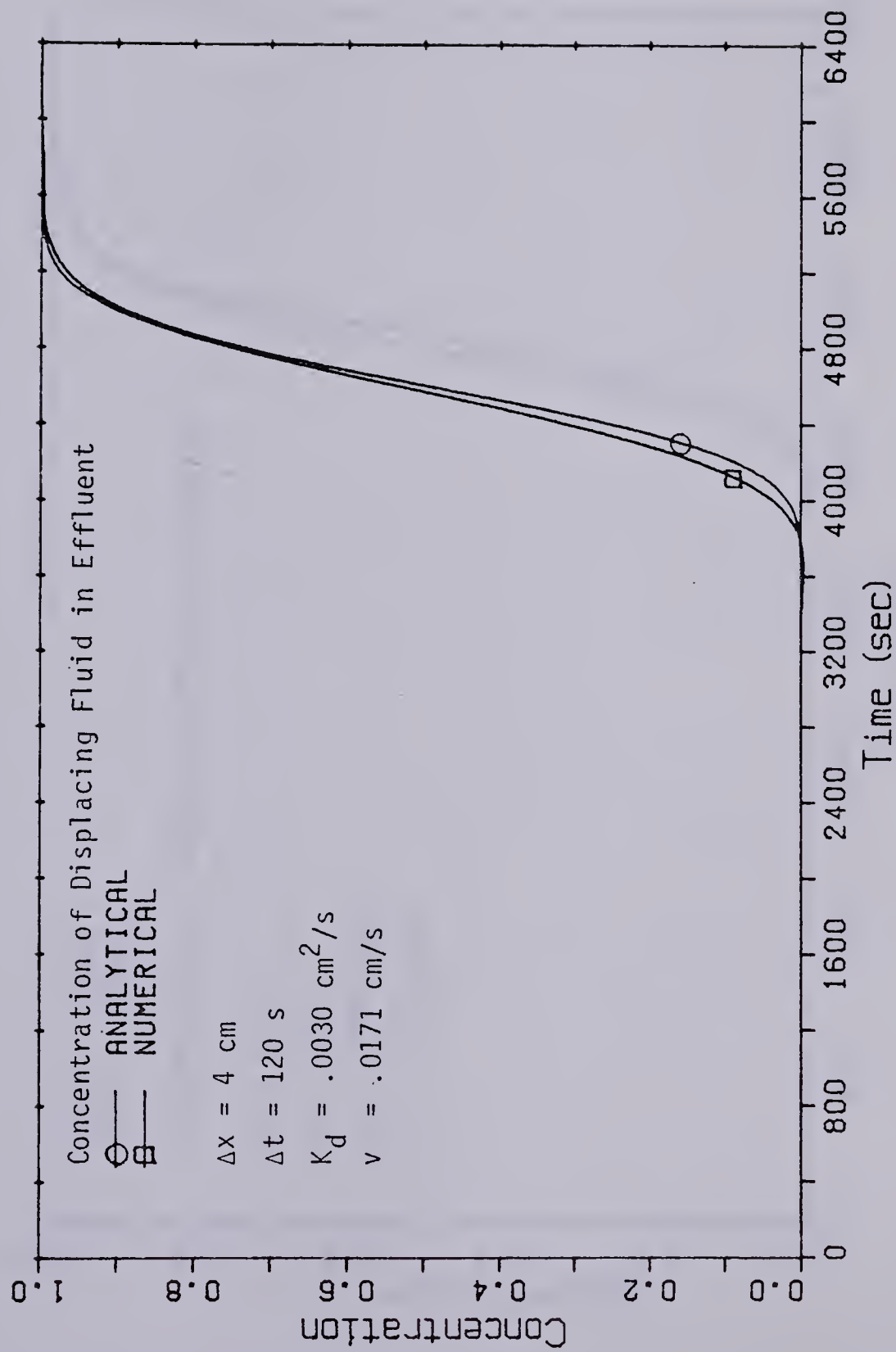


Figure 17 NUMERICAL SOLUTION AT  $\Delta T=120 \text{ S.}$



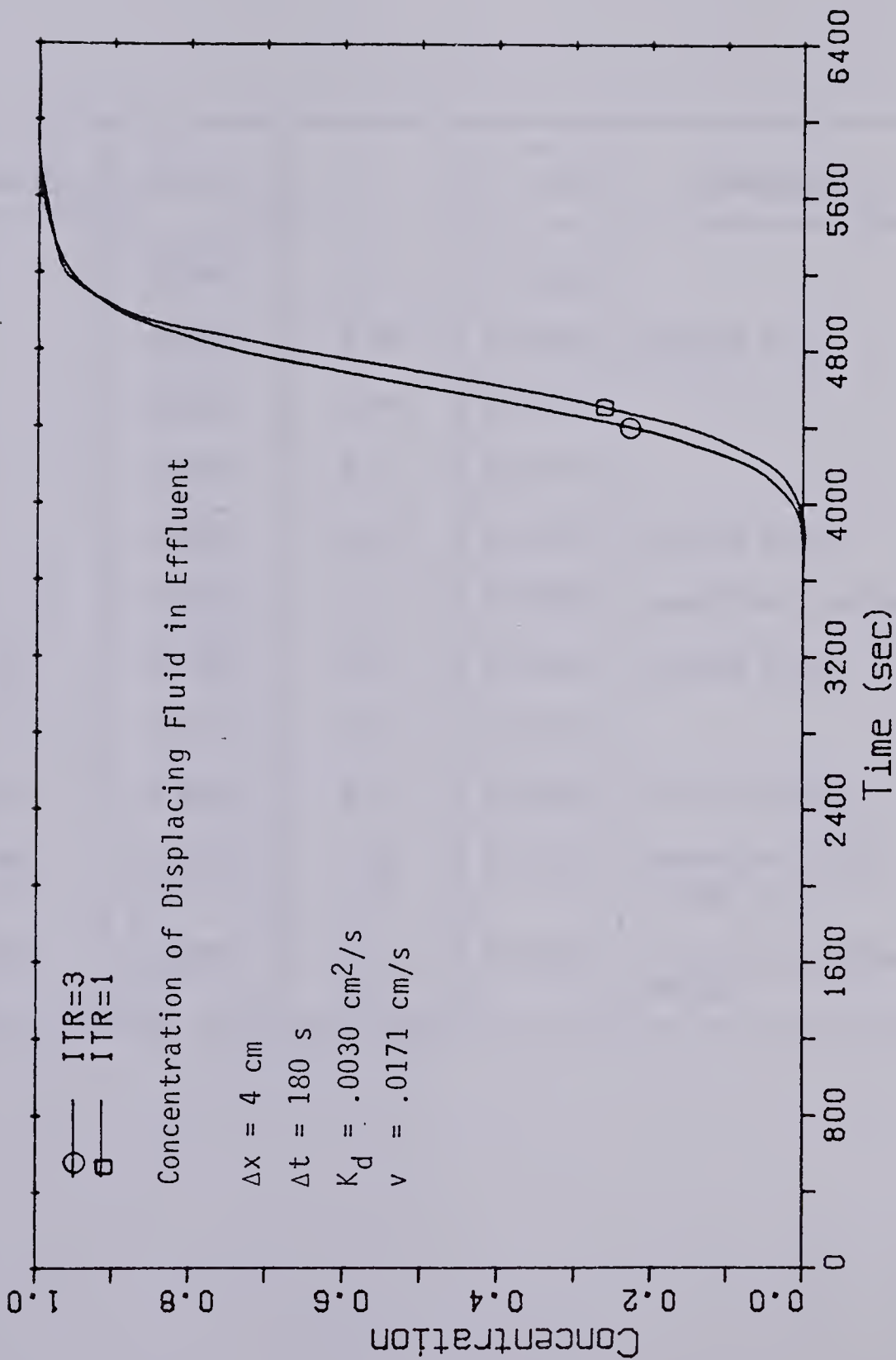


Figure 18 NUMERICAL SOLUTION AT 1 AND 3 ITERATIONS



Table 3  
Numerical Simulation of Experiments

Run No.	Inlet M.	$\sigma$	$v$ cm/s	Comments
1	0.089	1.61	0.00523	
3	0.089	1.60	0.00521	heated disp.
5	0.110	1.65	0.00528	
6	0.708	2.01	0.00475	
9	0.110	1.66	0.00544	heated disp.
8	0.0014	1.59	0.00538	numerical overshoot
10	0.708	2.01	0.00538	heated disp.
11	0.110	1.67	0.00127	
12	0.708	1.82	0.00538	chilled disp.
8A	0.0014	1.56	0.00538	repeat of R8 at larger $\Delta t$
3A	0.089	1.30	0.00521	pressure solution for R3



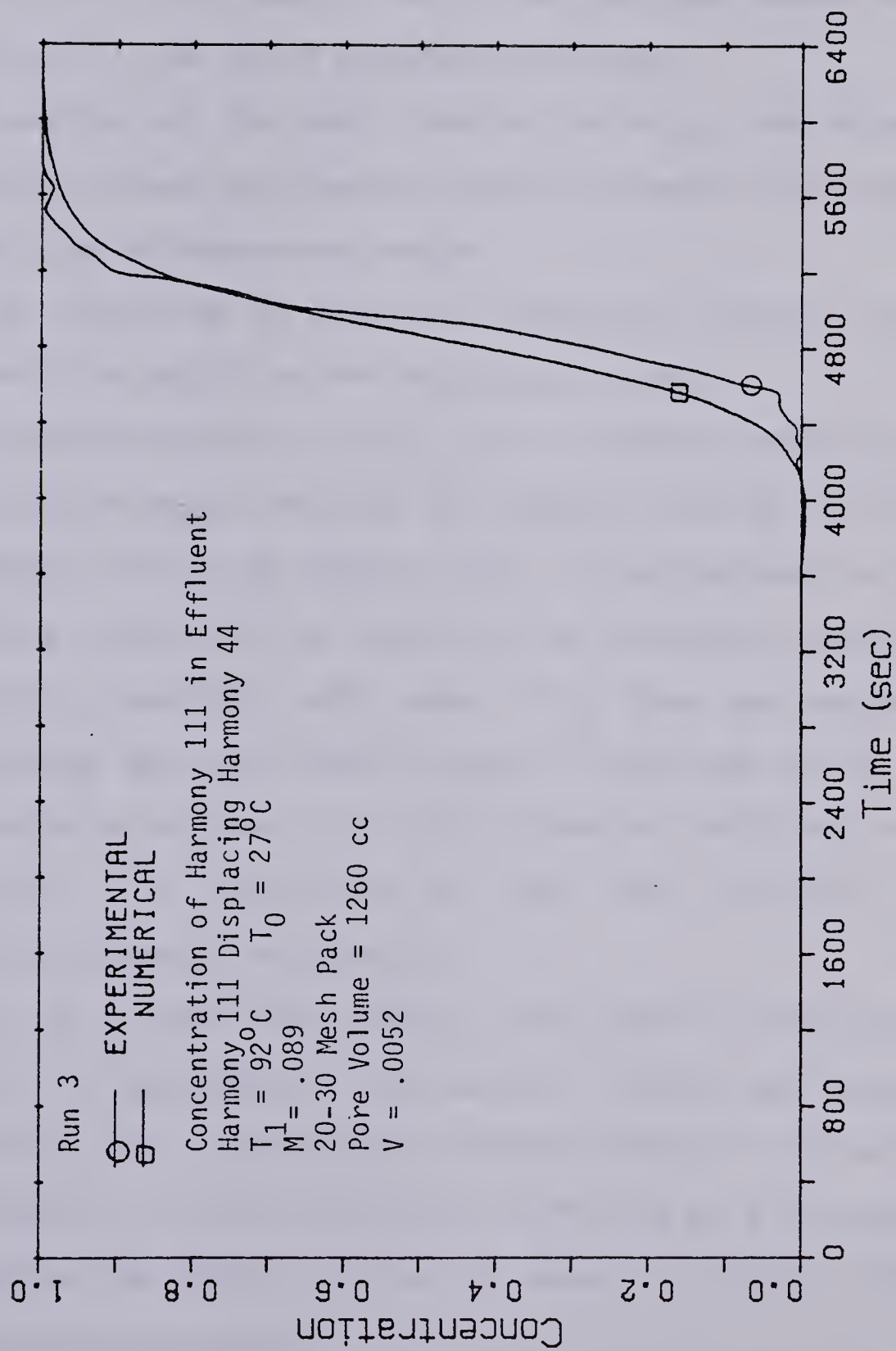


Figure 19 NUMERICAL SOLUTION FOR R3



simulations appear in Table 4.

The mixing coefficients obtained from the numerical curves were plotted against mobility ratio for a set of simulations of the 80-120  $\mu\text{m}$  pack (Figure 20). The numerical simulation predicted several effects that are present in the set of experiments performed:

1. The coupling of the heat transfer, velocity, and dispersion equations allowed the numerical system to predict the changes in velocity due to temperature changes.
2. Similar results may be obtained by employing a pressure solution and obtaining velocities from the pressure values.
3. The dispersion equation  $k_d = v d_p \sigma$  was not able to predict changes in dispersion due to injection of a heated or chilled fluid or due to changes in the inlet mobility ratio. It was necessary to supply a mixing coefficient by modifying the dispersion equation by including a mobility ratio term. This term was obtained by multiplying the local mobility ratio at each node by the local dispersion at each node. The local dispersion coefficient becomes  $k_d = v d_p \sigma M$ . A description of the local mobility ratio calculation appears in Appendix B.
4. The use of a linear local mobility ratio factor in the dispersion equation at each node in the numerical solution was capable of reproducing the experimentally observed effects for isothermal simulations. This local dispersion coefficient was also capable of reproducing the effect of injecting heated or chilled fluids in displacement experiments.
5. An increase in mixing was predicted when a heated displacing fluid



Table 4  
Numerical Stability Tests

Run No.	v (cm/s)	$\Delta t$ (s)	$\Delta x$ (cm)	Comments
S12	0.0025	120	8	overshoot
S13	0.0056	360	4	unstable
S14	0.0056	300	4	unstable
S15	0.0056	240	4	marginally unstable
S16	0.0056	220	4	stable
S17	0.0056	180	4	stable
S18	0.0056	90	4	stable
R8	0.0054	180	4	stable
R8a	0.0054	240	4	stable



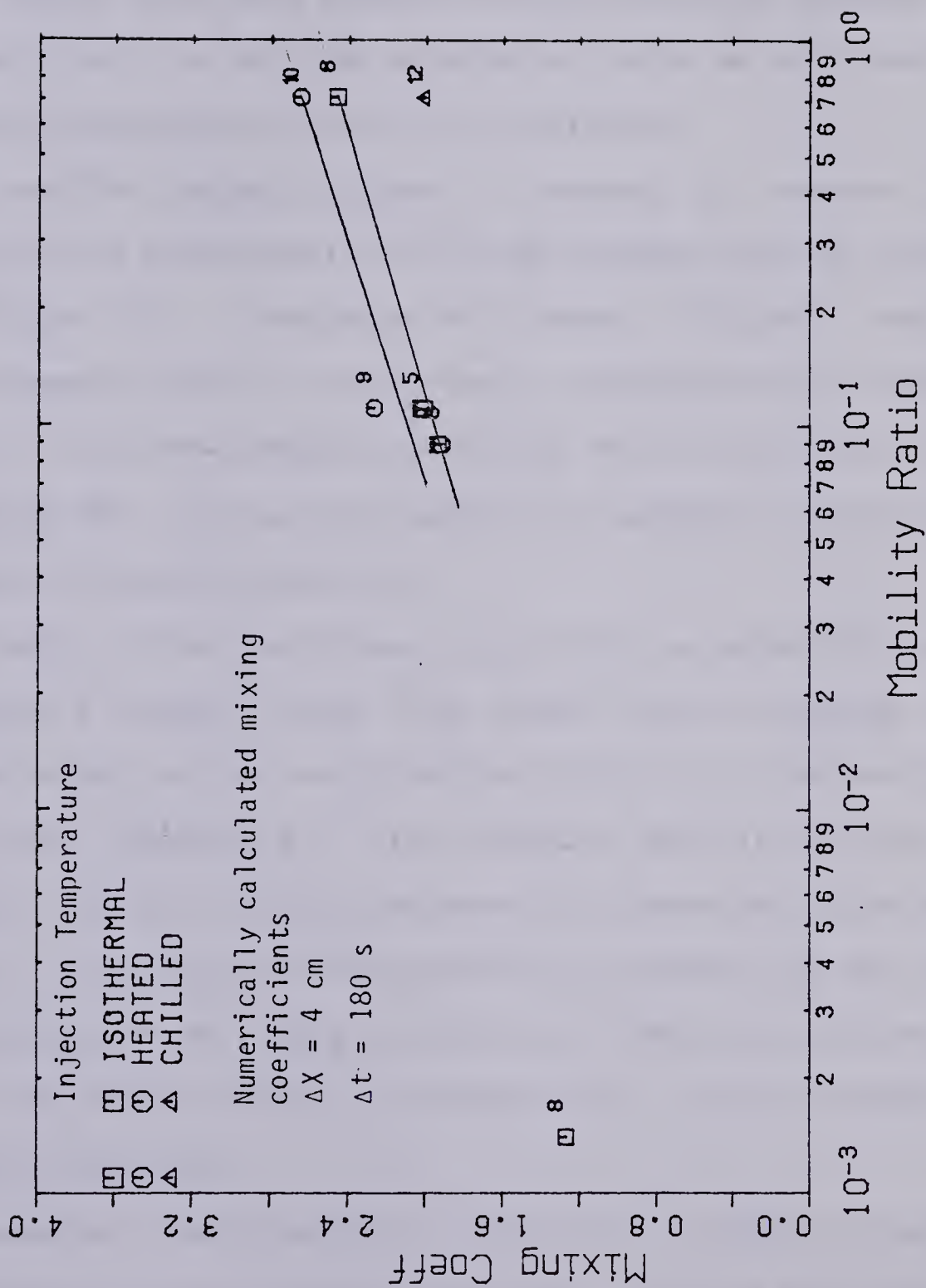


Figure 20 Numerical Simulation Data for 20-30 Mesh Pack



was used and a decrease in mixing when a chilled fluid was used. The magnitude of this effect was greater when the inlet viscosity ratio approached unity.

6. Isothermal simulations at differing velocities predicted mixing coefficients to be large relative to the coefficients expected from diffusion only, as the range of velocity studied was well above the velocity values where diffusion is significant.
7. The numerical system displayed a tendency to overshoot when simulation of displacements using large distance steps was attempted (Figure 14). Simulation of extremely favourable mobility displacements tended to display some overshoot behaviour (Table 3, test 8). This was remedied by modifying the time step used (Figure 21, test 8A). It was not possible to completely eliminate the overshoot from all simulations.
8. The results of the simulations, when plotted on probability paper, produced a slightly curved line rather than the straight line characteristic of the error function solution or of the experimental data, (Appendix F). The curvature made it difficult to estimate the exact slope of the numerically generated concentration curve. The presence of this curvature was assumed to be the result of numerical error. This curvature was found to be much smaller when the solution method was changed from a single iteration to multiple iterations.
9. The numerical simulation did not account for the effect of packing or porosity on the dispersion coefficient. This was due to the use of a fixed value of 1.75 for the mixing coefficient  $\sigma$ . Experiments on a number of different packs would be required in order to



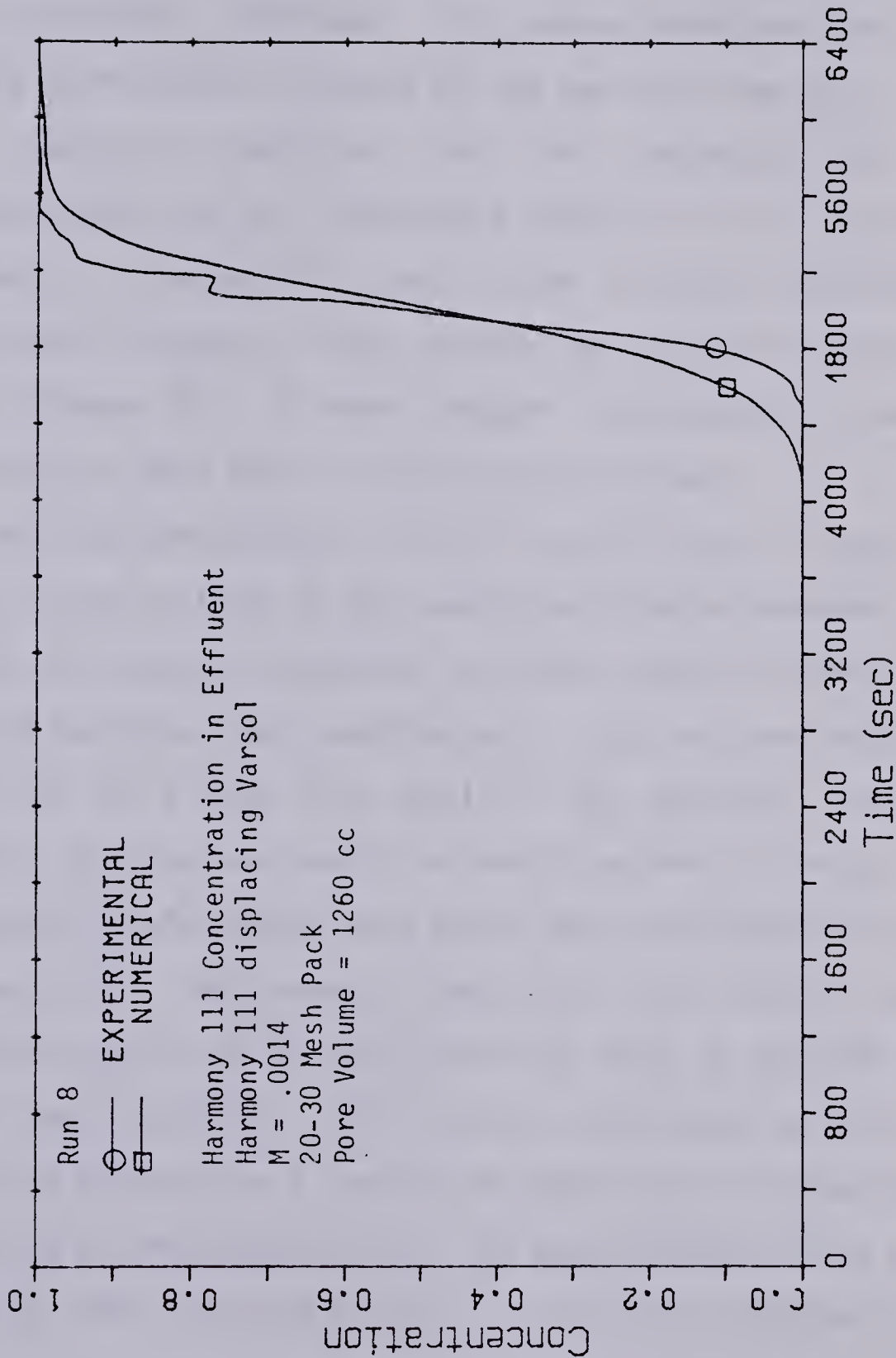


Figure 21 NUMERICAL SOLUTION FOR R8



determine the relationship between porosity and dispersion.

Perkins and Johnston(9) discussed the results of several investigators on the effect of packing. It was reported that for finer particles,  $\sigma$  increased. This general trend was found in the mixing coefficients calculated for the two pack sizes used.

10. The numerical simulation could not reproduce the curve characteristic of an unfavourable mobility ratio displacement (Figure 7). The use of a local  $M$  value to modify the dispersion coefficient produced a curve similar to the stable displacement curve (Figure 22). To model unstable displacement, it would be necessary to use a two- or three-dimensional model.
11. The model did not simulate heat loss from the core, as a heat loss term was not included in the convection-diffusion equation. This system of equations predicted a higher rate of thermal front advance than that found experimentally. This may have been due to the lack of a heat loss model in the numerical simulation. However, the model was capable of predicting that the thermal front (Figure 23) would advance more slowly than the concentration front (Figure 22). The numerical simulation could also be used to generate profiles of the local viscosity ratio in the pack at any given time (Figure 24). This plot was constructed by calculating the fluid viscosity as a function of composition and temperature at each node on the numerical grid. The local viscosity ratio at each node was then calculated as  $\frac{\mu_{i+1/2}}{\mu_{i-1/2}}$ . The profile indicates a ratio of less than unity at the stable displacement front and a ratio of greater than unity at the thermal front. A viscosity ratio profile for an isothermal experiment is also included in Figure 24.



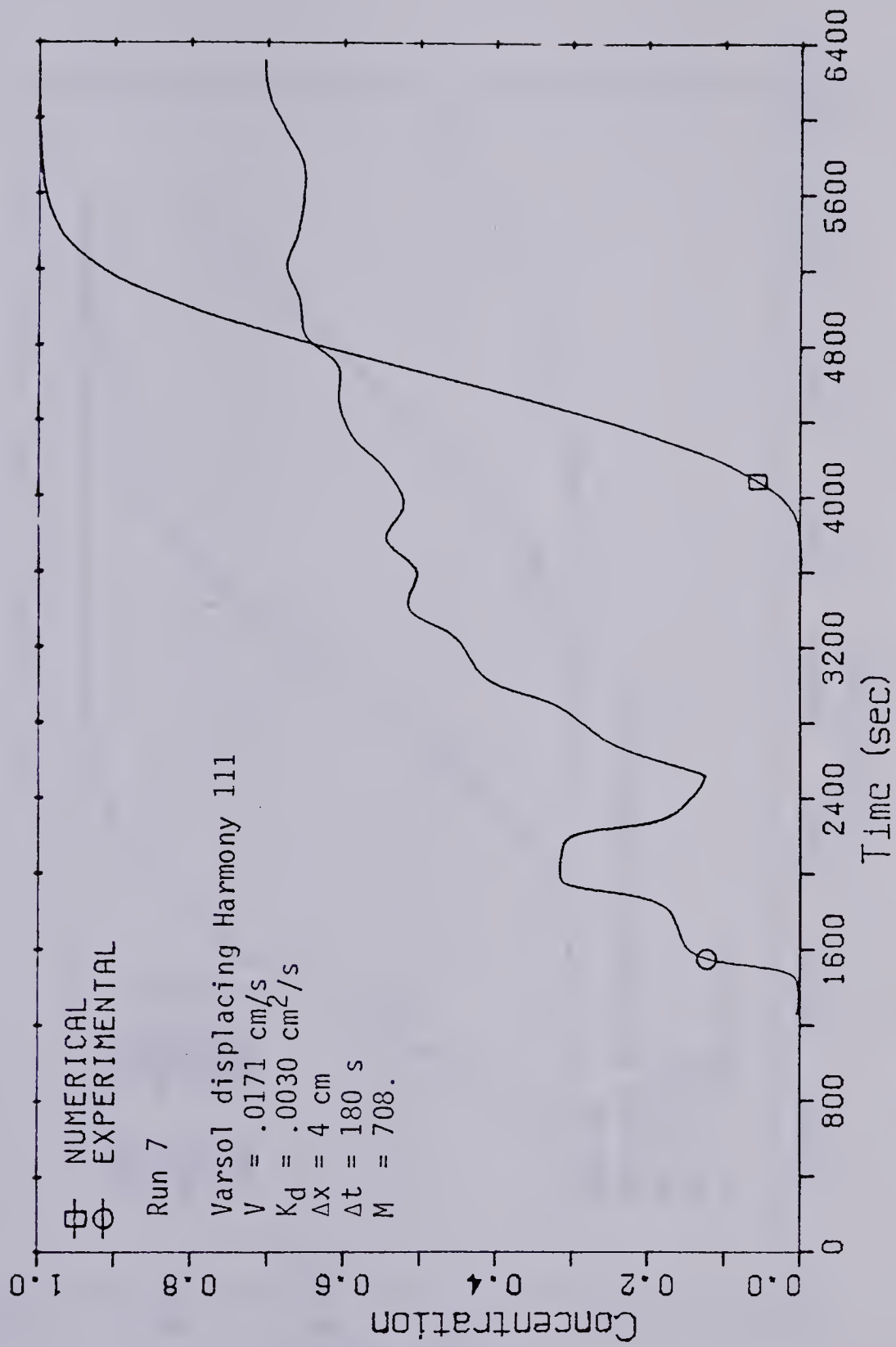


Figure 22 ADVERSE MOBILITY RATIO SIMULATION



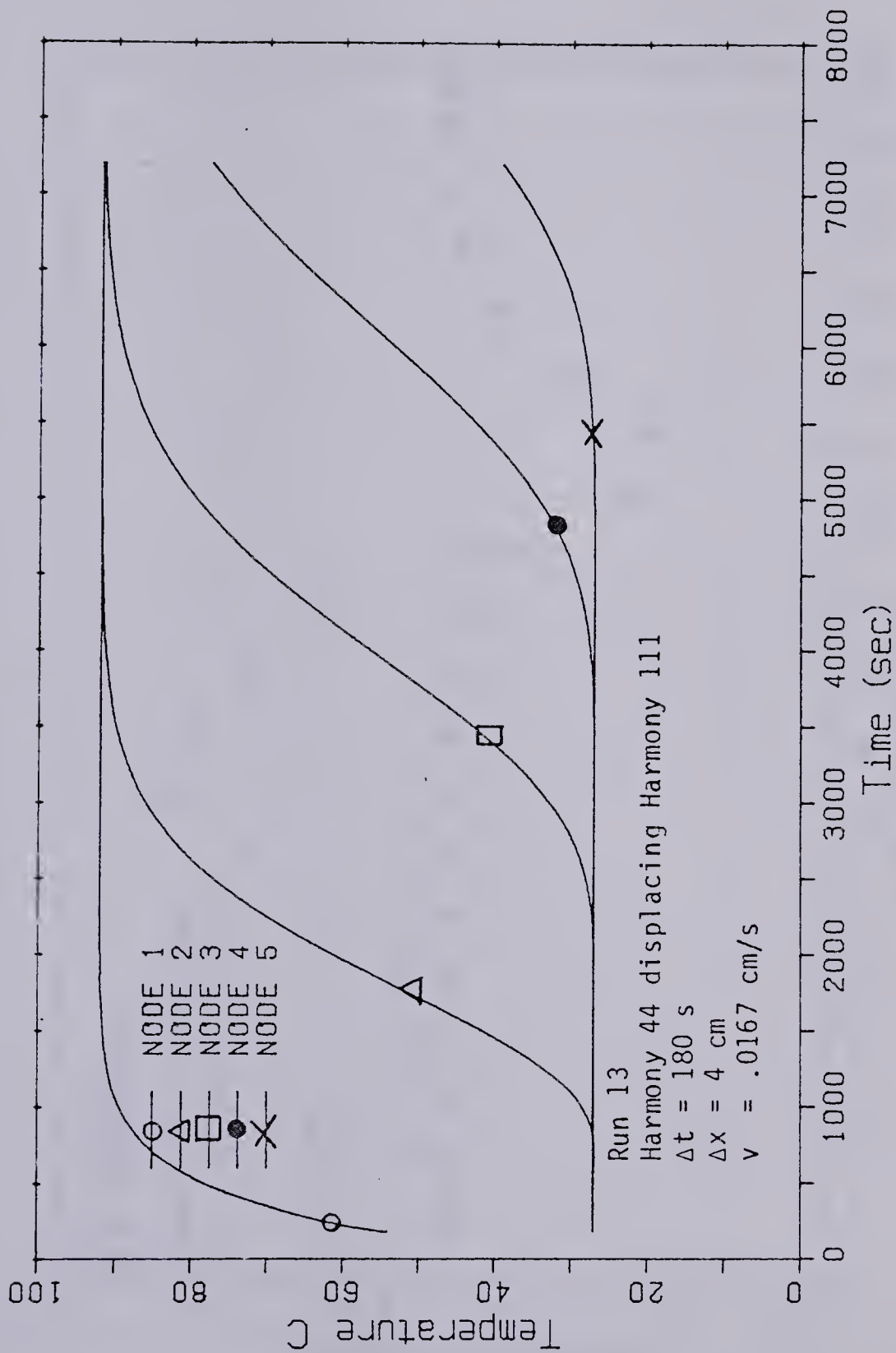


Figure 23 NUMERICAL TEMPERATURE PROFILES, R13



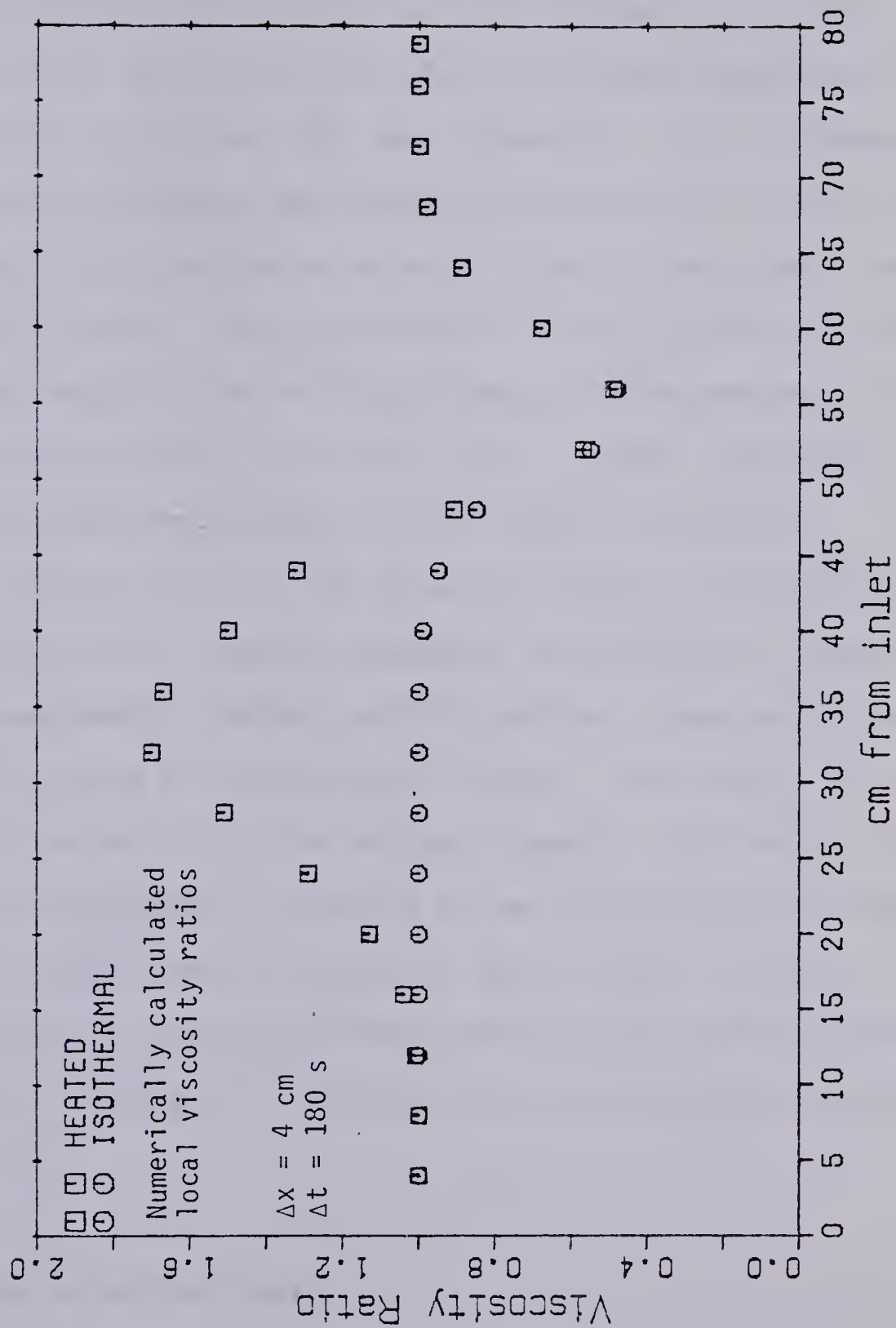


Figure 24 LOCAL VISCOSITY RATIO PROFILE AT T=3600 S



12. The numerical simulations which used fluid velocities from a pressure converged much more slowly than did the solutions using a direct solution for velocity. Pressure solutions required eight to eleven iterations to converge to the tolerances in C, 0.0001, in T, 0.01, and p, 0.001 while the velocity solutions required only three iterations to achieve the same tolerances. This difference in speed of convergence was thought to be due to the ability of the direct solution to provide velocity values at the current iteration of the solution. The calculation of velocity values from pressure values meant that the velocity values available were those from the previous iteration. This plus the increased complexity of the solution made the pressure solution slower to converge.
13. The numerical solution for pressure produced results (Figure 25) similar to the results determined experimentally (Figure 26). The experimental pressure profile contains a step at the pressure peak not found in the numerical solution. This step is due to the resistance to flow of the end cap assembly. This small increment of flow resistance is important as the resistance of the sand pack is very small when a 80-120  $\mu\text{m}$  sand is used. Figure 27 is a comparison of the concentration profile obtained from a numerical solution solving for pressure with an experimental concentration profile.

### C. Results of Scaling Study

The scaling study in Appendix A indicates a need to scale up both  $v$  and  $k$  as the model is scaled down. This would allow for modelling of pressure, gravity, heat transfer and viscous forces. However, it is



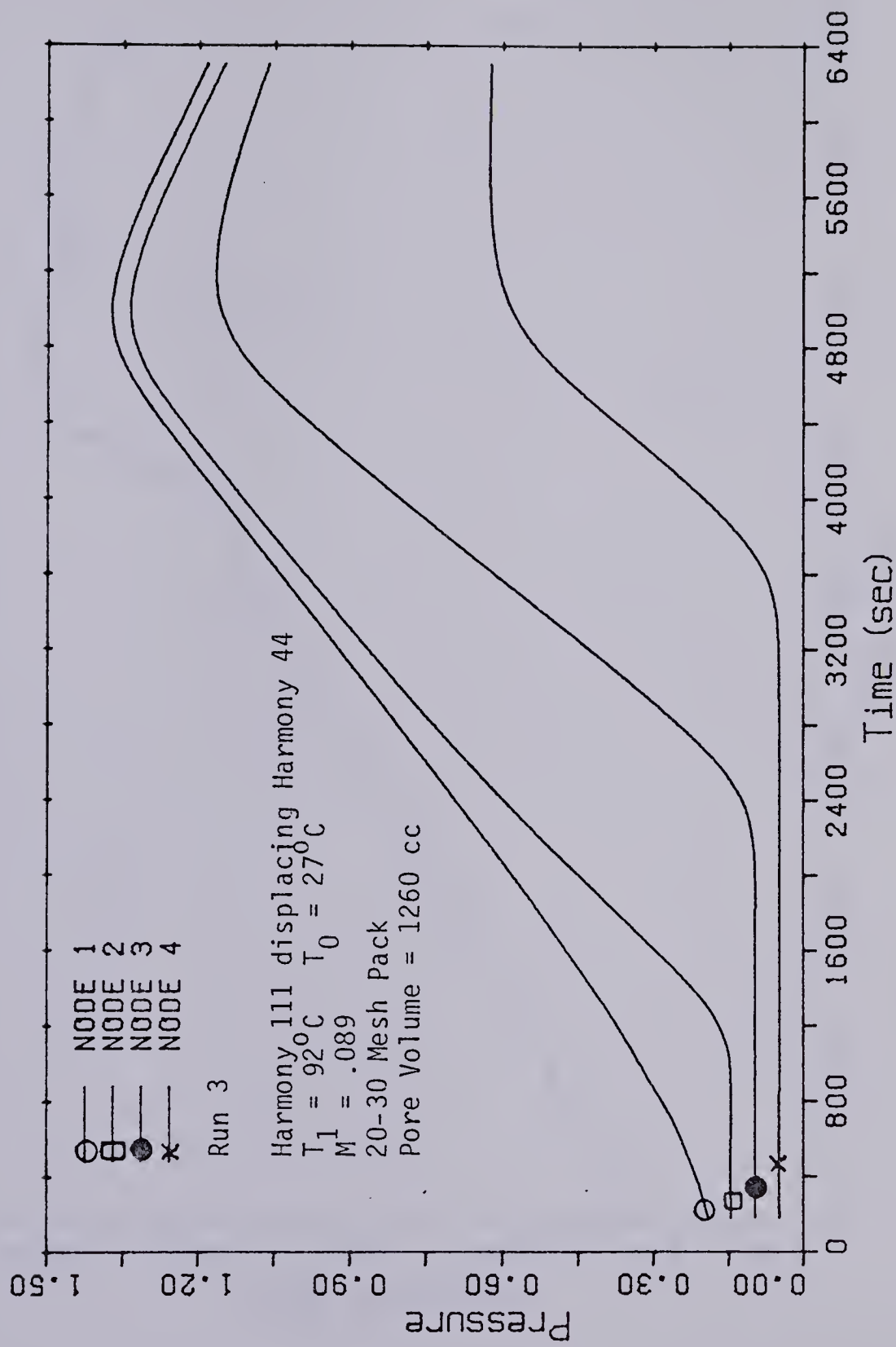


Figure 25 PRESSURE SOLUTION FOR R3



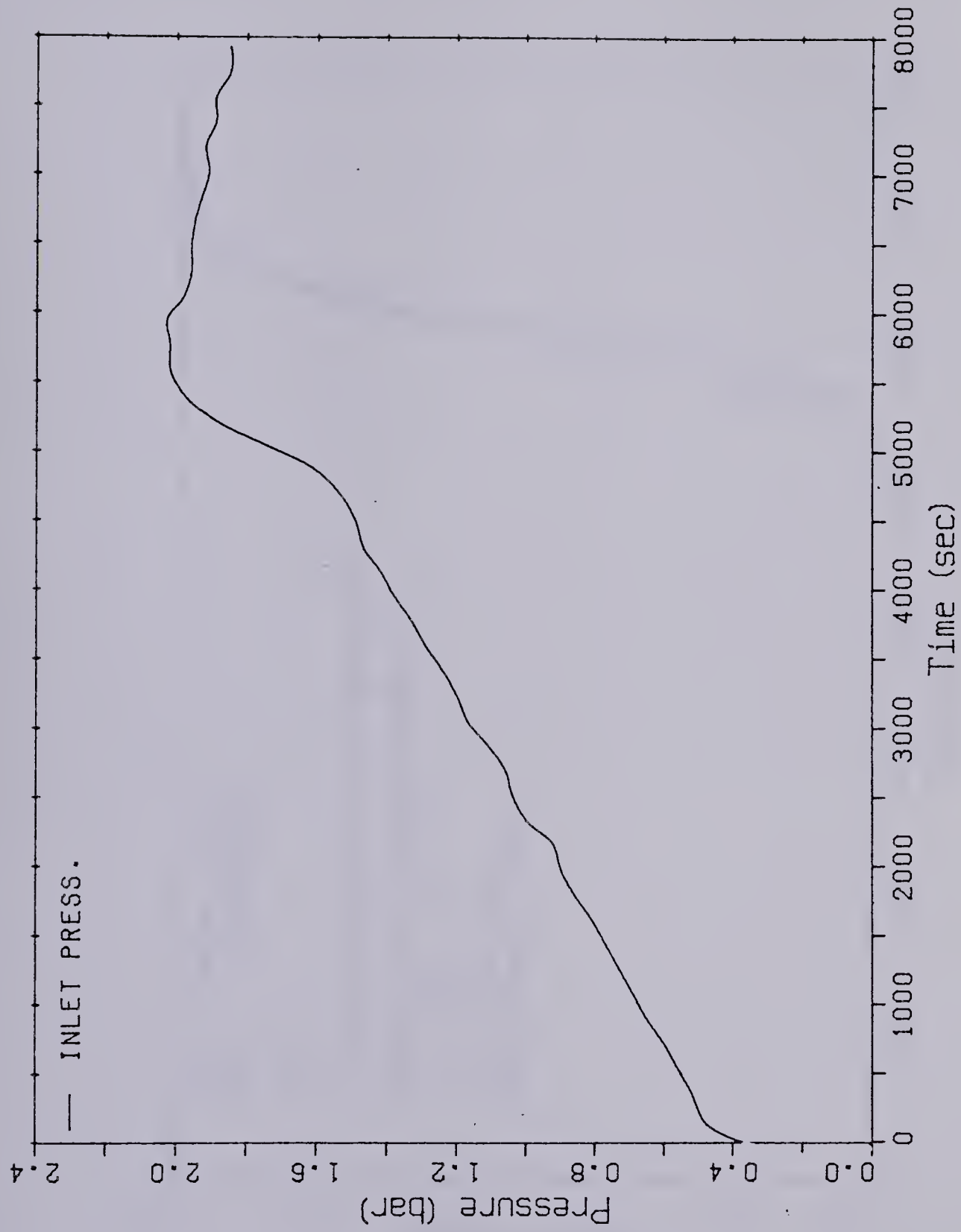


Figure 26 Experimental Pressure Profile, R3



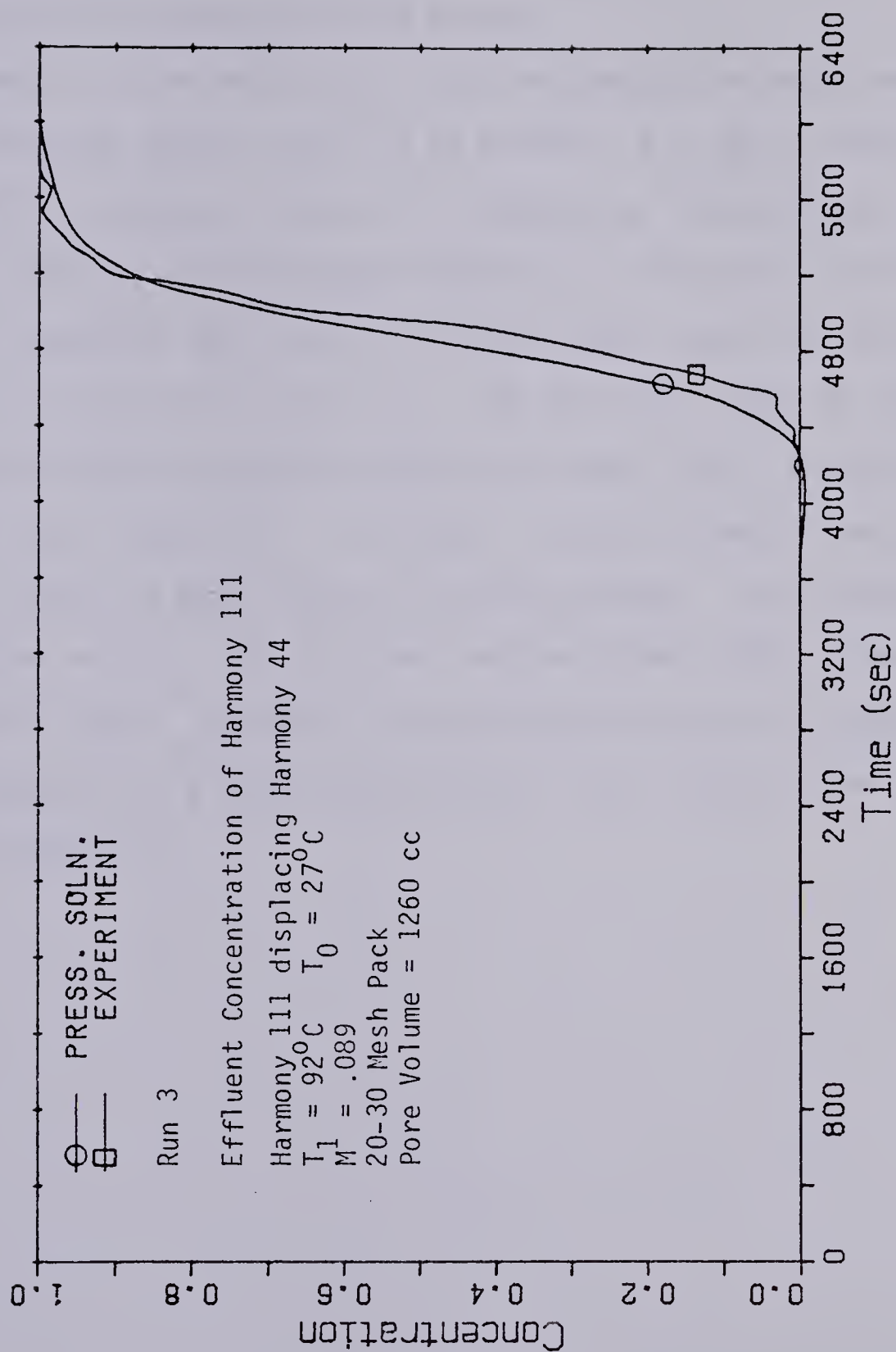


Figure 27 NUMERICAL SOLUTION FOR R3



necessary to scale down  $d_p$  as  $v$  is increased in order to model dispersion. However, this implies that  $k$  must be scaled down, which conflicts with the remaining scaling groups.

An example of the application of scaling groups for heat transfer, viscous forces and gravity forces is as follows: A  $1 \mu\text{m}^4$  (1 darcy), 78 m long section flowing at .152 m/d is modelled by a  $100 \mu\text{m}^2$  sand pack flowing at .0176 m/s. The prototype would be in a velocity region where diffusion dominates ( $D_0 > \sigma v d_p$ ) while the model would be dominated by mixing or dispersion ( $\sigma v d_p > D_0$ ). The sand pack would be able to scale gravity forces, pressure forces and viscous forces, but would be unable to scale dispersion. Conversely, a model correctly scaled for dispersion would not model gravity or viscous forces. The experiments support these results. The very low rate experiment (R25) produced a low dispersion value. Attempts to scale pressure forces by operating at a higher velocity in a larger particle pack (R5) produced much higher values of dispersion.



## V. CONCLUSIONS

### A. Experimental and Numerical Results:

1. The relationship  $k_d = D_0 + \sigma v d_p$  as described by Perkins and Johnston(9) was found to be valid for both sand packs (Figure 6).
2. The high values of the dispersion coefficient and the irregular displacement profiles occurring in the experiments at  $M > 1$  (Figure 5) suggested the presence of viscous fingering. This was noted by Brigham, Reed and Dew(4) and other studies.
3. The successful prediction of the increase in dispersion with an increase in mobility ratio (Figure 20) tends to support the use of a linear local viscosity ratio term in the calculation of local dispersion coefficients. However, this does not imply that  $k_d$  for the entire sand pack varies linearly with mobility ratio.
4. The modification of dispersion coefficients by a mobility ratio term is also useful for predicting the influence of temperature gradients on dispersion (Figure 20).
5. The differing rates of advance of the thermal front and the displacement front were predicted by the numerical model. The numerical model did not contain a heat loss term and therefore could not predict heat losses from the sand pack. Had a heat loss term been included, the numerical model would probably have predicted a smaller effect of injection temperature on dispersion. The lack of a heat loss term in the model and the difficulty in obtaining adiabatic conditions in the experimental displacements meant that it was not possible to make quantitative measurements of thermal dispersion in the sand pack.
6. The regions of stability for the numerical method used were



evaluated (Table 3) and were found to be dependent on the fluid velocity used.

7. The use of a pressure solution to calculate velocity produced a workable solution, though convergence of this numerical system was much slower than convergence for a system using a direct velocity solution.
8. The pressure solution is more versatile as it may be written for slightly compressible flow, and could be extended to a compressible flow case, while the direct velocity solution is limited to one-dimensional incompressible flow.
9. While the numerical system used contained several simplifying approximations, it was sufficiently accurate to allow qualitative predictions of rate, temperature and mobility ratio effects.

## B. Scaling Study

The implications of the velocity dependence of  $k_d$  and the scaling analysis are as follows:

From Appendix A, the value of  $k_d \text{ model} = k_d \text{ field}$ . If  $k_d = D_0 + \sigma v d_p$ , then  $d_{\text{particle}}$  must be decreased as  $v_{\text{model}}$  increases. This generates a conflict as the remaining scaling groups require that both  $v$  and  $d_p$  be increased when scaling down from field size to laboratory size. Therefore, a model of a process in which dispersion is significant will be limited by the dependence of dispersion on flow rate. Such a system may be scaled only if it is not necessary to model heat transfer, gravity forces, or viscous forces. Conversely, a system modelling heat transfer, viscous and gravity forces will not be able to simultaneously model dispersion.



### C. Practical Application

1. The criterion  $k_d \text{ model} = k_d \text{ field}$  will set a scaling limit of 2:1 if the "field" system is Harmony 87 displacing Harmony 44 in a 20-30  $\mu\text{m}$  (80-120 mesh) sand pack displaced at 0.00035 cm/s and the maximum permissible error is 15%. For a fluid pair with a higher diffusion coefficient, the scaling constraint will be somewhat less severe. At  $D_0 = 0.001 \text{ cm}^2/\text{s}$ , the system may be scaled 5:1 to maintain the same error (15%). This scaling factor is still insufficient for a convenient laboratory model of a petroleum reservoir.
2. The differing rates of movement of the concentration and thermal fronts and the resulting lack of a strong temperature effect on dispersion suggest that the direct injection of a heated solvent will leave the thermal front behind the solvent-oil interface. The resulting process will be equivalent to a cold solvent injection.
3. The numerical solution of the heat transfer-diffusion-pressure problem is of interest to several types of reservoir problems. The solution of the convection-diffusion and pressure equations in two or three dimensions would allow for simulation of systems with unfavourable mobility ratios or simulation of heterogeneous reservoirs. The simulation of thermal recovery schemes where there is significant miscibility of components would require the solution of all three equations in two or three dimensions.

### D. Recommendations For Future Work

1. The development of a two-or three-dimensional model of the non-isothermal displacement problem would be an asset to a thermal recovery reservoir simulation.



2. An investigation into the fundamentals of the dispersion process using an analytical or numerical model of a reservoir pore space would better define the relationship between mobility ratio and dispersion.
3. The difficulties in reproducing experiments in this work imply that the effects of packing, porosity, and residual saturation of a second phase, are parameters which must be carefully controlled in a displacement experiment.
4. The measurement of thermal diffusivity in a sand pack will require one of two approaches:
  - i. Run experiments in a low pressure model with vacuum insulation.
  - ii. Match the thermal profiles of experiments using a numerical model containing a heat loss term.



## VI. BIBLIOGRAPHY

1. Farouq Ali, S. M. and Alikhan, A.: "Oil Recovery by Hydrocarbon Slugs Driven by a Hot Water Bank" Soc. Pet. Eng. Jour., Dec. 1971, p. 432
2. Greenkorn, R. A.: "Flow Models and Scaling Laws for Flow through Porous Media" Industrial and Engineering Chemistry, vol. 56 no. 3, March 1964, p. 32
3. Geertsma, J., Croes. G. and Schwartz, N.: "Theory of Dimensionally Scaled Models of Petroleum Reservoirs" AIME Trans., vol. 207, 1956, p. 178
4. Brigham, W., Dew, J. and Reed, P.: "Experiments on Mixing During Miscible Displacement in Porous Media" Soc. Pet. Eng. Jour., March 1961, p. 1
5. Blackwell, R. J.: "Laboratory Studies of Microscopic Dispersion Phenomena" Soc. Pet. Eng. Jour., March 1962, p. 1
6. Pozzi, A. and Blackwell, R. J.: "Design of Laboratory Models for the Study of Miscible Displacement" Soc. Pet. Eng. Jour., March 1963, p. 28
7. van der Pol, C.: "Effect of Lateral Diffusivity on Miscible Displacement in Horizontal Reservoirs" Soc. Pet. Eng. Jour., Dec. 1962, p. 317
8. Green, B. W., Perry, R. H. and Babcock, R. E.: "Longitudinal Dispersion of Thermal Energy Through a Porous Media With a Flowing Fluid" A.I.Ch.E. Jour., vol 10 no. 5, Sept. 1964, p. 645
9. Perkins, T. K. and Johnston, O. C.: "A Review of Diffusion and Dispersion in Porous Media" Soc. Pet. Eng. Jour., March 1963, p. 70
10. Peaceman, D. W. and Rachford, H. H.: "Numerical Calculation of



- Multidimensional Miscible Displacement" Soc. Pet. Eng. Jour., Dec. 1962, p. 327
11. Chaudhari, N. M.: "An Improved Numerical Technique for Solving Multidimensional Miscible Displacement Equations" Soc. Pet. Eng. Jour., Sept. 1971, p. 277
  12. Laumbach, D.: "A High Accuracy Finite Difference Technique for Solving the Convection-Diffusion Equation" Soc. Pet. Eng. Jour., Dec. 1975, p. 517
  13. Awang, M. and Farouq Ali, S. M.: "Hot Solvent Miscible Displacement" presented at CIM, Calgary, June 1980
  14. Leventhal, Stephen H.: "The Operator Compact Method of Reservoir Simulation" Soc. Pet. Eng. Jour., June 1980, p. 120
  15. Reid, R., Prausnitz, J. and Sherwood, T.: The Properties of Liquids and Gases, McGraw Hill
  16. Anand, J., Somerton, W. H. and Gomaa, E.: "Predicting the Thermal Conductivities of Formations from Other Known Properties" Soc. Pet. Eng. Jour., Oct. 1973, p. 267
  17. Deston, A. P.: "On the Dependence of Thermal Conductivity of Oil Sands on Pressure" Research Council of Alberta, Internal Report
  18. Perry, R. and Chilton, C. H., editors, Chemical Engineer's Handbook McGraw Hill, Fifth Edition
  19. Weist, R. C., editor, Handbook of Chemistry and Physics, CRC Press
  20. Wygal, R. J.: "Construction of Models that Simulate Oil Reservoirs" Soc. Pet. Eng. Jour., Dec. 1963, p. 281
  21. Brigham, W. E.: "Mixing Equations in Short Laboratory Cores" Soc. Pet. Eng. Jour., Feb. 1974, p. 91
  22. Miller, C. A. and Jain, K.: "Stability of Fluid Systems with Heat



- and Mass Transport - Stability in the Absence of Surface Tension Effects" Chemical Engineering Science, 28, p. 157 (1973)
23. Miller, Clarence A.: "Stability of Moving Surfaces in Fluid Systems with Heat and Mass Transport - Combined Effects of Transport and Density Difference Between Phases" AIChE Journal, Sept. 1973, vol. 19 no. 5, p. 909
  24. Miller, Clarence A.: "Stability of Moving Surfaces in Fluid Systems with Heat and Mass Transport - Stability of Displacement Fronts in Porous Media" AIChE Journal, May 1975, vol. 21 no. 3, p. 474
  25. Kasraie, Mahnaz: "Influence of Rate and Various Immobile Fluid Saturations on Convective Mixing in a Porous Medium" M.Sc. Thesis Pennsylvania State University, Aug. 1979
  26. Chuoke, R. L., van Meurs, P. and van der Pol, C.: "A Theoretical Description of a Water Drive Process Involving Viscous Fingering", Trans. AIME (1959), 216, p. 188-194
  27. Peaceman, D. W.: Numerical Reservoir Simulation Elsevier North-Holland (1977)
  28. Farouq Ali, S. M.: Mineral Engineering 577 Lecture Notes (1977)



## VII. APPENDIX A

### A. Inspectional Analysis of Miscible Displacement

#### i. Differential Equations

##### 1. Fluid Displacement Equation

$$\frac{\partial}{\partial x} \left( k_d \frac{\partial (\rho C)}{\partial x} \right) - \frac{\partial (v \rho C)}{\partial x} = \frac{\partial (\phi \rho C)}{\partial t}$$

##### 2. Heat Transfer Equation

$$\frac{\partial}{\partial x} \left( k_h \frac{\partial T}{\partial x} \right) - \frac{\partial (\rho v c_p T)}{\partial x} = \frac{\partial [((1-\phi)\rho_r c_{p_r} + \phi \rho c_p) T]}{\partial t}$$

##### 3. Darcy's Law

$$\phi \frac{\partial x}{\partial t} = - \frac{k}{\mu} \left( \frac{\partial p}{\partial x} + \Delta \rho g \right) \quad \text{where } \phi \frac{\partial x}{\partial t} \text{ is the fluid velocity } v$$

##### 4. Dispersion Equation

$$k_d = \sigma v d_p + \frac{D_0}{f\phi}$$

#### ii. Boundary Conditions:

1.  $T(x,0)=T_0$  for all  $x$
2.  $T(0,t)=T_1$  for all  $t > 0$
3.  $T(x,\infty)=T_1$  for all  $x$
4.  $C(x,0)=0$  for all  $x$
5.  $C(0,t)=C_1$  for all  $t > 0$
6.  $C(x,\infty)=C_1$  for all  $x$
7.  $p(L,t)=0$  for all  $t$

#### iii. Define Dimensionless Variables

$$T^* = \frac{T-T_0}{T_1-T_0}$$

$$C^* = \frac{C}{C_1} = C$$



$$\varepsilon = \frac{x}{X_0}$$

$$\tau = \frac{t}{t_0}$$

$$p^* = \frac{P}{P_1}$$

where  $X_0$  and  $t_0$  are arbitrary values

iv. Substitute Dimensionless Variables into Equations and Simplify:

$$1. \quad \frac{\partial}{\partial \varepsilon X_0} \left( \frac{k_d \partial (\rho C^*)}{\partial \varepsilon X_0} \right) - \frac{\partial}{\partial \varepsilon X_0} (v \rho C^*) = \frac{\partial}{\partial \tau t_0} (\phi \rho C^*)$$

$$\frac{\partial C^*}{\partial \tau} = \frac{t_0 k_d}{\phi X_0^2} \frac{\partial^2 C^*}{\partial \varepsilon^2} - \frac{t_0 v}{\phi X_0} \frac{\partial C^*}{\partial \varepsilon}$$

$$2. \quad \frac{\partial}{\partial \varepsilon X_0} \left( k_h \frac{\partial}{\partial \varepsilon X_0} (T^*(T_1 - T_0) + T_0) \right) - \frac{\partial}{\partial \varepsilon X_0} (\rho c p v (T^*(T_1 - T_0) + T_0))$$

$$= \frac{\partial}{\partial \tau t_0} [T^*(T - T_0) ((1 - \phi) \rho_r c p_r + \phi \rho c p)]$$

$$\frac{\partial T^*}{\partial \tau} = \frac{k h t_0}{X_0^2} \frac{1}{[(1 - \phi) \rho_r c p_r + \phi \rho c p]} \frac{\partial^2 T^*}{\partial \varepsilon^2}$$

$$- \frac{t_0 v}{X_0} \frac{\rho c p}{(1 - \phi) \rho_r c p_r + \phi \rho c p} \frac{\partial T^*}{\partial \varepsilon}$$

$$3. \quad T(\varepsilon, 0) = T^* A + B = T_0$$

$$4. \quad T(0, \tau) = T^* A + B = T_1$$

$$5. \quad C(\varepsilon, 0) = C^* = 0$$

$$6. \quad C(0, \tau) = C^* = 1$$

$$7. \quad T(\varepsilon, \infty) = T^* A + B = T_1$$

$$8. \quad C(\varepsilon, \infty) = C^* = 1$$

$$9. \quad \phi \frac{\partial \varepsilon X_0}{\partial \tau t_0} = \frac{k}{\mu} \left( \frac{\partial p^* p_1}{\partial \varepsilon X_0} - \Delta \rho g \right)$$

$$\frac{\partial \varepsilon}{\partial \tau} = \frac{k}{\mu} \frac{t_0 p_1}{X_0^2 \phi} \frac{\partial p^*}{\partial \varepsilon} - \frac{k \Delta \rho g t_0}{\mu X_0 \phi}$$



or

$$\frac{\partial p^*}{\partial \epsilon} = \frac{\mu X_0 v}{k P_1} + \frac{\Delta \rho g X_0}{p_1}$$

$$10. \quad \sigma = \frac{k_d}{v d_p} - \frac{D_0}{v d_p}$$

v. Equate all Dimensionless Parameters to Unity:

$$1. \quad \frac{t_0 k_d}{\phi X_0^2} = 1$$

$$2. \quad \frac{t_0 v}{\phi X_0} = 1$$

$$3. \quad \frac{t_0 k_h}{X_0^2} \frac{1}{(\phi \rho c_p + (1-\phi) \rho_r c_{p_r})} = 1$$

$$4. \quad \frac{t_0 v}{X_0} \frac{\rho c_p}{((1-\phi) \rho_r c_{p_r} + \phi \rho c_p)} = 1$$

$$5. \quad \frac{k t_0 p_1}{\mu X_0^2 \phi} = 1$$

$$6. \quad \frac{k \Delta \rho g t_0}{\mu X_0 \phi} = 1$$

$$7. \quad \frac{k_d}{v d_p} = 1$$

$$8. \quad \frac{D_0}{v d_p} = 1$$

vi. Results:

If we assume that  $X_0 = L$ :

$$1. \quad t_0 = \frac{\phi L^2}{k_d}$$



$$\tau_1 = \frac{tk_d}{\phi L^2}$$

$$2. \quad t_0 = \frac{\phi L}{v}$$

$$\tau_2 = \frac{tv}{\phi L}$$

$$3. \quad t_0 = \frac{L^2((1-\phi) \rho_r c_{p_r} + \phi \rho c_p)}{k_h}$$

$$\tau_3 = \frac{tk_h}{L^2} \frac{1}{((1-\phi) \rho_r c_{p_r} + \phi \rho c_p)}$$

$$4. \quad t_0 = \frac{x_0}{v} \frac{((1-\phi) \rho_r c_{p_r} + \phi \rho c_p)}{\rho c_p}$$

$$\tau_4 = \frac{tv}{L} \frac{\rho c_p}{((1-\phi) \rho_r c_{p_r} + \phi \rho c_p)}$$

$$5. \quad t_0 = \frac{\mu L^2 \phi}{k \Delta p}$$

$$\tau_5 = \frac{tk \Delta p}{\mu L^2 \phi}$$

$$6. \quad t_0 = \frac{\mu L \phi}{k \Delta \rho g}$$

$$\tau_6 = \frac{tk \Delta \rho g}{\mu L \phi}$$

If we wish to solve for x:

1. combine 1 and 2:

$$x_0 = \frac{k_d}{v}$$



$$\varepsilon_1 = \frac{Xv}{k_d}$$

2. combine 1 and 4:

$$X_0 = \frac{k_d}{\phi v} \frac{(1-\phi) \rho_r c p_r + \phi \rho c p}{\rho c p}$$

$$\varepsilon_2 = \frac{Xv}{k_d} \frac{\phi \rho c p}{(1-\phi) \rho_r c p_r + \phi \rho c p}$$

3. combine 1 and 6:

$$X_0 = \frac{k_d \mu}{k \Delta \rho g}$$

$$\varepsilon_3 = \frac{X k \Delta \rho g}{k_d \mu}$$

4. combine 3 and 2:

$$X_0 = \frac{\phi k_h}{v} \frac{1}{(1-\phi) \rho_r c p_r + \phi \rho c p}$$

$$\varepsilon_4 = \frac{Xv}{k_h} \frac{\phi \rho c p + (1-\phi) \rho_r c p_r}{\phi}$$

5. combine 3 and 4:

$$X_0 = \frac{k_h}{v} \frac{1}{\rho c p}$$

$$\varepsilon_5 = \frac{Xv}{k_h} \frac{\rho c p}{1}$$

6. combine 3 and 6:

$$X_0 = \frac{k_h \mu}{\Delta \rho g k} \frac{\phi}{(1-\phi) \rho_r c p_r + \phi \rho c p}$$

$$\varepsilon_6 = \frac{X \Delta \rho g k}{k_h \mu} \frac{(1-\phi) \rho_r c p_r + \phi \rho c p}{\phi}$$



7. combine 5 and 2:

$$X_0 = \frac{k\Delta P}{\mu v}$$

$$\varepsilon_7 = \frac{Xv\mu}{k\Delta p}$$

8. combine 5 and 4:

$$X_0 = \frac{k\Delta p}{\mu v} \frac{\phi \rho c p + (1-\phi) \rho_r c p_r}{\phi \rho c p}$$

$$\varepsilon_8 = \frac{Xv\mu}{k\Delta p} \frac{\phi \rho c p}{\phi \rho c p + (1-\phi) \rho_r c p_r}$$

9. combine 5 and 6:

$$X_0 = \frac{\Delta p}{\Delta \rho g}$$

$$\varepsilon_9 = \frac{\Delta \rho g X}{\Delta p}$$

- vii. Scaling Results from Groups Obtained:

Let L be Scaled by a Factor of A

Let X=L

1. from  $\tau_3$ ,  $\frac{t_2}{t_1} = A^2$  (assume  $k_{h2} = k_{h1}$ )
2. from  $\tau_2$ ,  $\frac{v_2}{v_1} = \frac{1}{A}$
3. from  $\tau_1$ ,  $\frac{k_{d2}}{k_{d1}} = 1$
4. from  $\tau_6$ ,  $\frac{k_2}{k_1} = \frac{1}{A}$  (assume  $\mu_1 = \mu_2$ ,  $\Delta \rho_1 = \Delta \rho_2$ )



5. from  $\tau_5$ ,  $\frac{\Delta p_2}{\Delta p_1} = A$
6. from  $\varepsilon_9$ ,  $\frac{\Delta p_2}{\Delta p_1} = A$  (assume  $\Delta p_1 = \Delta p_2$ )
7. from  $\varepsilon_6$ ,  $\frac{k_2}{k_1} = \frac{1}{A}$  (assume  $\Delta p_1 = \Delta p_2$ )
8. from  $\varepsilon_7$ ,  $\frac{v_2}{v_1} = \frac{1}{A}$  (assume  $k_{h1} = k_{h2}$ )
9. from  $\varepsilon_3$ ,  $\frac{k_{d2}}{k_{d1}} = 1$
10. from  $\frac{k_d}{v d_p}$ ,  $\frac{dp_2}{dp_1} = A$
11. from  $\frac{D_0}{v d_p}$ ,  $\frac{dp_2}{dp_1} = A$

Note:

1. Group 9 conflicts with the other scaling groups as illustrated by groups 10 and 11.
2. The equation used is one-dimensional, therefore the geometric scaling groups do not appear.

## B. Dimensional Analysis of Non-Isothermal Miscible Displacement

### i. Variables

L	length	cm
d	diameter	cm
$\mu$	viscosity	gm/cm s
cp	fluid specific heat	J/gm K
$\rho$	fluid density	gm/cm <sup>3</sup>



$k_d$	dispersion coefficient	$\text{cm}^2/\text{s}$
$v$	fluid velocity	$\text{cm}/\text{s}$
$\Delta p$	pressure drop	$\text{gm}/\text{cm s}^2$
$\Delta T$	temperature differential	K
$g$	gravity	$\text{cm}/\text{s}^2$
$k$	permeability	$\mu\text{m}^2$
$k_h$	matrix thermal conductivity	$\text{J}/\text{cm K s}$

ii. Matrix of Variables

	1	2	3	4	5	6	7	8	9	10	11	12
	L	$\mu$	g	cp	$k_d$	k	$k_h$	$\Delta p$	d	v	$\Delta T$	$\rho$
M	0	1	0	0	0	0	1	1	0	0	0	1
L	1	-1	1	2	2	2	1	-1	1	1	0	-3
t	0	-1	-2	-2	-1	0	-3	-2	0	-1	0	0
$\Delta T$	0	0	0	-1	0	0	-1	0	0	0	1	0

iii. Determinant of Matrix to Far Right of Matrix of Variables

$$\begin{vmatrix} 0 & 0 & 0 & 1 \\ 1 & 1 & 0 & -3 \\ 0 & -1 & 0 & 0 \\ 0 & 0 & 1 & 0 \end{vmatrix}$$

$$D=1$$

iv. Number of Dimensionless Groups Obtained

$$N=n-r$$

where

n = number of independant variables



r = number of dimensions required to express them

$N=12-4=8$

v. Coefficient Equations

M :  $A_2+A_7+A_8+A_{12} = 0$

L :  $A_1-A_2+A_3+2A_4+2A_5+2A_6+A_7-A_8+A_9+A_{10}-3A_{12} = 0$

t :  $-A_2+2A_3-2A_4-A_5-3A_7-2A_8-A_{10} = 0$

$\Delta T$ :  $-A_4-A_7-A_{11} = 0$

vi. Solution of Coefficient Equations

$A_{12} = -A_2-A_7-A_8$

$A_{11} = A_7+A_4$

$A_{10} = -A_2-2A_3-2A_4-A_5-3A_7-2A_8$

$A_9 = -A_1-A_2+A_3-A_5-2A_6-A_7$

vii. Matrix of Solutions

	1	2	3	4	5	6	7	8	9	10	11	12
	L	$\mu$	g	cp	$k_d$	k	$k_h$	$\Delta p$	d	v	$\Delta T$	$\rho$
1	1								-1	0	0	0
2		1							-1	-1	0	-1
3			1						1	-2	0	0
4				1					0	-2	1	0
5					1				-1	-1	0	0
6						1			-2	0	0	0
7							1		-1	-3	1	-1
8								1	0	-2	0	-1

viii.Dimensionless Groups Obtained

1.  $\frac{L}{d}$



$$2. \quad \frac{\mu}{v d \rho}$$

$$3. \quad \frac{g d}{v^2}$$

$$4. \quad \frac{c_p \Delta T}{v^2}$$

$$5. \quad \frac{k_d}{d v}$$

$$6. \quad \frac{k}{d^2}$$

$$7. \quad \frac{k_h \Delta T}{\rho d v^3}$$

$$8. \quad \frac{\Delta p}{\rho v^2}$$

ix. Modify Groups to Obtain Meaningful Results

Assume:

$$\frac{\rho_2}{\rho_1} = \frac{c_{p2}}{c_{p1}} = \frac{g_2}{g_1} = \frac{k_{h2}}{k_{h1}} = 1$$

Assume that kinetic energy is negligible, therefore groups must be arranged so that kinetic energy terms do not appear explicitly. Also, since we desire that  $t_{\text{model}}$  be smaller than  $t_{\text{field}}$ , we do not wish to have the dimensionless permeability group to appear.

Useful groups are:

$$1. \quad \frac{L}{d}$$

$$2. \quad \frac{k_d}{L v}$$



$$3. \frac{k_h}{\rho c p v L}$$

$$4. \frac{\Delta p}{\rho g L}$$

$$5. \frac{\rho g k}{v \mu}$$

$$6. \frac{\rho c p \Delta T}{\Delta p}$$

$$7. \frac{g k}{d v^2}$$

Note: If heat transfer and mass transfer are not strongly coupled, group 6 may be ignored.

x. Results:

$$\text{let } \frac{L_2}{L_1} = A$$

$$\text{from 1 } \frac{d_2}{d_1} = A$$

$$\text{from 3 } \frac{v_2}{v_1} = \frac{1}{A}$$

$$\text{from 2 } \frac{k d_2}{k d_1} = 1$$

$$\text{from 4 } \frac{\Delta p_2}{\Delta p_1} = 1$$

$$\text{from 7 } \frac{k_2}{k_1} = \frac{1}{A}$$

$$\text{from 5 } \frac{\mu_2}{\mu_1} = 1$$



Fluid groups must also be duplicated if two fluids are used.

$$\frac{\mu_{s1}}{\mu_{01}} = \frac{\mu_{s2}}{\mu_{02}}$$

$$\frac{\rho_{s1}}{\rho_{01}} = \frac{\rho_{s2}}{\rho_{02}}$$

$$\frac{cp_{s1}}{cp_{01}} = \frac{cp_{s2}}{cp_{02}}$$



## VIII. APPENDIX B

### Development of Finite Difference Equations from Differential Equations

#### A. Convection-Diffusion Equation

$$\frac{\partial}{\partial x} \left( k_d \frac{\partial (\rho C)}{\partial x} \right) - \frac{\partial (v \rho C)}{\partial x} = \frac{\phi \partial (\rho C)}{\partial t}$$

may be modified to yield: (ignore cross derivatives)

$$k_d \frac{\rho \partial^2 C}{\partial x^2} + \left( \frac{\rho \partial k_d}{\partial x} + 2k_d \frac{\partial \rho(T)}{\partial x} - v \rho \right) \frac{\partial C}{\partial x} = \phi \rho \frac{\partial C}{\partial t}$$

where

$$\frac{\partial \rho(T)}{\partial x} = \frac{\partial \rho}{\partial T} \frac{\partial T}{\partial x}$$

The semi implicit finite difference formula is:

$$\begin{aligned} & \frac{k_d \rho}{2\Delta x^2} (C_{i-1}^{n+1} - 2C_i^{n+1} + C_{i+1}^{n+1} + C_{i-1}^n - 2C_i^n + C_{i+1}^n) \\ & + \left( \frac{\rho \partial k_d}{\partial x} + 2k_d \frac{\partial \rho(T)}{\partial x} - v \rho \right) \frac{1}{4\Delta x} (C_{i+1}^{n+1} - C_{i-1}^{n+1} + C_{i+1}^n - C_{i-1}^n) \\ & = \frac{\phi \rho}{\Delta t} (C_i^{n+1} - C_i^n) + \epsilon \end{aligned}$$

The truncation error from a Taylor series expansion is:

$$\begin{aligned} \epsilon &= \left( \frac{\rho \partial k_d}{\partial x} + 2k_d \frac{\partial \rho(T)}{\partial x} - v \rho \right) \frac{\Delta t^2}{8} \frac{\partial^3 C}{\partial x \partial t^2} \\ &+ \left( \frac{\rho \partial k_d}{\partial x} + 2k_d \frac{\partial \rho(T)}{\partial x} - v \rho \right) \frac{\Delta x^2}{6} \frac{\partial^3 C}{\partial x^3} \\ &- \rho \phi \frac{\Delta t^2}{24} \frac{\partial^3 C}{\partial t^3} \end{aligned}$$

rearrange:



$$\begin{aligned} \varepsilon = & \left( \left( \frac{\rho \partial k_d}{\partial x} + 2k_d \frac{\partial \rho(T)}{\partial x} - v\rho \right) \frac{v\Delta t^2}{-8\phi} \right. \\ & - \left( \frac{\rho \partial k_d}{\partial x} + 2k_d \frac{\partial \rho(T)}{\partial x} - v\rho \right) \frac{\phi \Delta x^2}{6v} \\ & \left. - \frac{v^2 \rho \Delta t^2}{24\phi} \right) \frac{\partial^3 C}{\partial x^2 \partial t} \end{aligned}$$

This is similar to Laumbach's truncation error term.

Let

$$\varepsilon = BB' \frac{\partial^3 C}{\partial x^2 \partial t}$$

or

$$\varepsilon = \frac{BB'}{\Delta x^2 \Delta t} (C_{i-1}^{n+1} - 2C_i^{n+1} + C_{i+1}^n - C_{i-1}^n + 2C_i^n - C_{i+1}^n)$$

let

$$BB = \frac{BB'}{\Delta x^2 \Delta t}$$

let

$$\begin{aligned} BB = & \frac{-v^2 \Delta t}{24\phi \Delta x^2} - \left( \frac{\rho \partial k_d}{\partial x} + 2k_d \frac{\partial \rho(T)}{\partial x} - v\rho \right) \frac{v\Delta t}{8\phi \Delta x^2} \\ & - \left( \frac{\rho \partial k_d}{\partial x} + 2k_d \frac{\partial \rho(T)}{\partial x} - v\rho \right) \frac{\phi}{6v\Delta t} \end{aligned}$$

let

$$AA = \frac{\phi \rho}{\Delta t}$$

let

$$CC = \frac{k_d \rho}{2\Delta x^2}$$



let

$$DD = \left( \frac{\rho \partial k_d}{\partial x} + 2k_d \frac{\partial \rho(T)}{\partial x} - v\rho \right) \frac{1}{4\Delta x}$$

rewrite the equation:

$$\begin{aligned} & AA(C_i^{n+1} - C_i^n) + BB(C_{i-1}^{n+1} - 2C_i^{n+1} + C_{i+1}^{n+1} - C_{i-1}^n + 2C_i^n - C_{i+1}^n) \\ &= CC(C_{i-1}^{n+1} - 2C_i^{n+1} + C_{i+1}^{n+1} + C_{i-1}^n - 2C_i^n + C_{i+1}^n) \\ &+ DD(C_{i+1}^{n+1} - C_{i-1}^{n+1} + C_{i+1}^n - C_{i-1}^n) \end{aligned}$$

or

$$AC_{i-1}^n + BC_i^n + CC_{i+1}^n = DC_{i-1}^{n+1} + EC_i^{n+1} + FC_{i+1}^{n+1}$$

for any point within the system.

At the inlet node, the system is supplied by a source of strength  $v\rho$ ;  $C_{inlet} = \text{constant} = C_1$  where  $C_{inlet}$  is a fluid source. If  $C$  is fixed at the inlet boundary, the equation at node two becomes:

$$\begin{aligned} & AA(C_2^{n+1} - C_2^n) + BB(-2C_2^{n+1} + C_3^{n+1} + 2C_2^n - C_3^n) \\ &= CC(C_3^{n+1} - 2C_2^{n+1} + C_3^n - 2C_2^n + 2C_1^n) + DD(C_3^{n+1} - 2C_2^{n+1} + C_3^n - 2C_2^n + 2C_1^n) \end{aligned}$$

Rewrite the equation:

$$A' \cdot C_1^n + B' C_2^n + CC_3^n = EC_2^{n+1} + FC_3^{n+1}$$

where

$$A' = \frac{2DD - 2CC}{2CC - AA} \quad B' = \frac{-AA - 2BB + 2CC}{2CC - AA}$$



At the outlet boundary the system is closed to diffusion but is open to mass transport via fluid convection. The convection-diffusion equation at the outlet becomes:

$$AA(C_i^{n+1} - C_i^n) + BB(2C_{i-1}^{n+1} - 2C_i^{n+1} - 2C_{i-1}^n + 2C_i^n)$$

$$= CC(2C_{i-1}^{n+1} - 2C_i^{n+1} + 2C_{i-1}^n - 2C_i^n)$$

$$+ 2DD(-C_{i-1}^{n+1} + C_i^{n+1} + C_i^n - C_{i-1}^n)$$

Now let:

$$A'' = \frac{-2BB - 2CC + 2DD}{-AA + 2CC}$$

$$B'' = \frac{-AA + 2BB + 2CC - 2DD}{-AA + 2CC}$$

$$D'' = \frac{-2BB + CC - 2DD}{-AA + 2CC}$$

$$E'' = \frac{-AA + 2BB - 2CC + 2DD}{-AA + 2CC}$$

Rewrite the equations in the following form:

$$A''C_{i-1}^n + B''C_i^n = D''C_{i-1}^{n+1} + E''C_i^{n+1}$$

Arrange the system of equations in matrix form:

$$\begin{array}{lcl} A' C_1^n + BC_2^n + CC_3^n & = & \begin{vmatrix} C_2^{n+1} \\ C_3^{n+1} \\ C_i^{n+1} \\ C_i^{n+1} \end{vmatrix} \quad \begin{vmatrix} E' & F' & 0 & 0 \\ D & E & F & 0 \\ 0 & D & E & F \\ 0 & 0 & D'' & E'' \end{vmatrix} \\ A C_2^n + BC_3^n + CC_4^n & = & \\ A C_{i-1}^n + BC_i^n + CC_{i+1}^n & = & \\ A'' C_{i-1}^n + B'' C_i^n + 0 & = & \end{array}$$



The tridiagonal matrix thus formed may be solved by the Thomas Algorithm. A similar solution applies to the conduction-convection equation for the heat transfer problem.

## B. Heat Transfer Equation

$$\frac{\partial}{\partial x} \left( k_h \frac{\partial T}{\partial x} \right) - \frac{\partial}{\partial x} (\rho c_p v T) = \frac{\partial}{\partial t} ((1-\phi) \rho_r c_{p_r} + \phi \rho c_p) T$$

may be modified to obtain:

$$k_h \frac{\partial^2 T}{\partial x^2} + \left( \frac{\partial k_h}{\partial x} - \rho c_p v \right) \frac{\partial T}{\partial x} = \frac{\partial}{\partial t} ((\phi \rho c_p + (1-\phi) \rho_r c_{p_r}) T)$$

The semi-implicit finite difference approximation is:

$$\begin{aligned} & \frac{k_h}{2\Delta x^2} (T_{i-1}^{n+1} - 2T_i^{n+1} + T_{i+1}^{n+1} + T_{i-1}^n - 2T_i^n + T_{i+1}^n) \\ & + \frac{\partial k_h}{\partial x} - \rho c_p v \quad \frac{1}{4\Delta x} (T_{i+1}^{n+1} - T_{i-1}^{n+1} + T_{i+1}^n - T_{i-1}^n) \\ & = \frac{[M]}{\Delta t} (T_i^{n+1} - T_i^n) + \epsilon \end{aligned}$$

where

$$[M] = (\phi \rho c_p + (1-\phi) \rho_r c_{p_r})$$

The truncation error term obtained from a Taylor series expansion is:

$$\begin{aligned} \epsilon &= -[M] \frac{\Delta t^2}{24} \frac{\partial^3 T}{\partial t^3} + \left( \frac{\partial k_h}{\partial x} - v \rho c_p \right) \left( \frac{\Delta x^2}{6} \frac{\partial^3 T}{\partial x^3} + \frac{\Delta t^2}{8} \frac{\partial^3 T}{\partial x \partial t^2} \right) \\ \epsilon &= \left( \frac{-(v \rho c_p)^2}{[M]} \frac{\Delta t^2}{24} + \frac{[M] \Delta x^2}{\sigma v \rho c_p} \left( \frac{\partial k_h}{\partial x} - v \rho c_p \right) \right. \\ & \left. + \left( \frac{\partial k_h}{\partial x} - v \rho c_p \right) \frac{\Delta t^2}{8} \frac{v \rho c_p}{[M]} \right) \frac{\partial^3 T}{\partial x^2 \partial t} \end{aligned}$$



let

$$\epsilon = BB' \frac{\partial^3 T}{\partial x^2 \partial t}$$

or

$$\epsilon = \frac{BB'}{\Delta x^2 \Delta t} (T_{i-1}^{n+1} - 2T_i^{n+1} + T_{i+1}^{n+1} - T_{i-1}^n + 2T_i^n - T_{i+1}^n)$$

let

$$BB = \frac{BB'}{\Delta x^2 \Delta t}$$

let

$$BB = \left( \frac{[M]\Delta x^2}{v\rho cp} + \frac{\Delta t^2 v\rho cp}{8 [M]} \right) \left( \frac{\partial k_h}{\partial x} - v\rho cp \right) + \frac{-(v\rho cp)^2 \Delta t^2}{[M] 24}$$

let

$$AA = \frac{\phi\rho cp + (1-\phi)\rho_r cp_r}{\Delta t} = \frac{[M]}{\Delta t}$$

let

$$CC = \frac{k_h}{2\Delta x^2}$$

let

$$DD = \frac{v\rho cp}{4\Delta x}$$

rewrite the equation as for the convection-diffusion problem:

$$AT_{i-1}^n + BT_i^n + CT_{i+1}^n = DT_{i-1}^{n+1} + ET_i^{n+1} + FT_{i+1}^{n+1}$$

### C. Fluid Flow Equation in One Dimension

The mass balance for the total system is:



$$\frac{\partial(\rho v)}{\partial x} = -\frac{\phi \partial \rho}{\partial t}$$

This may be rewritten as the continuity equation for one dimensional non-isothermal flow:

$$\frac{v \partial \rho}{\partial x} + \frac{\rho \partial v}{\partial x} = \frac{-\phi \partial \rho}{\partial t}$$

where  $\rho = \rho(T)$

or

$$\frac{\partial \rho(T)}{\partial x} = \frac{\partial \rho}{\partial T} \frac{\partial T}{\partial x}$$

$$\frac{\partial \rho(T)}{\partial t} = \frac{\partial \rho}{\partial T} \frac{\partial T}{\partial t}$$

In finite difference form:

$$\begin{aligned} & \frac{(v_{i+\frac{1}{2}}^{n+1} + v_{i-\frac{1}{2}}^{n+1})}{2} \frac{\partial \rho}{\partial T} \frac{(T_{i+1}^{n+1} - T_{i-1}^{n+1})}{2\Delta x} + \rho_i^{n+1} \frac{(v_{i+\frac{1}{2}}^{n+1} - v_{i-\frac{1}{2}}^{n+1})}{\Delta x} \\ & = \frac{\phi \partial \rho}{\partial T} \frac{(T_i^{n+1} - T_i^n)}{\Delta t} \end{aligned}$$

This may be solved directly if velocity is given at node 1.

#### D. Pressure Equation

Derivation of the pressure equation for non-isothermal slightly compressible flow

for a slightly compressible fluid:

$$\frac{\partial(\rho v)}{\partial x} = -\phi \rho C \frac{\partial p}{\partial t} \quad \text{where } C \text{ is the fluid compressibility}$$

for a non-isothermal fluid flow:



$$\frac{\partial(\rho v)}{\partial x} = \frac{-\phi \partial \rho}{\partial t}$$

where  $\rho = \rho(T)$

combine the equations:

$$\frac{\partial(\rho(T)v)}{\partial x} = -\phi \left( \frac{\partial \rho(T)}{\partial t} + \rho C \frac{\partial p}{\partial t} \right)$$

Darcy's Law

$$v = \frac{-k}{\mu} \frac{\partial p}{\partial x}$$

Note: The gravity term is neglected as gravity forces are small compared to viscous forces at experimental flow rates.

$$\frac{\partial}{\partial x} \left( \rho(T) \frac{k}{\mu} \frac{\partial p}{\partial x} \right) = \phi \left( \frac{\partial \rho(T)}{\partial t} + \rho C \frac{\partial p}{\partial t} \right)$$

The change in density due to pressure is very small at experimental pressure drops, so the fluid density should be written as a function of temperature only. The dependence of fluid density on variables other than pressure complicates the problem in that it requires an iterative solution, as an analytical solution will become intractable.

Define transmissibility as follows:

$$\rho_{i-1/2} Tr_{i-1/2} = \frac{(\rho_{i-1} + \rho_i)}{2} \frac{2k}{(\mu_{i-1} + \mu_i) \Delta x}$$

Place pressure equation in finite difference form:

$$\begin{aligned} & \rho_{i+1/2} Tr_{i+1/2} (p_{i+1}^{n+1} - p_i^{n+1}) - \rho_{i-1/2} Tr_{i-1/2} (p_i^{n+1} - p_{i-1}^{n+1}) \\ &= \frac{\phi \Delta x}{\Delta t} ((p_i^{n+1} - p_i^n) \rho_i^{n+1} C + \frac{\partial \rho}{\partial T} (T_i^{n+1} - T_i^n)) \end{aligned}$$



### Boundary Conditions:

The boundary conditions common to both heat and mass transfer are as follows:

At the inlet:

$$C(0,t) = C_1 = 1$$

$$C(x,0) = 0$$

$$T(0,t) = T_1$$

$$T(x,0) = T_0$$

$$v(0,t) = v_1$$

At the outlet:

$$p(L,t) = 0$$

The equations used for the fluid and rock properties are as follows:

#### 1. Fluid Density

$$\rho = A + BT + CT^2 \quad \frac{\text{gm}^2}{\text{cm}^3}$$

The constants A, B and C were determined for each oil used by fitting a least squares curve to the densities measured at 22°C, 50°C and 70°C for each oil used.

#### 2. Density of Fluid Mixtures

$$\rho_m = \frac{1}{C_1/\rho_1 + (1-C_1)/\rho_2} \quad \frac{\text{gm}}{\text{cm}^3}$$

This is an adaptation of a specific volume formula found in "The Properties of Gases and Liquids" p. 86 (15).

#### 3. Fluid Viscosities

$$\mu = A \exp \left( \frac{B}{T} \right)$$

This correlation is known as Andrade's equation, (Ref. 15) p. 437. The constants A and B were determined by fitting the viscosities found in the manufacturer's literature to the equation.



#### 4. Viscosities of Mixtures

$$L_1 = \frac{1000 \ln 20}{\ln \mu_1 - \ln .0005}$$

$$L_m = C_1 L_1 + (1 - C_1) L_2$$

$$\mu_m = .0005 \exp \frac{1000 \ln 20}{L_m}$$

The correlation used by Awang (Cragoe's equation) and a logarithmic correlation (Equation 19-8, Ref. 15) were compared with viscosities measured with a Nametre viscometer for several oil mixtures. Cragoe's correlation (above) was considered to be more accurate, (Appendix F).

#### 5. Diffusivity of the Bulk Oil

$$D_o = Au^q \frac{\text{cm}^2}{\text{s}}$$

where  $q$  is valued between -0.5 and -1.0; from Ref. 15 p. 574.

#### 6. Dispersion Coefficient in Sand Pack

$$k_d = \frac{D_o}{F\phi} + 1.75 v_{dp} \frac{\text{cm}^2}{\text{s}}$$

This correlation was proposed by Blackwell(5). Brigham et al (4) noted that the dispersion coefficient  $k_d$  appeared to be a function of the mobility ratio. Therefore the dispersion coefficient was defined as follows:

$$k_d = \frac{D_o}{F\phi} + 1.75 v_{dp} M \frac{\text{cm}^2}{\text{s}}$$



## 7. Thermal Conductivity of Sand Pack

$$k_{ht} = .0189 - .000017T \frac{J}{cm \cdot s \cdot ^\circ C}$$

From data of Anand, et al (15). The properties of Boise sandstone were assumed to be similar to that of the sand pack. The value obtained here is slightly higher than the value obtained for tar sand by Deston(17). These values were considered useful approximations as no correlations for heat transfer in unconsolidated sand packs saturated with refined oils were available.

## 8. Thermal Diffusivity of Sand Pack

$$k_h = k_{ht} + .1728(vd_p)^{1.4} \frac{J}{cm \cdot s \cdot ^\circ C}$$

This equation was proposed by Green et al(8) as a best fit of the data they obtained for thermal diffusion in an unconsolidated sand pack.

## 9. Mobility Ratio

This is defined as the oil viscosity at the  $i+1/2$  node divided by the viscosity at the  $i-1/2$  node. This ratio can be approximated by:

$$M = \frac{\mu_{i+1} + \mu_i}{\mu_{i-1} + \mu_i}$$

## 10. Heat Capacity of Oil

The "Chemical Engineer's Handbook"(18) p.3-136 lists the following correlation for the thermal capacity of oils:

$$c_p = \frac{1.778}{\sqrt{\rho_{15}}} + .00377 (T-15) \frac{J}{gm^\circ C}$$



$\rho_{15}$  is the oil density at a reference temperature, (15°C).

#### 11. Heat Capacity of Rock

The specific heat of quartz can be determined from a correlation found in Ref. (19) p. f-68:

$$c_{pr} = .753 + .0025T \quad \frac{\text{J}}{\text{gm}^\circ\text{C}}$$

#### 12. Rock Density

A formula for the density of quartz may be obtained by combining data from Ref.(19) p. f-68 and Ref.(18) p. 3-20:

$$\rho_r = 2.645 - 5.5 \times 10^{-7}T \quad \frac{\text{gm}}{\text{cm}^3}$$



## IX. APPENDIX C

### A. Stability Analysis

A stability analysis of the Truncation Cancellation Procedure via the Karplus Criterion (28):

1. Write the equation in the form used by the matrix solution:

$$\begin{aligned}
 & AA(C_i^{n+1} - C_i^n) + BB(C_{i-1}^{n+1} - 2C_i^{n+1} + C_{i+1}^{n+1} - C_{i-1}^n + 2C_i^n - C_{i+1}^n) \\
 & = CC(C_{i-1}^{n+1} - 2C_i^{n+1} + C_{i+1}^{n+1} + C_{i-1}^n - 2C_i^n + C_{i+1}^n) \\
 & + DD(C_{i+1}^{n+1} - C_{i-1}^{n+1} + C_{i+1}^n - C_{i-1}^n)
 \end{aligned}$$

Rearrange

$$\begin{aligned}
 & AA(C_i^{n+1} - C_i^n) + BB(C_{i-1}^{n+1} - C_i^n) - 2BB(C_i^{n+1} - C_i^n) \\
 & + BB(C_{i+1}^{n+1} - C_i^n) - BB(C_{i-1}^n - C_i^n) - BB(C_{i+1}^n - C_i^n) \\
 & - CC(C_{i-1}^{n+1} - C_i^n) + 2CC(C_i^{n+1} - C_i^n) - CC(C_{i+1}^{n+1} - C_i^n) \\
 & - CC(C_{i-1}^n - C_i^n) - CC(C_{i+1}^n - C_i^n) - DD(C_{i+1}^{n+1} - C_i^n) \\
 & + DD(C_{i-1}^{n+1} - C_i^n) - DD(C_{i+1}^n - C_i^n) + DD(C_{i-1}^n - C_i^n) = 0
 \end{aligned}$$

Terms will cancel to yield the stability criterion:

$$-AA + 2BB + 2CC = 0$$

When the isothermal case is considered; the stability criterion becomes:

$$\frac{-2\phi\rho}{3\Delta t} + \frac{v^2\rho\Delta t}{6\phi\Delta x^2} + \frac{k_d\rho}{\Delta x^2} \leq 0$$

or



$$\frac{-2\phi\rho}{3} + \frac{v^2\rho\Delta t^2}{6\phi\Delta x^2} + \frac{k_d\rho\Delta t}{\Delta x^2} \leq 0$$

For a typical experiment:

$$\phi = .328$$

$$\rho = .87 \text{ gm/cm}^3$$

$$v = .00561 \text{ cm/s}$$

$$\Delta x = 4.0 \text{ cm}$$

$$k_d = .0030 \text{ cm}^2/\text{s}$$

-  $.1902 + .8696 \times 10^{-6} \Delta t^2 + .000163 \Delta t < 0$ . The system is stable for  $\Delta t < 300 \text{ s}$ .

Actual instability occurs at  $\Delta t = 240 \text{ s}$ .



## X. APPENDIX D

### A. Heat Transfer Calculations for Miscible Displacement Test Core

Heat Transfer Through Sand

$k_{ht} = .865 \text{ W/m } ^\circ\text{K} (0.5 \text{ btu/hr ft } ^\circ\text{F})$  (Green, Perry & Babcock, Ref. 8)

$$Q_{sand} = (K_{ht} A \Delta T)/d$$

$$Q_{sand} = .865 .00492 \text{ 70}/.0792$$

$Q_{sand} = 3.77 \text{ W} (7.13 \text{ btu/hr})$  where  $d$  is the core diameter in m

$K_{sleeve} = 16.5 \text{ W/m } ^\circ\text{K} (9.5 \text{ btu/hr ft } ^\circ\text{F})$  for 316 stainless steel

$$Q_{sleeve} = 16.5 .000113 \text{ 70}/.0792$$

$q_{sleeve} = 1.64 \text{ W} (3.12 \text{ btu/hr})$  for a .018" wall stainless steel sleeve

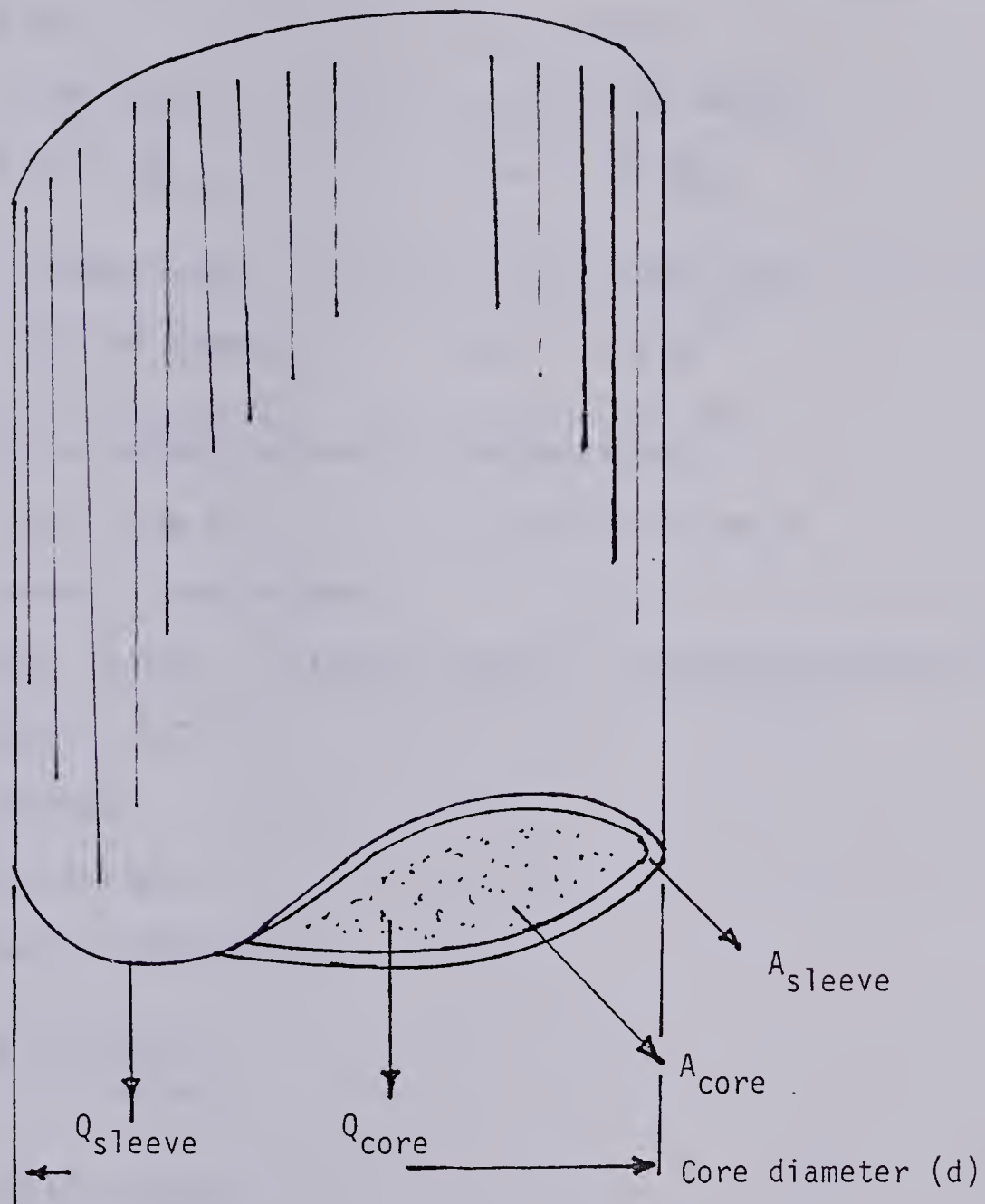
for a .010" thick stainless sleeve,  $Q_{sleeve} = .91 \text{ W}$

$$\text{for a .010" sleeve, } Q_{sleeve}/Q_{sand} = .24$$

The .010" sleeve chosen in order to minimize the contribution of the sleeve to total heat conduction, and to allow the overburden pressure used to act on the core.



Figure 28 Core Heat Transfer Problem



$\frac{Q_{\text{sleeve}}}{Q_{\text{core}}}$  must be small for experimental accuracy



## XI. APPENDIX E

### A. Miller Stability Criterion for Stable Thermal Displacement Front

$$T_1 = 25^\circ\text{C}$$

$$T_2 = 90^\circ\text{C}$$

$$\rho_1 = .888 \text{ gm/cm}^3$$

$$\rho_2 = .847 \text{ gm/cm}^3$$

$$\mu_1 = 8.00 \frac{\text{gm}}{\text{cm s}}$$

$$\mu_2 = .34 \frac{\text{gm}}{\text{cm s}}$$

$$v_1 = .00540 \text{ cm/s}$$

$$v_2 = .00561 \text{ cm/s}$$

$$k_1 = 100 \text{ um}^2 \text{ (darcys)}$$

$$k_2 = 100 \text{ um}^2$$

$$k_{h2} = .020 \text{ J/cm s } ^\circ\text{C}$$

$$v_2 = .005 \text{ cm/s}$$

(relative velocity of rock to thermal front)

$$cp_1 = 2.01 \text{ J/gm } ^\circ\text{C}$$

$$cp_2 = 2.25 \text{ J/gm } ^\circ\text{C}$$

The system is stable when:

(gravity forces) + (viscous forces) - (stabilizing effect of heat transfer) > 0.0

Gravity term

$$- (\rho_2 - \rho_1) g \alpha$$

$$= (.847 - .888) 981.0 \alpha$$

$$= + 40.18 \alpha \frac{\text{gm}}{\text{cm}^3 \text{ sec}^2}$$

$$= + 40.18 \alpha \frac{\text{dynes}}{\text{cm}^2}$$

Viscosity term

$$\left( - \frac{\mu_1 v_1}{k_1} + \frac{\mu_2 v_2}{k_2} \right) \alpha \cdot 10^8$$

$$= -41,200 \alpha \frac{\text{dynes}}{\text{cm}^2}$$

Thermal stability



$$- \left( \frac{\mu_1}{\rho_1 k_1} + \frac{\mu_2}{\rho_2 k_2} \right) \frac{k_h \gamma (\gamma_2 - \gamma) (T_1 - T_2)}{H_1 - H_2 - c p_2 (T_1 - T_2) \frac{(\gamma_2 - \gamma)}{\alpha}} 10^8$$

$$= - \left( \frac{8.00}{.888 \times 100} + \frac{.34}{.847 \times 100} \right) \frac{.020 \gamma (\gamma_2 - \gamma) (-65)}{-127.32 - 2.25 (-65) \frac{(\gamma_2 - \gamma)}{\alpha}} 10^8$$

$$\gamma = \frac{\rho_2 c p_2}{K_h} \phi \left( v - \frac{v_2}{\phi} \right) + \frac{\rho_r c p_r (1 - \phi) v}{K_h} = \frac{\text{convective heat transfer}}{\text{conductive heat transfer}}$$

$$\gamma = -.722$$

$$\gamma_2 = \frac{\gamma}{2} + \sqrt{\alpha^2 + \frac{\gamma^2}{4}}$$

$$\gamma_2 = .5096 \text{ or } \gamma_2 = .175 \text{ for } \lambda = 2. d_{\text{sandpack}} \text{ or } \lambda = d_{\text{sandpack}}$$

$$\alpha = \frac{2\pi}{\lambda} \quad (\lambda \text{ is the largest probable wave length})$$

$$\alpha = .7923 \text{ or } \alpha = .3961$$

Gravity forces

$$- (\rho_2 - \rho_1) g \alpha$$

$$= +15.9 \text{ dynes/cm}^2$$

Viscous forces

$$\alpha \left( - \frac{\mu_1 v_1}{k_1} + \frac{\mu_2 v_2}{k_2} \right) 10^8$$

$$= - 16310. \frac{\text{dynes}}{\text{cm}^2}$$

Stability due to heat transfer

$$- \left( \frac{\mu_1}{\rho_1 k_1} + \frac{\mu_2}{\rho_2 k_2} \right) \frac{k_h \gamma (\gamma_2 - \gamma) (T_1 - T_2)}{H_1 - H_2 - c p_2 (T_1 - T_2) \frac{(\gamma_2 - \gamma)}{\alpha}} 10^8$$

$$= 33,324. \frac{\text{dynes}}{\text{cm}^2} \quad \text{assuming } \alpha = .3961$$



The sum of the forces is:

$$+ 17,020. \frac{\text{dynes}}{\text{cm}^2}$$

The thermal front is therefore stable.

However, the displacement front travels faster than the thermal front and is therefore isothermal. The displacement front stability criterion is simplified from Miller's criterion to yield:

$$\left( -\frac{\mu_1 v_1}{k_1} + \frac{\mu_2 v_2}{k_2} \right) 10^8 \alpha - (\rho_2 - \rho_1) g \alpha > 0$$

For Harmony 44 displacing Harmony 87:

$$\begin{aligned} & \left( -\frac{2.56 \times 0.0056}{100} + \frac{.25 \times 0.0056}{100} \right) 10^8 (.3961) - (.848 - .869) 981 (.3961) \\ & = -5098 \frac{\text{dynes}}{\text{cm}^2} \end{aligned}$$

Therefore the displacement front is unstable at experimental velocities.



## XII. APPENDIX F

### Raw Data and Data Work-Up

This section contains a numerical simulation flow chart, an illustration of experimental strategy, examples of probability plots for experimental and numerical results, and a summary of raw data. Examples of refractive index and viscosity calibration curves are also included.



Figure 29 Flowchart of Numerical Program

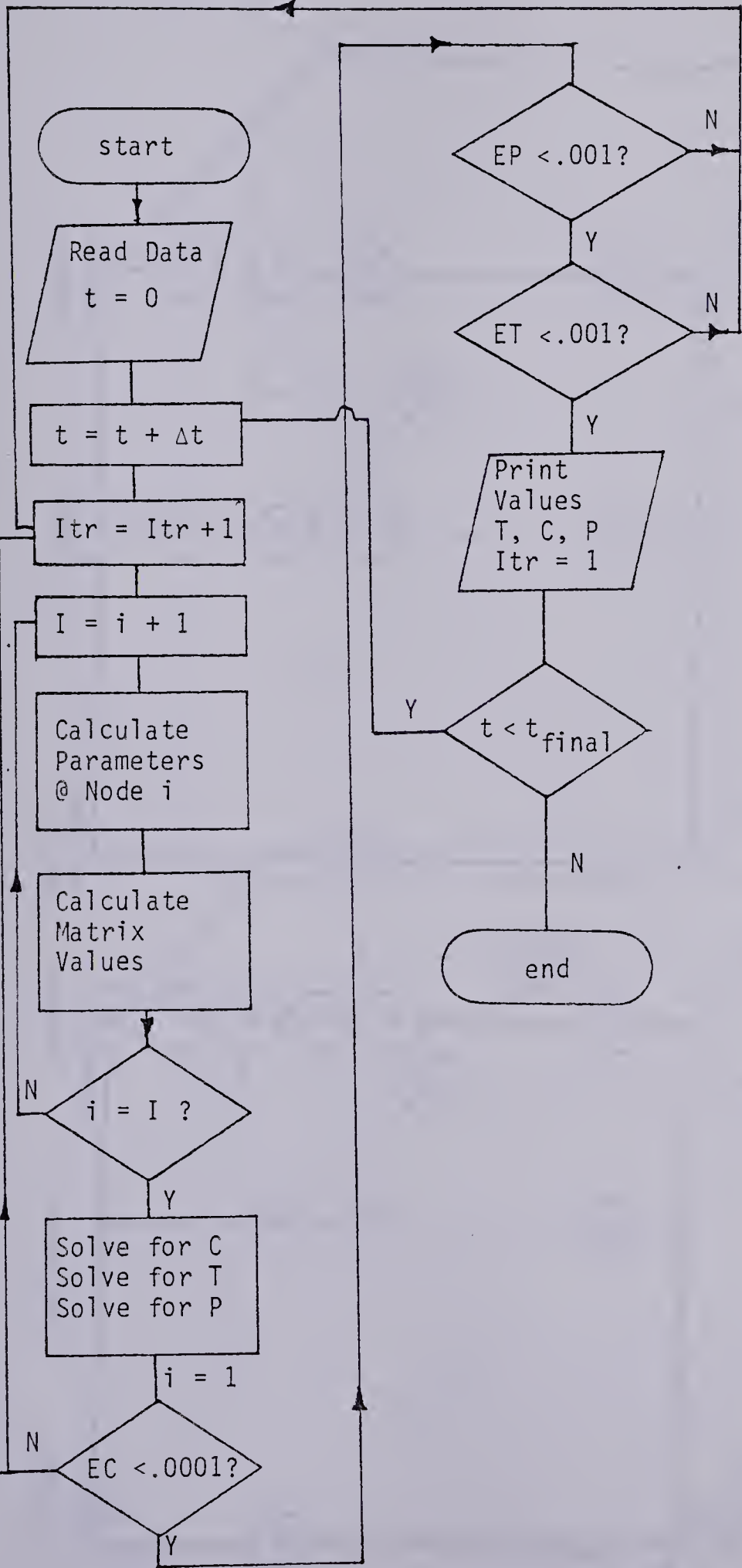
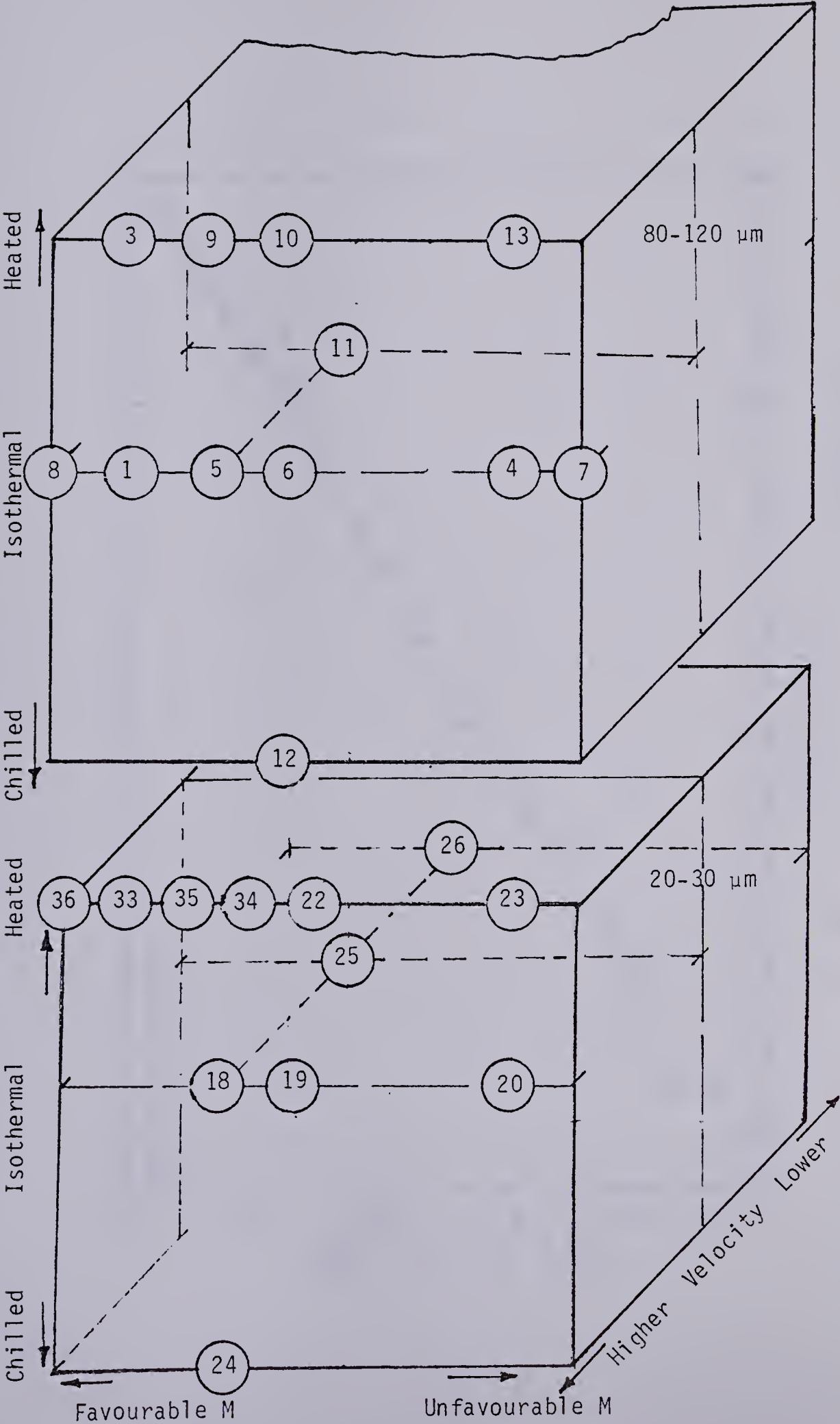




Figure 30 Experimental Strategy





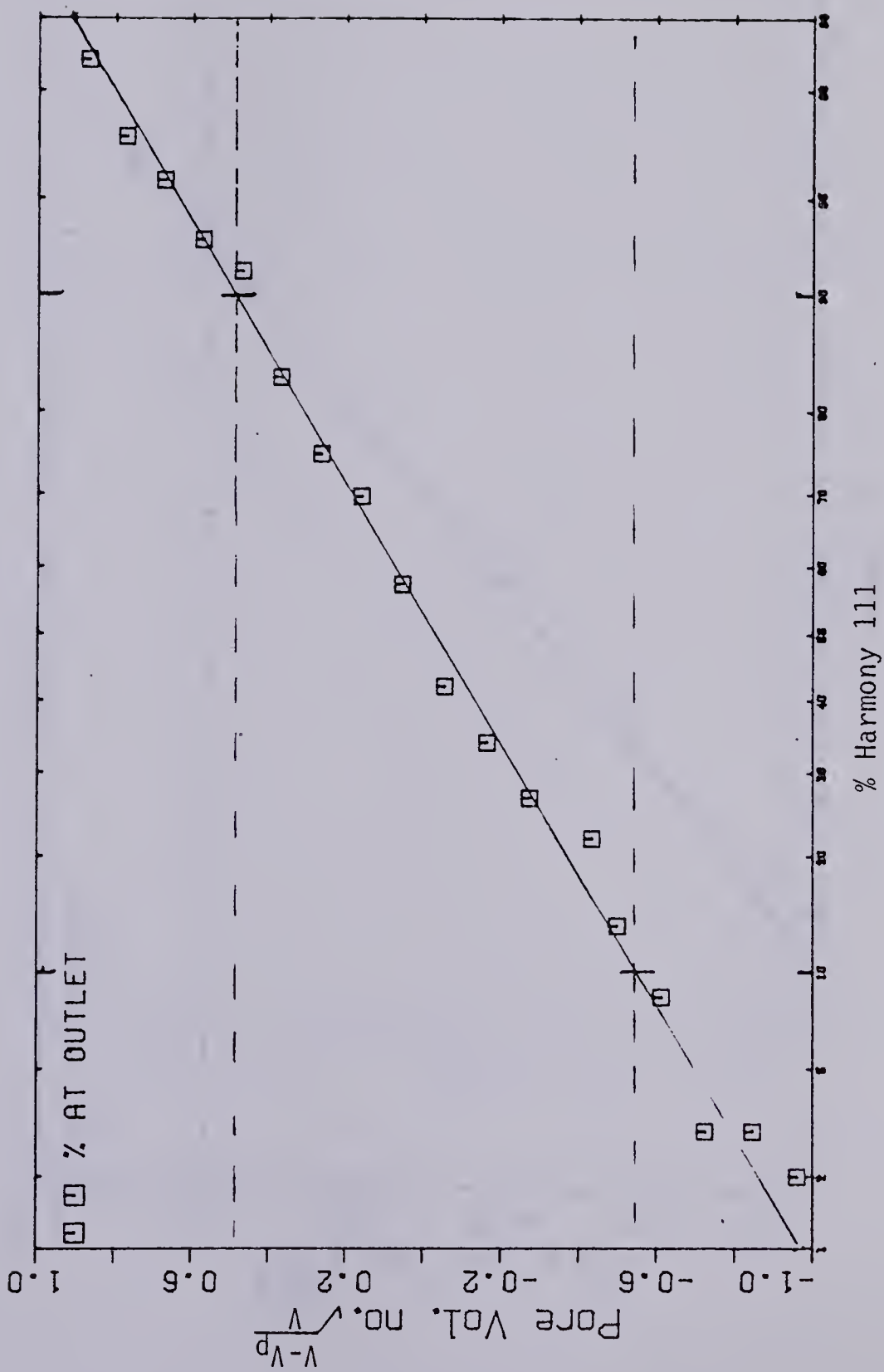


Figure 31 Probability Plot of Dispersion Profile, R3



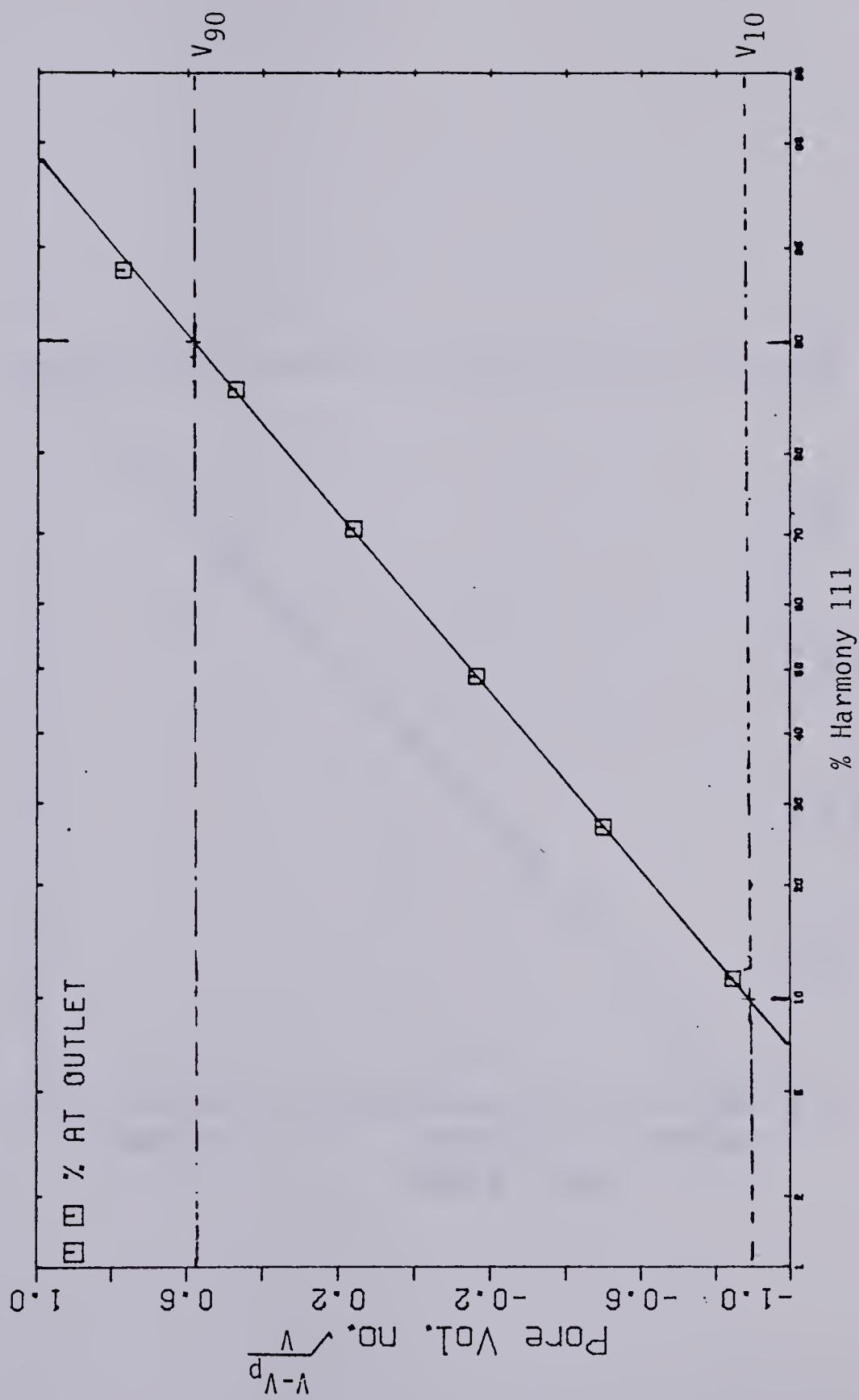


Figure 32 Probability Plot of Numerical Dispersion Profile



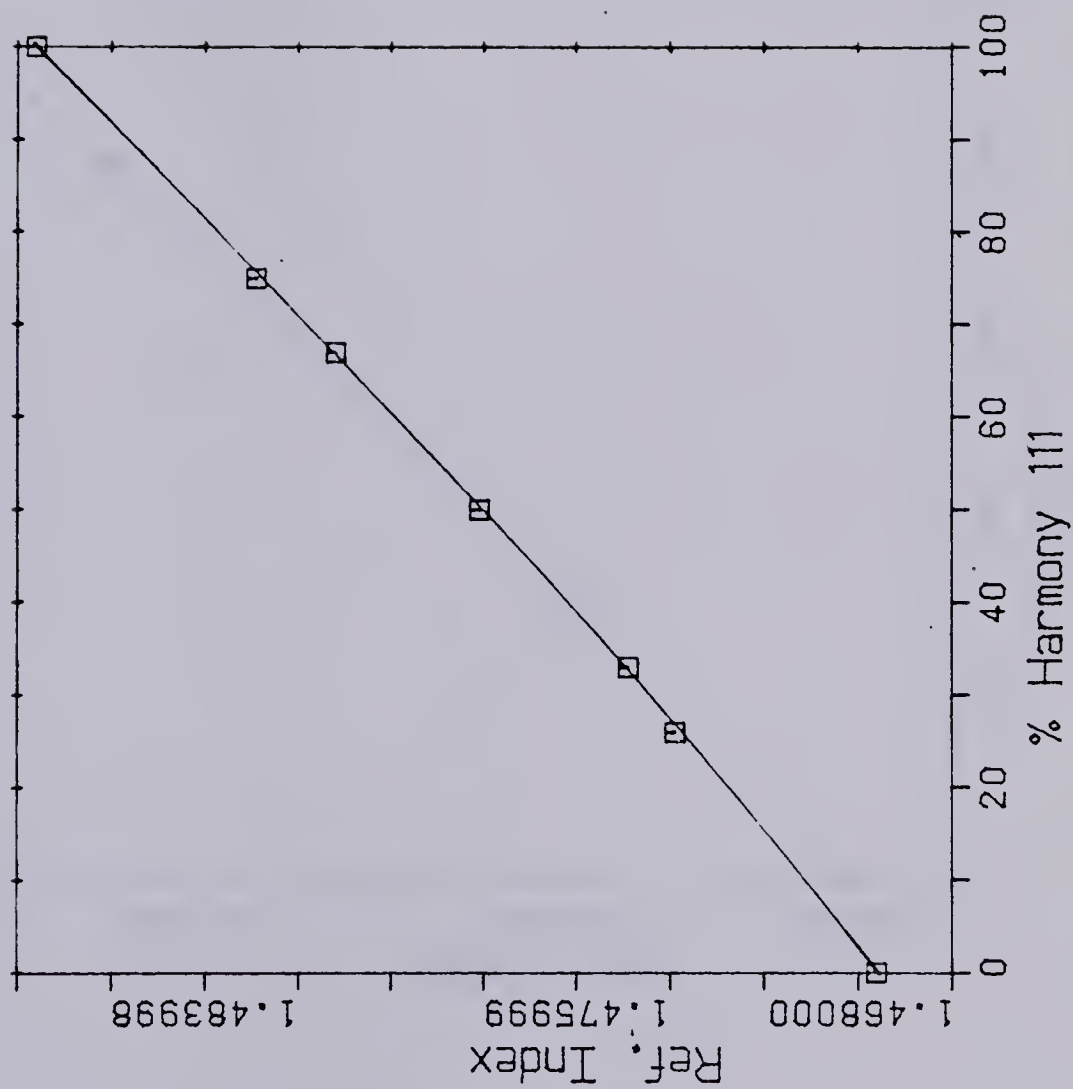


Figure 33 Harmony 44-111, Refractive Index



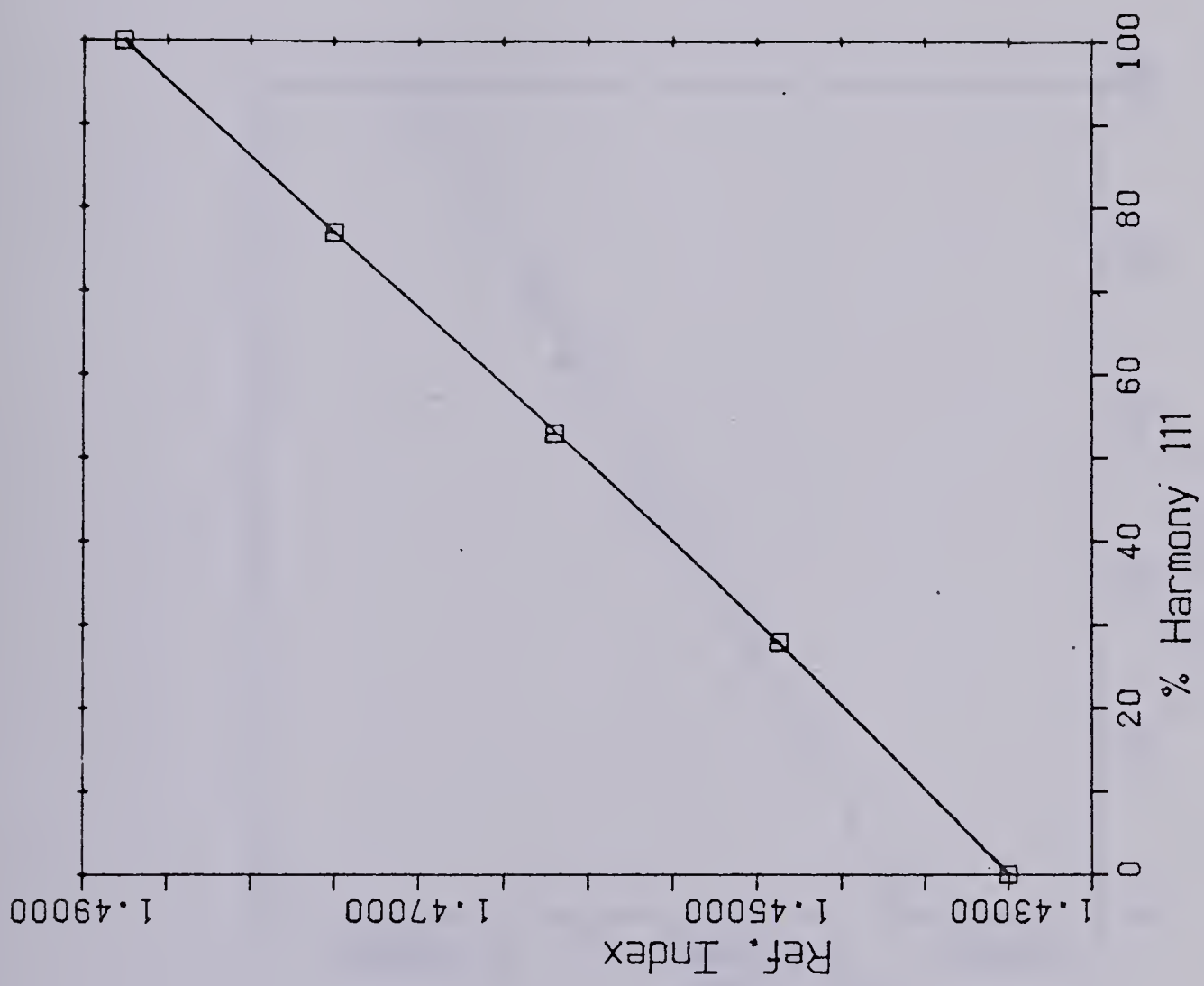


Figure 34 varsol-Harmony 111, Refr. Index



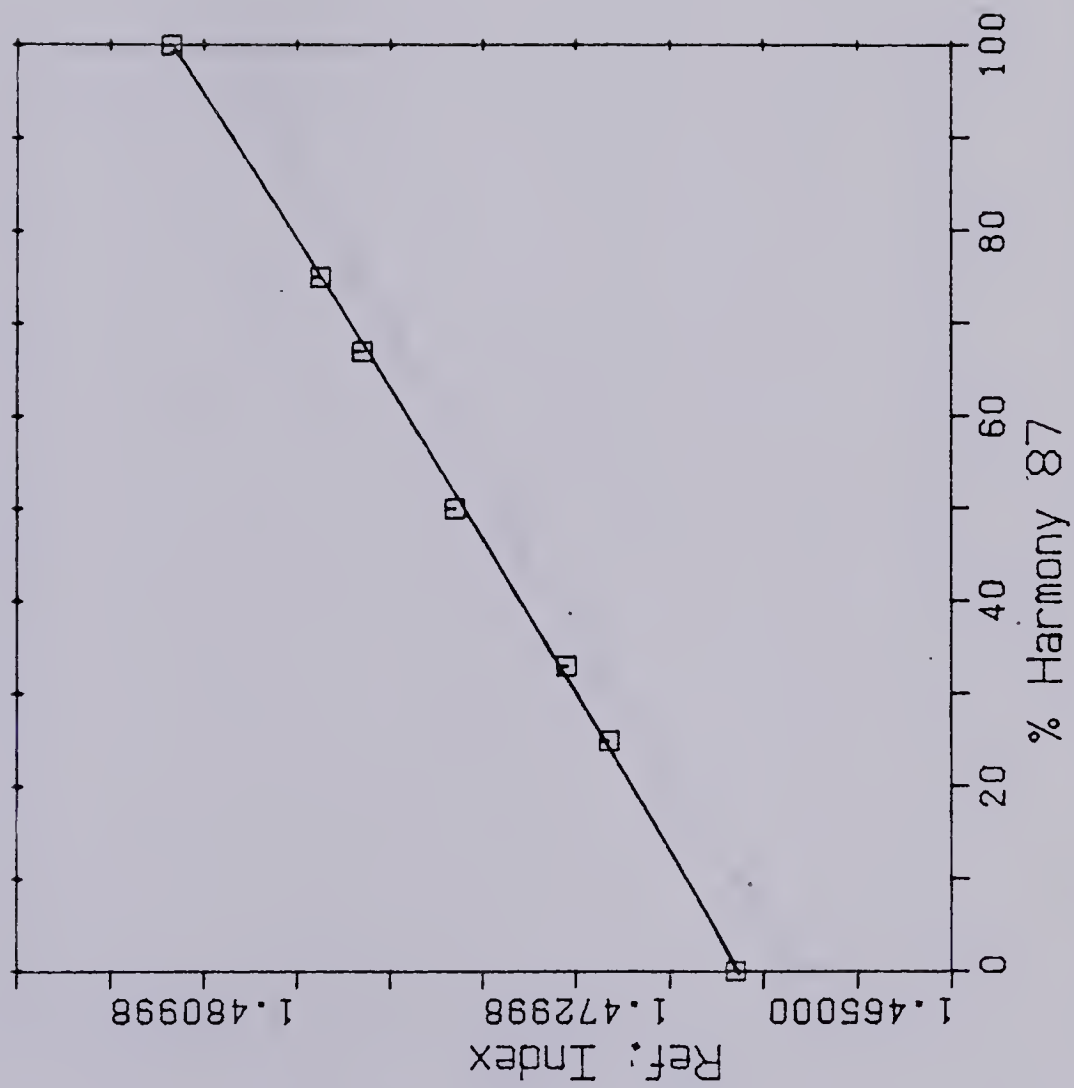


Figure 35 Harmony 44-87, Refractive Index



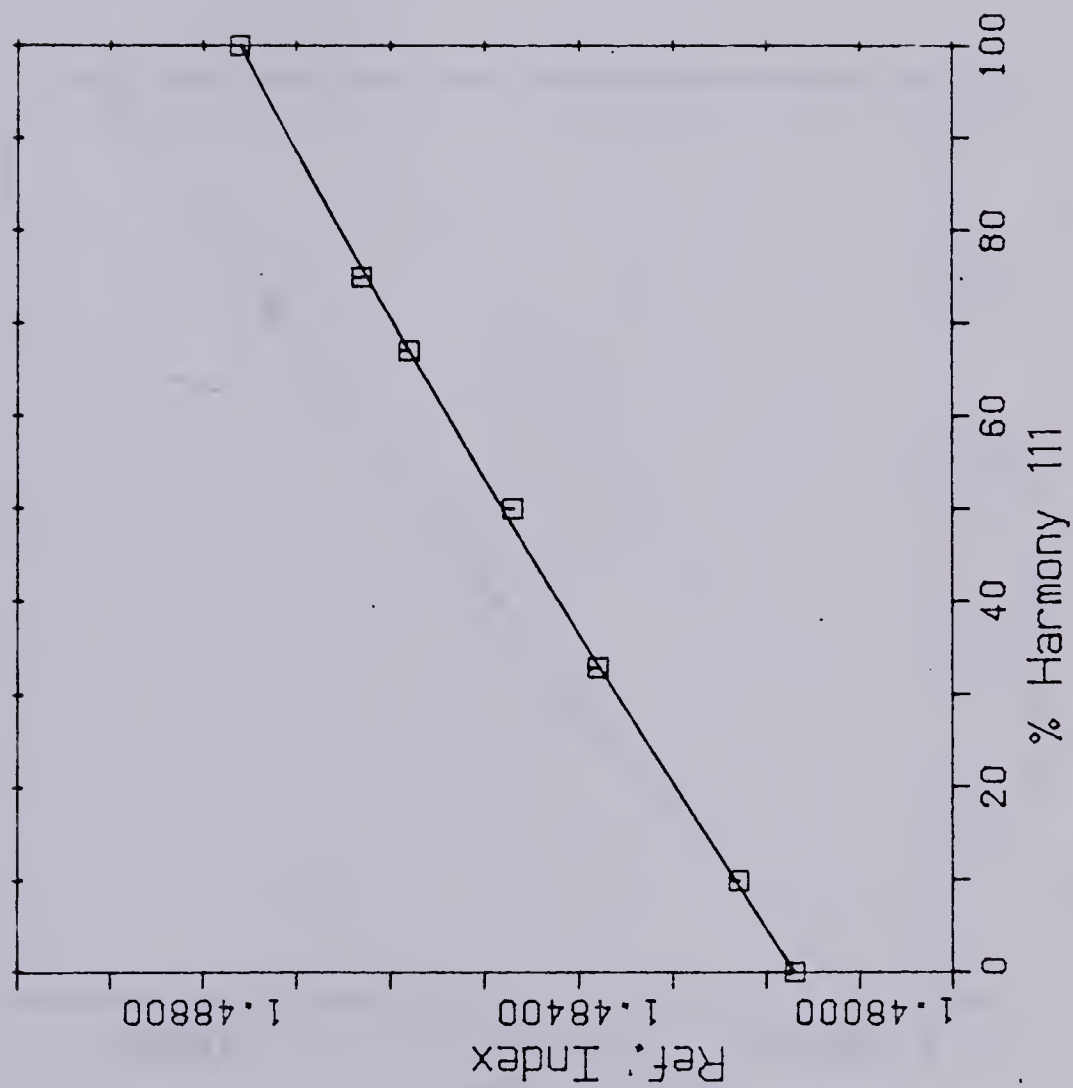


Figure 36 Harmony 87-111, Refractive Index



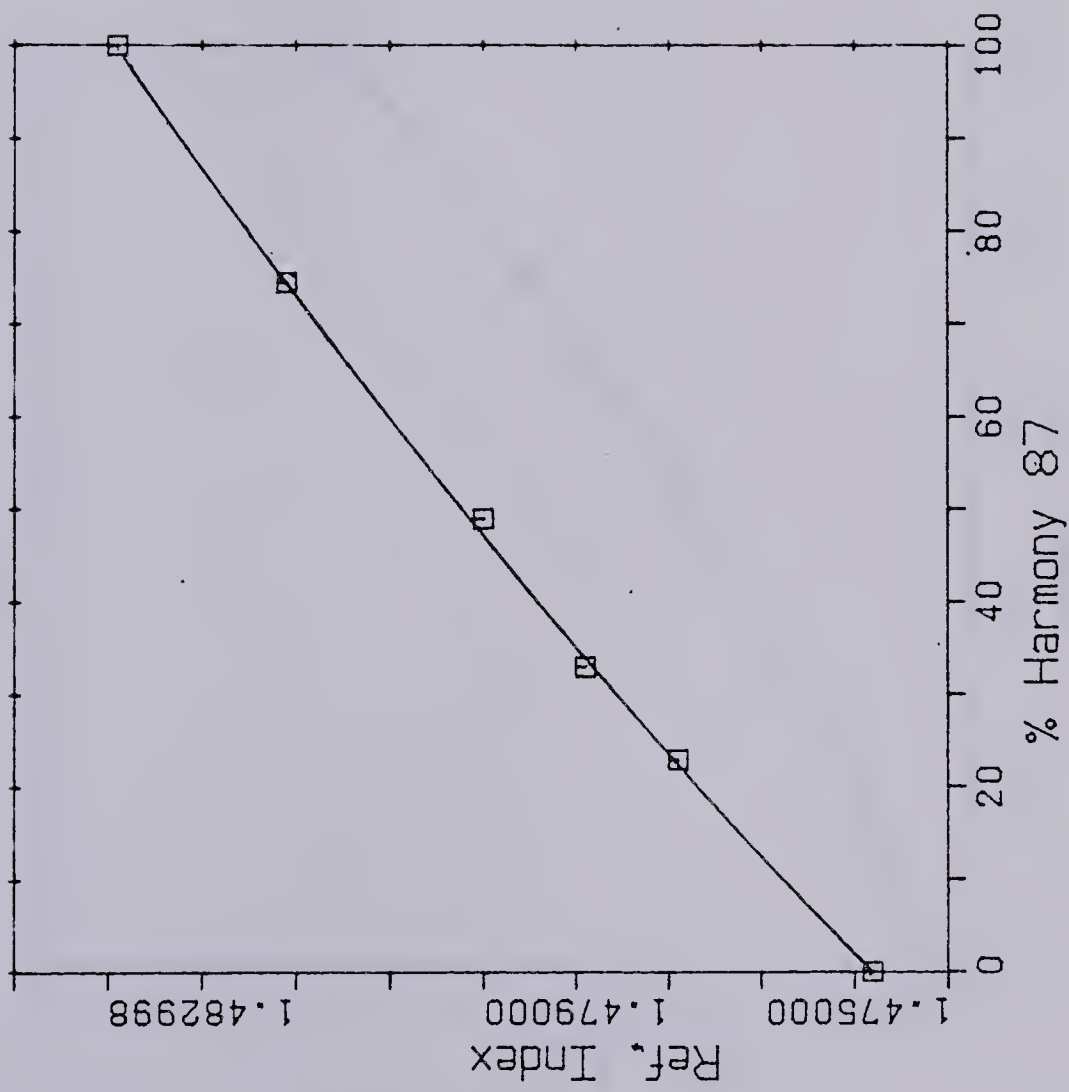


Figure 37 Harmony 53-87 , Refractive Index



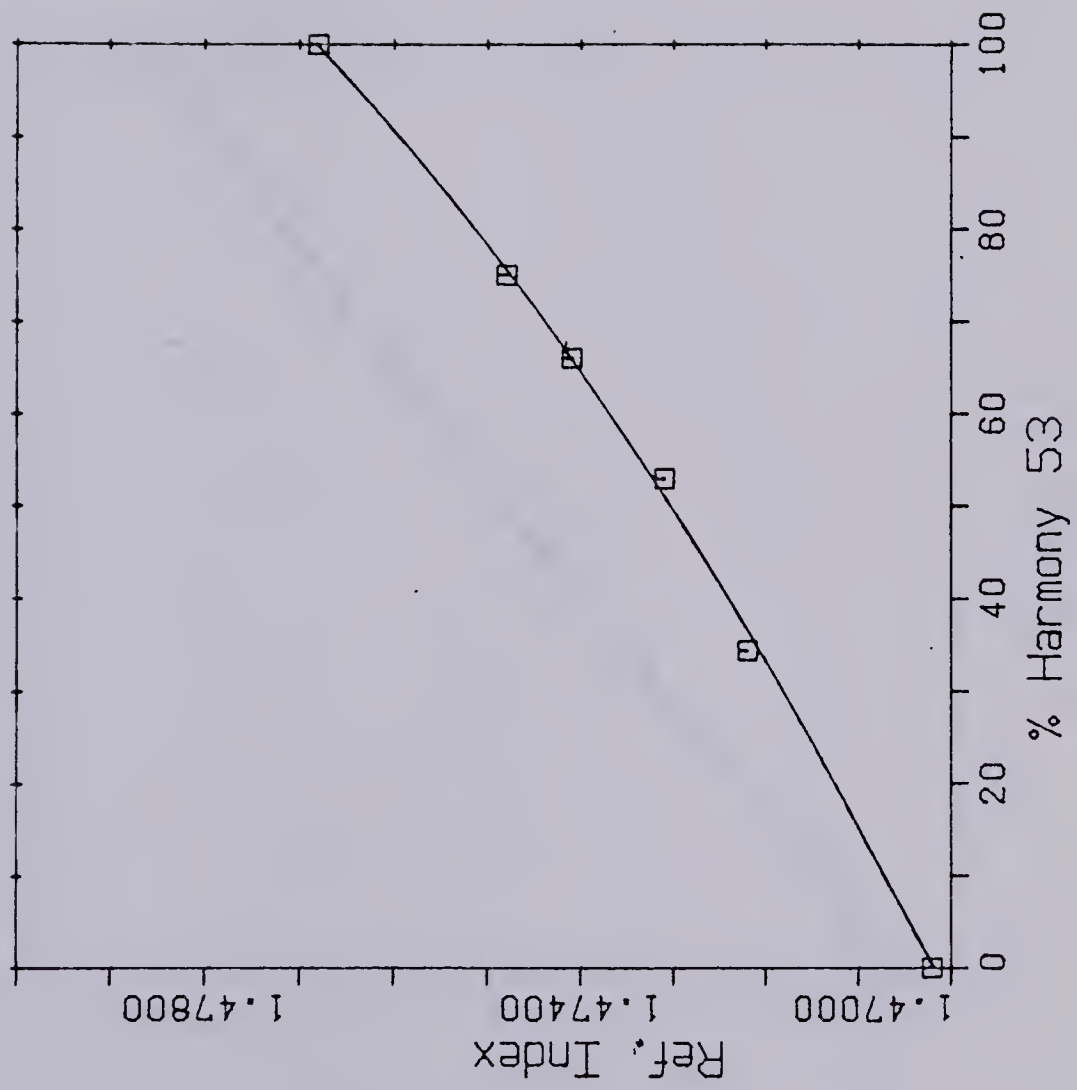


Figure 38 Harmony 44-53 , Refractive Index



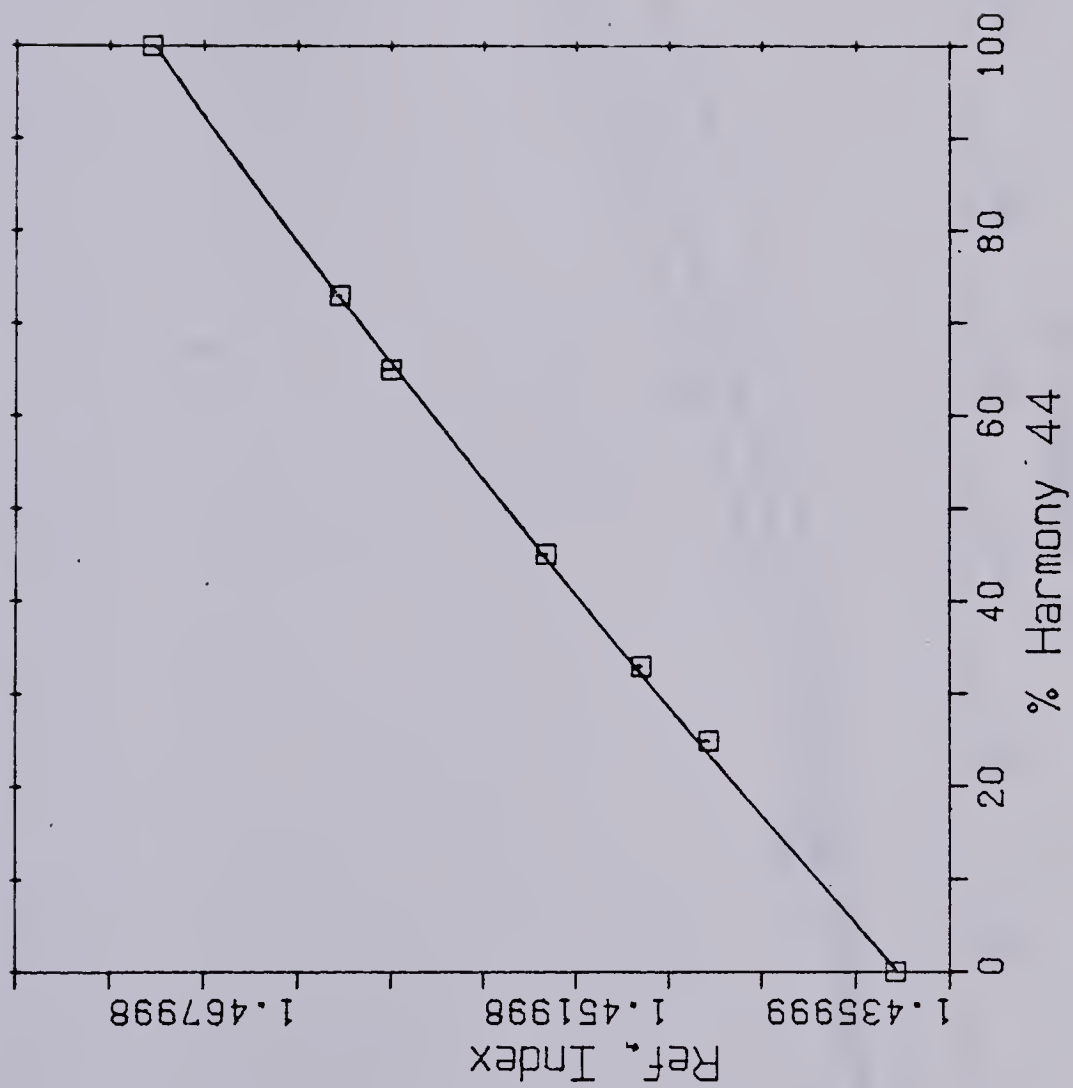


Figure 39 varsol-Harmony 44, Refractive Index



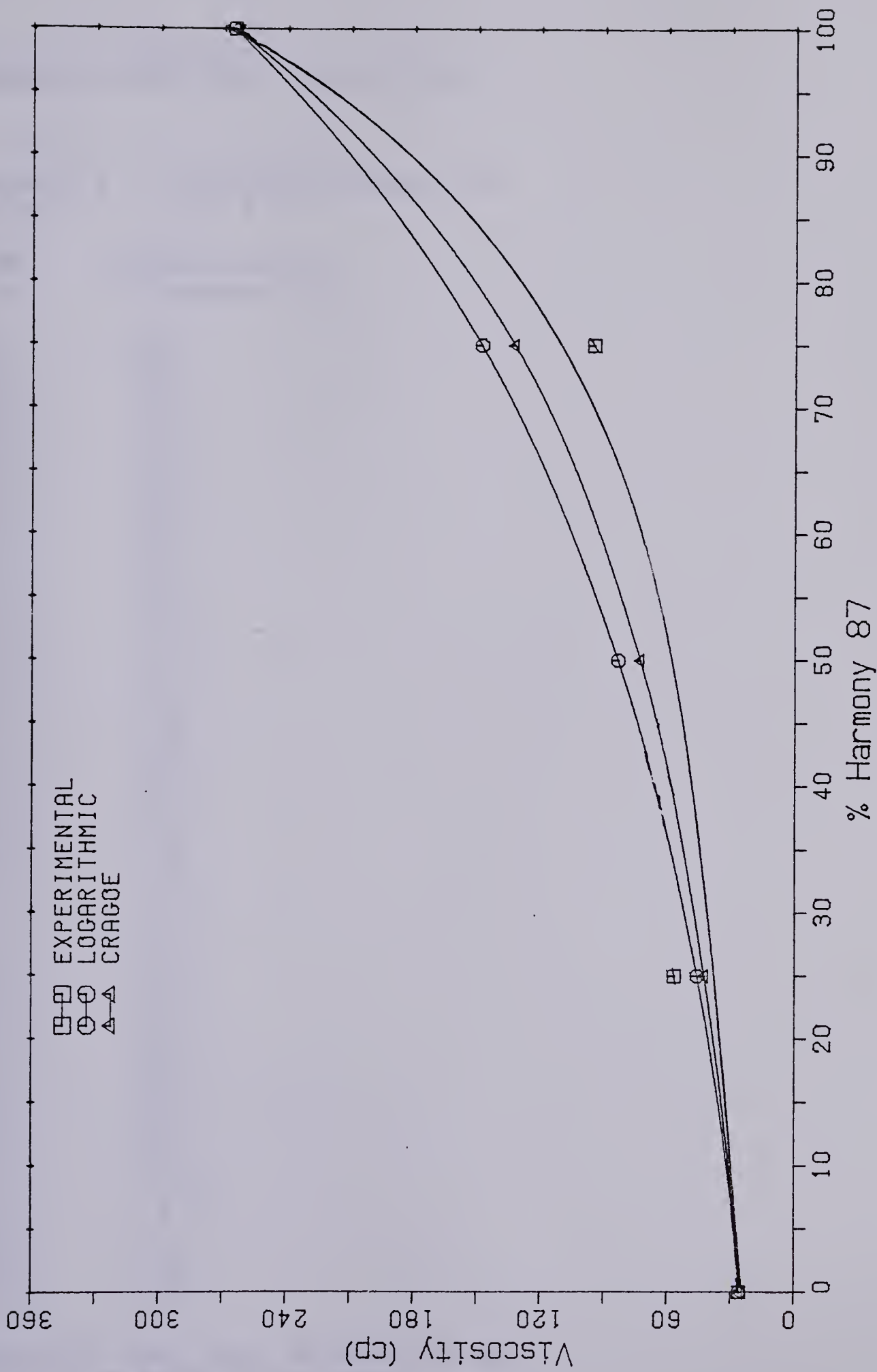


Figure 40 Viscosity of Mixtures, Harmony 44-87



TABLE 5  
Summary of Raw Data, Runs 1-36

Run 1  
Harmony 111 displacing Harmony 44  
T0=26.7 C T1=27.4 C

Time (s)	Concentration (% Harmony 111)
-------------	----------------------------------

240.	.020
300.	.035
3960.	.000
4020.	.000
4080.	.000
4140.	.000
4200.	.007
4260.	.000
4320.	.007
4380.	.007
4440.	.020
4500.	.030
4560.	.030
4620.	.085
4680.	.135
4740.	.206
4800.	.268
4860.	.341
4920.	.422
4980.	.575
5040.	.699
5100.	.752
5160.	.834
5220.	.915
5280.	.932
5340.	.957
5400.	.970
5460.	.985
5520.	.995
5580.	.990
5640.	.985
5700.	.995
5760.	1.000
5820.	1.0
5880.	1.00
5940.	1.00
6000.	1.0

porosity=.328 pore volume=1260 cm3  
80 -120 um sand (20-30 mesh)



Run 2

Harmony 44 displacing Harmony 111

T0=27.5 T1=23.5

Time (s)	Concentration (% Harmony 44)
-------------	---------------------------------

600.	.576
630.	.757
660.	.548
690.	.576
720.	.565
750.	.630
780.	.585
810.	.570
840.	.550
870.	.527
900.	.522
930.	.613
960.	.545
990.	.580
1020.	.585
1050.	.576
1080.	.576
1110.	.522
1140.	.505
1170.	.522
1200.	.477
1230.	.465
1260.	.494
1290.	.494
1320.	.450
1350.	.438
1380.	.430
1410.	.387
1440.	.340
1470.	.325
1500.	.312
1530.	.315
1560.	.307
1590.	.290
1620.	.285
1650.	.285
1680.	.250
1710.	.240
1740.	.240
1770.	.250
1800.	.245
1830.	.240
1860.	.228
1890.	.240
1910.	.228
1940.	.240

porosity = .328 pore volume=1260 cm3



## Run 3

Harmony 111 displacing Harmony 44  
 Heated injection, T0=27 C T1=92 C

Time (s)	Concentration (% Harmony 111)
-------------	----------------------------------

3600.	.015
4140.	.007
4200.	.007
4260.	.007
4320.	.007
4380.	.022
4440.	.015
4500.	.030
4560.	.042
4620.	.062
4680.	.075
4740.	.152
4800.	.222
4860.	.307
4920.	.410
4980.	.465
5040.	.500
5100.	.737
5160.	.798
5220.	.845
5280.	.895
5340.	.895
5400.	.960
5460.	.985
5520.	.980
5580.	.995
5640.	.995
5700.	1.00
5760.	.995
5820.	1.00
5880.	1.00

Oil flow rate = 948 cm<sup>3</sup>/hr

porosity = .328 pore volume = 1260 cm<sup>3</sup>

80-120 um sand



## Run 4

Harmony 44 displacing Harmony 111  
 T0=25.3 C T1=25.6 C

Time (s)	Concentration (% Harmony 44)
-------------	---------------------------------

180.	1.00
360.	1.00
540.	.995
720.	1.00
900.	1.00
1080.	1.00
1260.	1.00
1440.	.995
1620.	.990
1800.	.700
1980.	.748
2169.	.848
2340.	.740
2520.	.815
2700.	.715
2880.	.695
3060.	.730
3240.	.647
3420.	.630
3600.	.705
3780.	.630
3960.	.565
4140.	.565
4320.	.510
4500.	.515
4680.	.420
4860.	.420
5040.	.515
5220.	.460
5400.	.440
5580.	.365
5760.	.308
5940.	.308
6120.	.330
6300.	.302
6480.	.295
6660.	.273
6840.	.270
7020.	.245
7200.	.285

porosity= .328 pore volume = 1260 cm3  
 80-120 um sand (20-30 mesh)  
 Oil flow rate =937 cm3/hr



## Run 5

Harmony 87 displacing Harmony 44

T0=27.6 C T1=27.2 C

Time (s)	Concentration (% Harmony 87)
-------------	---------------------------------

3600.	.000
4140.	.000
4200.	.023
4260.	.023
4320.	.023
4380.	.031
4440.	.031
4500.	.041
4560.	.095
4620.	.135
4680.	.192
4740.	.285
4800.	.396
4860.	.482
4920.	.585
4980.	.664
5040.	.74 1
5100.	.824
5160.	.895
5220.	.910
5280.	.932
5340.	.970
5400.	.980
5460.	.988
5520.	.995
5580.	.988
5640.	.995
5700.	.988
5760.	1.00
5880.	.980
5940.	.995

porosity = .328 pore volume = 1260 cm3

80-120 um sand (20-30 mesh)

Oil flow rate = 945 cm3/hr

note: Concentrations were normalized to 1.0 and 0.0



Run 6

Harmony 111 displacing Harmony 87

T0=27.2 C T1=26.7 C

Time (s)	Concentration (% Harmony 111)
-------------	----------------------------------

4560.	.000
4620.	.000
4680.	.000
4740.	.052
4800.	.020
4860.	.020
4920.	.052
4980.	.052
5040.	.068
5100.	.115
5160.	.130
5220.	.145
5280.	.195
5340.	.305
5400.	.402
5460.	.450
5520.	.482
5580.	.465
5640.	.755
5700.	.755
5760.	.740
5820.	.917
5880.	.932
5940.	.968
6000.	.932
6060.	.987
6120.	.968
6180.	.987

porosity=.328 pore volume=1260 cm3

80-120 um sand

Oil flow rate=851 cm3/hr



## Run 7

varsol displacing Harmony 111

T0=27.0 C T1=27.5 C

Time (s)	Concentration (% varsol)
-------------	-----------------------------

180.	.995
360.	.995
540.	.995
720.	.945
900.	.596
1080.	.484
1260.	.436
1440.	.436
1620.	.447
1800.	.405
1980.	.328
2160.	.287
2340.	.255
2520.	.250
2700.	.243
2880.	.242
3060.	.232
3240.	.214
3600.	.213
3780.	.210
3960.	.202
4140.	.203
4320.	.204
4500.	.207
4680.	.197
5040.	.184
5220.	.181
5400.	.177
5580.	.176
5760.	.177
5940.	.178
6120.	.179
6300.	.177
6480.	.177
6660.	.177
6840.	.178
7020.	.177
7200.	.186

porosity=.328 pore volume=1260. cm3

80-120 um sand

Oil flow rate=970 cm3/hr

Concentrations were normalized to 1.0 and 0.0



## Run 8

Harmony 111 displacing varsol

T0=28.2 C T1=28 C

Time (s)	Concentration (% Harmony 111)
-------------	----------------------------------

3660.	.000
4500.	.000
4560.	.009
4620.	.014
4680.	.032
4740.	.062
4800.	.117
4860.	.210
4920.	.362
4980.	.486
5040.	.604
5100.	.778
5160.	.771
5220.	.910
5280.	.952
5340.	.957
5400.	.976
5460.	.985
5520.	.999
5580.	.997
5640.	.997
5700.	.997
5760.	.997
5820.	.998
5880.	1.00
6000.	1.00

porosity=.328 pore volume=1260 cm3

80-120 um sand

Oil flow rate=963 cm3/hr

Concentrations were normalized to 1.0 and 0.0



## Run 9

Harmony 87 displacing Harmony 44  
Heated injection, T0=26 C T1=94 C

Time (s)	Concentration (% Hamony 87)
-------------	--------------------------------

3660.	.000
4200.	.000
4260.	.000
4320.	.020
4380.	.038
4440.	.085
4500.	.094
4560.	.175
4620.	.265
4680.	.352
4740.	.442
4800.	.575
4860.	.622
4920.	.782
4980.	.830
5040.	.855
5100.	.925
5160.	.940
5220.	.972
5280.	.990
5340.	.995
5400.	.990
5460.	1.00
5520.	1.00
5580.	.995
5640.	1.00
5940.	1.00

porosity=.328 pore volume=1260 cm3

80-120 um sand

Oil flow rate=980 cm3/hr



Run 10  
Harmony 111 displacing Harmony 87  
Heated injection, T0=26.5 C T1=96.0 C

Time (s)	Concentration (% Hamony 111)
-------------	---------------------------------

3660.	.000
4080.	.000
4140.	.020
4200.	.000
4260.	.000
4320.	.020
4380.	.020
4440.	.020
4500.	.090
4560.	.115
4620.	.162
4680.	.210
4740.	.290
4800.	.385
4860.	.482
4920.	.500
4980.	.585
5040.	.688
5100.	.792
5160.	.810
5220.	.845
5280.	.898
5340.	.934
5400.	.950
5460.	.970
5520.	.987
5580.	1.00
5640.	1.00
5700.	1.00
6000.	1.00

porosity=.328 pore volume=1260 cm3  
80-120 um sand  
Oil flow rate=966 cm3/hr



Run 11

Hamony 87 displacing Harmony 44

T0=26.1 C T1=26 C

Time (s)	Concentration (% Hamony 87)
-------------	--------------------------------

14400.	.000
18000.	.000
18240.	.000
18480.	.000
18720.	.012
18960.	.066
19200.	.076
19440.	.103
19680.	.195
19920.	.285
20160.	.430
20400.	.528
20640.	.621
20880.	.753
21120.	.783
21360.	.845
21600.	.903
21840.	.924
22080.	.934
22320.	.980
22560.	1.00
22800.	1.00
23040.	1.00
23760.	1.00

porosity=.328 pore volume=1260 cm3

80-120 um sand

low flow rate



Run 12

Hamony 111 displacing Harmony 87

Chilled injection, T 0=80 C T1=19.5 C

Time (s)	Concentration (% Harmony 111)
-------------	----------------------------------

3360.	.000
4200.	.000
4260.	.000
4320.	.000
4380.	.017
4440.	.033
4500.	.069
4560.	.158
4620.	.230
4680.	.318
4740.	.389
4800.	.578
4860.	.578
4920.	.653
4980.	.789
5040.	.808
5100.	.925
5160.	.944
5220.	.967
5340.	.985
5400.	.985
5460.	1.00
5520.	1.00
5580.	1.00
6000.	1.00

porosity=.328 pore volume=1260 cm3

80-120 um sand

Concentrations were normalized to 1.0 and 0.0



Run 13

Harmony 44 displacing Harmony 111

Heated injection, T 0=26.0 C T1=90 C

Time (s)	Concentration (% Harmony 44)
-------------	---------------------------------

1260.	.005
1440.	.005
1620.	.150
1800.	.170
1980.	.315
2160.	.310
2340.	.160
2520.	.125
2700.	.252
2880.	.315
3060.	.420
3240.	.451
3420.	.516
3600.	.505
3780.	.545
3960.	.522
4140.	.545
4320.	.590
4500.	.607
4680.	.607
4860.	.652
5040.	.658
5220.	.675
5400.	.660
5580.	.653
5760.	.653
5940.	.676
6120.	.698
6300.	.704
6480.	.698
6660.	.704
6840.	.698
7020.	.738
7200.	.732

porosity=.328 pore volume=1260 cm3

80-120 um sand

Oil flow rate=979 cm3/hr



Run 14

Harmony 87 displacing Harmony 44  
T0=26.3 C T1=26.7 C

Time (s)	Concentration (% Harmony 87)
-------------	---------------------------------

3660.	.000
4080.	.000
4140.	.000
4200.	.000
4260.	.005
4320.	.012
4380.	.046
4440.	.100
4500.	.193
4560.	.282
4620.	.360
4680.	.493
4740.	.640
4800.	.692
4860.	.815
4920.	.870
4980.	.894
5040.	.915
5100.	.963
5160.	.970
5220.	.988
5280.	.988
5340.	.988
5400.	1.00
5460.	1.00
5520.	.996
5580.	1.00
5640.	1.00
6000.	1.00

porosity=.328 pore volume=1260 cm3  
80-120 um sand  
Oil flow rate=975 cm3/hr



Run 15

Harmony 111 displacing Harmony 87

T0=28.0 C T1=28.0 C

Time (s)	Concentration (% Harmony 111)
-------------	----------------------------------

3660.	.000
3840.	.000
3900.	.000
3960.	.000
4020.	.007
4080.	.038
4140.	.022
4200.	.038
4260.	.053
4320.	.100
4380.	.117
4440.	.133
4500.	.230
4560.	.297
4620.	.297
4680.	.424
4720.	.475
4800.	.634
4860.	.634
4920.	.791
4980.	.808
5040.	.808
5100.	.841
5160.	.881
5220.	.936
5280.	.936
5340.	.963
5400.	.982
5460.	1.00
5520.	.982
5580.	1.00
5640.	1.00
6000.	1.00

porosity=.328 pore volume=1260 cm3

80-120 um sand

Oil flow rate=964 cm3/hr

concentrations were normalized to 1.0 and 0.0



Run 16  
Harmony 111 displacing Harmony 44  
T0=26.9 C T1=27.8 C

Time (s)	Concentration (% Harmony 111)
3660.	.000
4140.	.000
4200.	.000
4260.	.000
4320.	.007
4380.	.007
4440.	.048
4500.	.068
4560.	.110
4620.	.195
4680.	.250
4740.	.370
4800.	.494
4860.	.602
4920.	.685
4980.	.778
5040.	.845
5100.	.880
5160.	.900
5220.	.942
5280.	.942
5340.	.950
5400.	.962
5460.	.962
5520.	.985
5580.	.985
5640.	.985
5940.	.995

porosity=.328 pore volume=1260 cm3  
80-120 um sand  
Oil flow rate=963 cm3/hr



Run 17

Hamony 111 displacing Harmony 87

T0=27 C T1=27.2 C

Time (s)	Concentration (% Harmony 111)
-------------	----------------------------------

3660.	.000
4320.	.000
4380.	.000
4440.	.000
4500.	.017
4560.	.017
4620.	.051
4680.	.180
4740.	.218
4800.	.273
4860.	.419
4920.	.419
4980.	.557
5040.	.597
5100.	.735
5160.	.752
5220.	.784
5280.	.816
5340.	.834
5400.	.834
5460.	.957
5520.	.957
5580.	.957
5640.	.957
5700.	.977
5820.	1.000
5880.	1.000
6000.	1.000

porosity=.328 pore volume=1260 cm3

80-120 um sand

oil flow rate=927 cm3/hr

Concentration was normalized to 1.0 and 0.0



Run 18

Harmony 87 displacing Harmony 44

T0=27.0 C T1=26.8 C

Time (s)	Concentration (% Harmony 87)
-------------	---------------------------------

3660.	.000
5040.	.000
5100.	.000
5160.	.000
5220.	.010
5280.	.032
5340.	.090
5400.	.175
5460.	.302
5520.	.446
5580.	.597
5640.	.680
5700.	.835
5760.	.934
5820.	.934
5880.	.970
5940.	.993
6000.	1.00
6060.	.993
6120.	1.00
6180.	1.00
6240.	1.00
6300.	1.00

porosity=.368 pore volume=1411 cm3

20-30 um (80-120 mesh) sand

oil flow rate=908 cme/hr



Run 19  
 Harmony 111 displacing Harmony 87  
 T 0=24.9 C T1=25.3 C

Time (s)	Concentration (% Harmony 111)
4860.	.035
5100.	.000
5400.	.020
5460.	.085
5520.	.085
5580.	.130
5640.	.146
5700.	.257
5760.	.322
5820.	.450
5880.	.567
5940.	.620
6000.	.755
6060.	.810
6120.	.810
6180.	.933
6240.	.950
6300.	.950
6360.	.950
6420.	.970

porosity=.368 pore volume=1411 cm3  
 20-30 um sand



RUN 20

Harmony 44 displacing Harmony 111

T0=24.2 C T1=24.4 C

Time (s)	Concentration (% Hamony 44)
-------------	--------------------------------

00180.	.005
00360.	.005
01980.	.005
02160.	.005
02340.	.150
02520.	.105
02700.	.212
2880.	.160
03060.	.165
03240.	.195
03420.	.212
03600.	.222
03780.	.222
03960.	.295
04140.	.360
04320.	.370
04500.	.420
04680.	.425
04860.	.435
05040.	.470
05220.	.480
05400.	.535
05580.	.545
05760.	.590
05940.	.590
06120.	.630
06300.	.635
06480.	.635
06660.	.640
06840.	.675
7020.	.698
7200.	.705

porosity=.368 pore volume=1411 cm3

20-30 um sand

Oil flow rate=900 cm3/hr



Run 21  
Harmony 87 displacing Harmony 44  
Heated injection, T0=25.5 C T1=91.5 C

Time (s)	Concentration (% Harmony 87)
4800.	.000
4860.	.000
4920.	.022
4980.	.085
5040.	.156
5100.	.246
5160.	.407
5220.	.556
5340.	.832
5400.	.903
5460.	.960
5520.	.994
5580.	1.00
5640.	1.000
5700.	1.00
5880.	1.00

porosity=.368 pore volume=1411 cm3  
20-30 um sand  
oil flow rate=972 cm3/hr



Run 22

Harmony 111 displacing Harmony 87

Heated injection, T0=28.1 C T1=92.4 C

Time (s)	Concentration (% Harmony 111)
-------------	----------------------------------

4260.	.000
4620.	.000
4680.	.000
4740.	.024
4800.	.000
4860.	.054
4920.	.134
4980.	.134
5040.	.167
5100.	.284
5160.	.365
5220.	.479
5280.	.619
5340.	.691
5400.	.778
5460.	.816
5520.	.835
5580.	.871
5640.	.928
5700.	.962
5760.	.962
5820.	.962
5880.	.979
5940.	1.00
6000.	1.00
6600.	1.00

porosity=.368 pore volume=141.1 cm3

20-30 um sand

oil flow rate=950 cm3/hr

Concentrations were normalized to 1.0 and 0.0



Run 23

Harmony 44 displacing Harmony 111

Heated injection, T0=28.7 C T1=89.0 C

Time (s)	Concentration (% Harmony 44)
-------------	---------------------------------

0180.	.000
01440.	.000
1620.	.000
1800.	.047
1980.	.091
2160.	.136
2340.	.145
2520.	.179
2700.	.205
2880.	.205
3060.	.224
3240.	.273
3420.	.310
3600.	.354
3780.	.364
3960.	.354
4140.	.389
4320.	.414
4500.	.467
4680.	.480
4860.	.530
5040.	.563
5220.	.575
5400.	.574
5580.	.581
5760.	.586
5940.	.591
6120.	.636
6300.	.662
6480.	.662
6660.	.690
6840.	.702
7020.	.729
7200.	.747

porosity=.368 pore volume=1411 cm3

20-30 um sand

Oil flow rate=925 cm3/hr

Concentrations were normalized to 1.0 and 0.0



Run 24

Harmony 87 displacing Harmony 44

Chilled injection, T0=80.3 C T1=26.9 C

Time (s)	Concentration (% Harmony 87)
-------------	---------------------------------

4860.	.046
5100.	.000
5340.	.046
5400.	.046
5460.	.067
5520.	.074
5580.	.142
5640.	.181
5700.	.315
5760.	.450
5820.	.600
5880.	.756
5940.	.837
6000.	.920
6060.	.936
6120.	.936
6180.	.982
6240.	1.00
6300.	1.00
6360.	1.00
6600.	1.00

porosity=.368 pore volume=1411 cm3

20-30 um sand

oil flow rate=855 cm3/hr

Concentrations were normalized to 1.0 and 0.0



Run 25

Harmony 87 displacing Harmony 44

T0=30.0 C T1=30.0 C

Time (s)	Concentration (% Harmony 87)
-------------	---------------------------------

21600.	.000
23040.	.000
23280.	.000
23540.	.011
23760.	.000
24000.	.011
24240.	.045
24480.	.108
24720.	.190
24960.	.311
25200.	.405
25440.	.494
25680.	.602
25920.	.670
26180.	.761
26420.	.847
26660.	.892
26900.	.926
27140.	.943
27380.	1.00
27620.	1.00
28340.	1.00

porosity=.368 pore volume=1411 cm3

20-30 um sand

Low flow rate (210 cm3/hr)

Concentrations were normalized to 1.0 and 0.0



Run 26

Harmony 87 displacing Harmony 44

T0=29 C T1=29.3 C

Time (s)	Concentration (% Harmony 87)
-------------	---------------------------------

65700.	.000
72900.	.000
73800.	.000
74700.	.000
75600.	.000
76500.	.011
77400.	.022
78300.	.072
79200.	.172
80100.	.250
81000.	.327
81900.	.544
82800.	.588
83700.	.672
84600.	.758
85500.	.844
86400.	.917
87300.	.950
88200.	1.00
89100.	1.00
90000.	1.00

porosity=.368 pore volume=1411 cm3

20-30 um sand

Field displacement rate (61 cm3/hr)

Concentrations were normalized to 1.0 and 0.0



Run 27  
water wet sand pack  
Harmony 87 displacing Harmony 44  
T0=29.C T1=29.2 C

Time (s)	Concentration (% Harmony 87)
-------------	---------------------------------

3660.	.000
4200.	.000
4260.	.000
4320.	.028
4380.	.055
4440.	.075
4500.	.170
4560.	.274
4620.	.432
4680.	.545
4740.	.692
4800.	.787
4860.	.871
4920.	.921
4980.	.936
5040.	.952
5100.	.952
5160.	1.00
5220.	.995
5280.	.995
5460.	1.00

porosity=.356 pore vol.=1354 cm3

volume of residual water in pack=174 cm3

oil flow rate = 975 cm3/hr

Oil concentrations are normalized to 0.0 and 1.0 .



Run 28

Harmony 111 displacing Hamony 87

water wet pack 20-30 um sand (80-120 mesh)

T0=27.2 C T1=27.5 C

Time (s)	Concentration (% Harmony 111)
-------------	----------------------------------

3660.	.000
4200.	.000
4260.	.000
4320.	.043
4380.	.043
4440.	.116
4500.	.189
4560.	.226
4620.	.371
4680.	.429
4740.	.560
4800.	.597
4860.	.719
4920.	.777
4980.	.899
5040.	.859
5100.	.940
5160.	.959
5220.	1.00
5280.	1.00
5340.	1.00
5940.	1.00

porosity=.356 pore vol.=1354 cm<sup>3</sup>

volume of residual water=75 cm<sup>3</sup>

oil flow rate=975 cm<sup>3</sup>/hr

Concentrations are normalized to 1.0 and 0.0



## Run 29

water wet sand pack

Harmony 44 displacing Harmony 111

T0=27.5 C T1=27.8 C

Time (s)	Concentration (% Harmony 44)
-------------	---------------------------------

360.	.000
540.	.000
900.	.000
1260.	.000
1620.	.000
1800.	.005
1980.	.039
2160.	.157
2340.	.222
2520.	.264
2700.	.292
2880.	.365
3060.	.519
3400.	.481
3780.	.562
4320.	.632
4680.	.686
5040.	.697
6840.	.768
7020.	.773

porosity=.356 pore volume=1354cm<sup>3</sup>

The volume of residual water could not be calculated.

oil flow rate=975 cm<sup>3</sup>/hr

Concentrations were normalized to 1.0 at endpoint.



Run 30

Heated displacement, T0=26. C T1=92.0 C  
Harmony 44 displacing varsol

Time (s)	Concentration (% Harmony 44)
-------------	---------------------------------

3660.	.000
3720.	.000
4080.	.000
4140.	.000
4200.	.000
4260.	.000
4320.	.000
4380.	.000
4440.	.000
4500.	.018
4560.	.026
4620.	.041
4680.	.116
4740.	.223
4800.	.331
4860.	.420
4920.	.570
4980.	.770
5040.	.883
5100.	.931
5160.	.958
5220.	.970
5280.	.990
5340.	1.00
5400.	1.00
5460.	1.00
6000.	1.00

porosity=.356 pore volume=1354. cm3

20-30 um sand (80-120 mesh)

Some aqueous phase was present in the pack.

Calculated volume=27. cm3

The concentrations of the end points  
were normalized to 1.0 and 0.0



Run 31  
Harmony 87 displacing Harmony 44  
T0=25.2 C T1=25.8 C

Time (s)	Concentration (% Harmony 87)
3600.	.000
3900.	.000
4200.	.000
4500.	.000
4740.	.000
4800.	.020
4860.	.020
4920.	.080
4980.	.145
5040.	.145
5100.	.370
5160.	.535
5220.	.690
5280.	.810
5340.	.880
5400.	.920
5460.	1.00
5520.	1.00
5700.	1.00
6000.	1.00

porosity=.356 pore volume=1354 cm3  
oil flow rate=970. cm3/hr  
20-30 um sand



Run 32

Harmony 111 displacing Harmony 87

T0=27.0 C T1=27.5 C

Time (s)	Concentration (% Harmony 111)
-------------	----------------------------------

3660.	.025
3900.	.000
4200.	.000
4500.	.000
4800.	.000
4860.	-.056
4920.	.000
4980.	.018
5040.	.037
5100.	.194
5160.	.233
5220.	.342
5280.	.420
5340.	.582
5400.	.624
5460.	.726
5520.	.810
5580.	.828
5640.	.873
5700.	.873
5760.	.936
5820.	.958
5880.	.978
5940.	1.00
6060.	1.00

porosity=.356 pore volume=1354 cm3

20-30 um sand (80-120 mesh)

oil flow rate =940 cm3/hr

Concentrations were normalized to 0.0 and 1.0 at endpoints.



Run 33

Harmony 111 displacing Harmony 44

Heated displacement T0=27 C T1=86.4 C

Time (s)	Concentration (% Harmony 111)
-------------	----------------------------------

4740.	.000
4800.	.000
4860.	.016
4920.	.036
4980.	.095
5040.	.213
5100.	.323
5160.	.462
5220.	.546
5280.	.753
5340.	.829
5400.	.930
5460.	.943
5520.	.963
5580.	.950
5640.	.985
5700.	.985
5760.	1.00
5820.	1.00
5940.	.995
6000.	1.00

Oil flow rate =975 cm3/hr

Porosity =.356 pore volume=1354 cm3

20-30 um (80-120 mesh) sand

concentrations were normalized to 1.0 and 0.0 at end points.



Run 34

Harmony 53 displacing Harmony 44  
 Heated injection, T0=25 C T1=92.5 C

Time (s)	Concentration (% Harmony 53)
4200.	.000
4500.	.000
4560.	.000
4620.	.025
4680.	.025
4740.	.069
4800.	.167
4860.	.243
4920.	.389
4980.	.531
5040.	.645
5100.	.772
5160.	.861
5220.	.890
5280.	.861
5340.	.984
5400.	.984
5460.	.984
5700.	1.00
6000.	1.00

oil flow rate =1020 cm3/hr  
 porosity =.356 pore volume=1354 cm3  
 20-30 um sand



Run 35  
Harmony 87 displacing Harmony 53  
Heated displacement, T0=25 C T1=89.2 C

Time (s)	Concentration (% Harmony 87)
-------------	---------------------------------

3660.	.000
3900.	.000
4200.	.000
4500.	.000
4800.	.000
4860.	.010
4920.	.076
4980.	.123
5040.	.244
5100.	.408
5160.	.532
5220.	.720
5280.	.846
5340.	.871
5400.	.888
5460.	.990
5520.	.990
5580.	1.00
5700.	1.00
6000.	1.00

porosity=.356 pore volume=1354 cm3  
20-30 um (80-120 mesh) sand



Run 36

Harmony 44 displacing varsol

Heated injection, T0=25 C T1=91.5 C

Time (s)	Concentration (% Harmony 44)
-------------	---------------------------------

3660.	.000
3900.	.000
4200.	.000
4500.	.005
4560.	.015
4620.	.020
4680.	.031
4740.	.066
4800.	.153
4860.	.306
4920.	.463
4980.	.648
5040.	.814
5100.	.890
5160.	.949
5220.	.969
5280.	.995
5340.	.995
5400.	1.00
5460.	1.00
5640.	1.00
6000.	1.00

pore volume=1354 cm3 porosity=.356  
20-30 um sand (80-120 mesh)









B30315